République Algérienne Démocratique et Populaire

Ministère de l'Enseignement Supérieur et de la Recherche Scientifique

Ecole National Polytechnique

Department of Automatic Control

Submitted By:

Mr. SELAM KARIM

Title

Fault Tolerant Control of Wind Energy Conversion Systems

Dissertation Submitted to the Department of Automatic as Partial Fulfilment of the Requirement for the Degree of PhD in Automatic Control Studies

Examinators:	*Pr. NEZLI Lazhari*	*ENP*	*President*
	Pr. Tadjine Mohamed	*ENP*	*Thesis director*
	Pr. Allaoui Tayeb	*Ibn khaldoun Univ*	*Thesis director*
	Pr BOUCHAFA Faarid	*USTHB*	*Examinator*
	Pr BOUCHHIDA Ouahid	*Yahia Fares Univ*	*Examinator*
	Dr BOUDANA Djamel	*MCA ENP*	*Examinator*
	Pr BENZINEB Omar	*Kasdi Merbah Univ*	*Examinator*

ENP 2020

République Algérienne Démocratique et Populaire

Ministère de l'Enseignement Supérieur et de la Recherche Scientifique

Ecole National Polytechnique

Department of Automatic Control

Submitted By:

Mr. SELAM KARIM

Title

Fault Tolerant Control of Wind Energy Conversion Systems

Dissertation Submitted to the Department of Automatic as Partial Fulfilment of the Requirement for the Degree of PhD in Automatic Control Studies

Examinators:	*Pr. NEZLI Lazhari*	*ENP*	*President*
	Pr. Tadjine Mohamed	*ENP*	*Thesis director*
	Pr. Allaoui Tayeb	*Ibn khaldoun Univ*	*Thesis director*
	Pr BOUCHAFA Faarid	*USTHB*	*Examinator*
	Pr BOUCHHIDA Ouahid	*Yahia Fares Univ*	*Examinator*
	Dr BOUDANA Djamel	*MCA ENP*	*Examinator*
	Pr BENZINEB Omar	*Kasdi Merbah Univ*	*Examinator*

ENP 2020

République Algérienne Démocratique et Populaire

Ministère de l'Enseignement Supérieur et de la Recherche Scientifique

Ecole National Polytechnique

Département de l'Automatique

Réalisé par :

Mr. SELAM KARIM

Thème

Commande Tolérante aux Défauts Appliquées au Système Eolien

Thèse de Doctorat en Automatique

Composition du jury :	*Pr. NEZLI Lazhari*	*ENP*	*Président*
	Pr. Tadjine Mohamed	*ENP*	*Directeur de thèse*
	Pr. Allaoui Tayeb	*Ibn khaldoun Univ*	*Co_Directeur de thèse*
	Pr BOUCHAFA Faarid	*USTHB*	*Examinator*
	Pr BOUCHHIDA Ouahid	*Yahia Fares Univ*	*Examinateur*
	Dr BOUDANA Djamel	*MCA ENP*	*Examinateur*
	Pr BENZINEB Omar	*Kasdi Merbah Univ*	*Examinateur*

ENP 2020

ملخص:

يركز هذا العمل على تصميم استراتيجيات التحكم اثناء حدوث اعطاب لتعزيز استقرار عمل توربينات الرياح في ظل ظروف استثنائية للموليدات. الفكرة الرئيسية هي استخدام مفهوم تكرار المراقبين لإنشاء مجموعة الكشف الفعال عن الاعطاب بالاشتراك مع مجموعة من أنظمة التحكم التي يتم من خلالها تحديد استراتيجية التحكم المناسبة تلقائيًا للحفاظ على تشغيل النظام وضمان استمرار و مصدر طاقة موثوق به أثناء حدوث عطل. في عملنا هذا ، يتم استخدام بنك من أربعة مراقبين لاكتشاف الأخطاء بما في ذلك مراقب كالمان ومراقب الوضع المنزلق ومراقب مراقب ليونبرغ ومراقب الكسب العالي. أثناء حالة عدم وجود خطأ (الوضع الصحي) ، يتم استخدام نظام التحكم المتقدم ، عند حدوث خطأ ، يتحول النظام تلقائيًا إلى وحدة تحكم مناسبة اعتمادًا على طبيعة الخطأ وموقعه. بشكل عام ، يتم استخدام وحدة التحكم المعروفة بخصائص المتانة الممتازة ضد التغيرات الاساسية لنظام. بسبب تصميمه البسيط. يمكن تشغيل النظام بأداء منخفض للحفاظ على توصيل الطاقة المستمر.

الأطروحة مقسمة إلى أربعة أجزاء رئيسية. أولاً: العرض العام لطاقة تحويل الرياح ، في الجزء الثاني النمذجة والتحكم الكلاسيكي أكثر مما قمنا بتطوير عنصر تحكم جديد متقدم في القسم الثالث ، هذه الأجزاء ضرورية تم وضع الأساس فيما يتعلق بنماذج توربينات الرياح الديناميكية ، ويشكل هذا الجزء أساسًا لـ الجزء الأخير من تشخيص الأعطال والتحكم في التسامح مع الخطأ ، حيث يتم وصف تشخيص الأخطاء وأنظمة التحكم في تحمل الأخطاء وتطبيقها على سيناريوهات عديدة للأعطال.

كلمات مفتاحية : *تشخيص الأخطاء ، التحكم اثناء حدوث اعطاب ، نظام التحكم المتقدم ،طاقة تحويل الرياح ، توربينات الرياح*

Résume

Ce travail se concentre sur la conception de stratégies de commande tolérantes aux défauts pour améliorer la stabilité des éoliennes dans des conditions de défaut d'actionneur. L'idée principale est d'utiliser le concept de redondance des observateurs pour générer un ensemble résiduel pour une détection efficace des défauts en combinaison avec un ensemble de schémas de contrôle à partir desquels la stratégie de contrôle adéquate est automatiquement sélectionnée pour maintenir le fonctionnement du système et assurer une alimentation en énergie fiable lors de l'apparition d'un défaut. Dans ce travail, une banque de quatre observateurs est utilisée pour la détection des défauts, y compris le filtre de Kalman, l'observateur en mode glissant, l'observateur Luenberger et l'observateur à gain élevé. En condition sans défaut (mode sain), un contrôleur gaussien quadratique linéaire est utilisé. Cependant, lorsqu'un défaut survient, le système bascule automatiquement sur un contrôleur approprié en fonction de la nature et de l'emplacement du défaut. On utilise généralement le contrôleur connu pour avoir d'excellentes propriétés de robustesse face aux variations paramétriques. En raison de sa conception simple. Le système peut être exploité à de faibles performances pour maintenir la délivrance constante de l’énergie.

La thèse est divisée en quatre parties principales. Premièrement La présentation générale de l'énergie de conversion éolienne, Dans la deuxième partie nous avons développé la Modélisation et la commande PI, Dans la troisième section commande avance sont présentées, Cette partie constitue une base pour la dernière partie de Diagnostic des défauts et commande tolérante des défauts, où les schémas de diagnostic des défauts et de commande à haute disponibilité sont décrits et appliqués à plusieurs scénarios de défaut.

Mots clés : *Diagnostic des défauts, Commande tolérante aux défauts, Contrôleur gaussien quadratique linéaire, Energie de conversion éolienne, Éoliennes*

Abstract

This work focuses on the design of fault-tolerant control strategies to enhance the stability of wind turbines under actuator fault conditions. The main idea is to use the concept of observers redundancy to generate a residual set for an effective detection of faults in combination with a set of control schemes from which the adequate control strategy is automatically selected to maintain the operation of the system and ensure continuous and reliable energy supply during the occurrence of a fault. In our this work a bank of four observers is used for fault detection including Kalman filter, Sliding Mode observer, Luenberger observer and High gain observer. During no-fault condition (healthy mode), a Linear Quadratic Gaussian controller is used. However, when a fault occurs, the system automatically switches to a suitable controller depending on the fault nature and location. Generally, the controller known to have excellent properties of robustness against the parametric variations is used. due to it simple design. The system can be operated at low performance to keep the constant power deliverance.

The thesis is divided in four main parts. First The general presentation of Wind conversion energy, In the second part Modeling and classical Control than we developed a new advanced control in third section, this parts are necessary groundwork is laid out concerning the dynamic wind turbine models ,This part form a basis for the last part Fault Diagnosis and Fault-Tolerant Control, where the fault diagnosis and fault-tolerant control schemes are described and applied to several fault scenario.

Keywords: *Fault diagnosis, Fault-tolerant control, Linear Quadratic Gaussian controller, Wind conversion energy, Wind turbines.*

Dedication

This work is dedicated:

To my beloved Mother, my Great Father, my Wife and all my family. I am truly grateful for having you in my life and for your support, encouragement and constant love that have sustained me throughout life.

To my brothers and sisters;

to all my relatives and friends

and finally to you, dearest reader.

Acknowledgements

I would like to thank my supervisors Professor Mohamed Tadjine and Professor Allaoui Tayeb for giving me many opportunities and guiding me all time through the PhD. I would also like to thank my parents for their support and encouragement.

CONTENTS

FIGURES

LIST OF ABBREVIATIONS

FTC	Fault Tolerant Control
FOC	Field Oriented Control
SM	Sliding Mode
DTC	Direct Torque Control
DPC	Direct Power Control
LQR	Linear Quadratic Control
LQG	Linear Quadratic Gaussian
DFIG	Doubly fed induction machine
DC / AC	Direct current alternating current
PWM	Pulse Width Modulation
PI	Proportional Integrator
IP	Integrator Proportional.

LIST OF SYMBOLS

Ω	Mechanical speed
Ω_{ref}	Mechanical speed reference
G	Slip
C_r	Load Torque
C_{em}, T_e	Electromagnetic torque
ω_s	Stator Pulsation
ω_r	Rotor Pulsation
θ	Angular phase between stator and rotor
θ_s	Stator angle
θ_r	Rotor angle
v_{sabc}, v_{rabc}	Stator and rotor voltages
i_{sabc}, i_{rabc}	Stator and rotor currents
Φ_{sabc}, Φ_{rabc}	Stator and rotor Fluxes
R_s, R_r	Stator and rotor Resistances
R_f	Fault resistance
T_c	Load torque.
T_s , T_r	Rotor and rotor Time gain
l_s, l_r	Self-Inductances of the rotor and stator
m_s, m_r	Inductance mutuelle statorique et rotorique
L_s , L_r	Mutual Inductances of the rotor and stator
M_{sr}	Cyclic Inductance stator and rotor
L_{so}, L_{ro}	Homopolar stator and rotor inductance
M_{sr}	Maximum value of stator rotor mutual inductance coefficients
Cc	Short-circuit
v_{sd} , v_{sq}	Stator and rotor voltages in the Park reference frame
i_{sd} , i_{rq}	Stator and rotor currents in the Park reference frame
v_{s0}, v_{r0}	Homopolar component of the stator and rotor voltage in the Park reference frame
i_{s0}, i_{r0}	Homopolar component of the stator and rotor current in the Park reference frame
σ	Coefficient of dispersion
V_p	Voltage Amplitude
Φ_{sd_mes} Φ_{sq_mes}	Estimated stator Fluxes

v_{rd}^{r} , v_{rq}^{r}	Regulated voltage
K_f	Coefficient of friction
ω_n	Electric pulstation
K_{pi} ,, K_{qi} ,, $K_{p\Omega}$	Proportional Regulator gains
K_{ii}, $K_{i\Omega}$	Integrator regulator gains

GENERAL INTRODUCTION

General Introduction

In the present , various forms of renewable energy sources have gained prominence, with wind energy emerging as the most widely adopted, thanks to its rapid growth, averaging a remarkable 30% annual increase. To sustain this ongoing wind energy expansion, optimizing its operations becomes imperative. Equally crucial is the delivery of high-quality energy harnessed from the wind, underscoring the need to understand wind speed fluctuations and wind turbine parameters.[1]

Meeting these challenges has led to the utilization of the Doubly Fed Induction Generator (DFIG) in various wind turbine configurations due to its control adaptability, superior energy efficiency, and ability to function effectively across varying wind speeds. Typically, DFIGs are controlled through the rotor, reducing power stress on the converters [3] [2].

In contemporary industrial facilities, sophisticated and dependable control systems are essential due to heightened demands for operational reliability, safety, and system availability. Applying conventional feedback control methods to intricate systems may result in subpar performance or even instability in the presence of sensor, actuator, or plant faults. Fault-tolerant controllers have been developed to maintain acceptable system performance and stability under faulty conditions. The primary objective of fault-tolerant control is to employ fault detection mechanisms, using measured process data to detect, isolate, and reconfigure the controller to compensate for faults.

Initially, fault-tolerant control found application in safety-critical systems such as aircraft, nuclear power plants, and chemical/petrochemical processes [3] [4]. However, recent advancements in microelectronics, coupled with the growing demand for high-performance and reliable operation, have expanded its scope to encompass new areas. Power systems, automotive systems, motor and drive systems, air conditioning systems, and heat exchange systems are among the emerging fields where fault-tolerant control principles can be effectively employed [5].

The thesis is structured into four chapters, each briefly summarized as follows:

- Chapter 1 provides an overview of terminology and methodologies within the field of wind turbines and their applications.
- Section 2 and Section 3 delve into the mathematical model of wind turbines, with a focus on addressing short-circuit faults, and explore classical control methods utilizing Field Oriented Control (FOC) based on Proportional-Integral (PI) and Sliding Mode

(SM) regulators. Additionally, advanced control strategies such as Direct Power Control (DPC) and Linear Quadratic Gaussian (LQG) are introduced in Section 3.

- Section 4 offers a comprehensive examination of fault-tolerant control (FTC) systems, encompassing definitions and various aspects. Existing approaches to Fault Detection and Identification (FDD) systems for fault diagnosis and fault-tolerant control of wind turbines are also explored.
- The concluding section presents simulations of the overall system behavior, featuring a turbine emulator controlled with Maximum Power Point Tracking (MPPT) strategy, including actuator faults. The thesis culminates with discussions on conclusions drawn and potential avenues for future research.

CHAPTER 01

WIND ENERGY CONVERSION SYSTEMS

1.1 INTRODUCTION

Wind energy, a plentiful and exploitable resource found on the Earth's surface, stands out as one of the most rapidly expanding forms of energy technology. Over the past several years, it has experienced an impressive global growth rate, averaging more than 30% annually. By the end of 2006, the total installed wind energy capacity worldwide had reached 74 GW [6]. The ever-increasing demand for energy, coupled with the advantages presented by wind turbines, has spurred a vigorous drive to optimize their performance. From a control perspective, the challenge extends beyond ensuring smooth operation; it encompasses the efficient reduction of loads and seamless integration into the power grid. Additionally, a significant hurdle lies in delivering high-quality energy from an intermittent and irregular primary energy source, which is the wind itself. To effectively harness wind energy, it is essential to comprehend the characteristics of wind energy systems.

One critical aspect to consider is that the energy available in the wind is directly proportional to the cube of the wind speed. This means that small changes in wind speed can lead to significant variations in available energy. Furthermore, wind patterns exhibit high variability, both spatially and temporally [7].

Renewable energy, often referred to as clean energy, comes from natural sources or processes that are constantly replenished. For example, sunlight or wind keep shining and blowing, even if their availability depends on the time and weather conditions.

While renewable energy is often thought of as a new technology, harnessing nature’s power has long been used for heating, transportation, lighting, and more. Wind has powered boats to sail the seas and windmills to grind grain. The sun has provided warmth during the day and helped kindle fires to last throughout the evening. But over the past 500 years or so, humans have turned to non-renewable, harmful to the environment energy sources such as coal and fracked gas.

1.2 History of Wind Energy

It is worthwhile to consider some of the history of wind energy which serves to illustrate the issues that wind energy systems still face today and provides insight into why turbines look the way they do. In the following summary, emphasis is given to those concepts which are particularly relevant nowadays.

The reader interested in a more detailed description of the history of wind energy is referred to Park (1981), Eldridge (1980), Inglis (1978), Freris (1990), Shepherd (1990), Dodge (2009), and

Ackermann and Soder (2002). Golding (1977) presents a history of wind turbine design from the ancient Persians to the mid-1950s. In addition to a summary of the historic uses of wind power, Johnson (1985) presents a history of wind electricity generation, and the US research work of the 1970–85 period on horizontal axis, vertical axis, and innovative types of wind turbines. The most recent comprehensive historical reviews of wind energy systems and wind turbines are contained in the books of Spera (1994), Gipe (1995), Harrison et al. (2000), and Gasch and Twele (2002). Eggleston and Stoddard (1987) give a historical perspective of some of the key components of modern wind turbines. Berger (1997) provides a fascinating picture of the early days of wind energy's re-emergence, particularly of the California wind farms.

1.3 Modern Wind Turbines

A wind turbine converts the kinetic energy in the wind into electricity. This is in contrast to a 'windmill', which is a machine which converts the wind's power into mechanical power as for electricity generators, wind turbines are connected to some electrical network. These networks include battery-charging circuits, residential scale power systems, isolated or island networks, and large utility grids. The most frequently found wind turbines are actually quite small – on the order of 10 kW or less. In terms of total generating capacity, the turbines that make up the majority of the capacity are, in general, rather large – in the range of 1.5 to 5 MW.

A typical modern wind turbine, in a wind farm configuration, connected to a utility network, is illustrated in Figure 20. The turbine shown is a General Electric 1.5 MW.

1.4 Wind Energy conversion systems

Over many years, different types of wind turbines have been developed. Wind turbine can be classified into Horizontal Axis Wind Turbine (HAWT) and Vertical Axis Wind Turbines (VAWT) based on the orientation of their spin axis. The wind turbine can also be classified into the fixed speed wind turbine and variable speed wind turbine based on the rotor speed control strategy. The configuration of the Wind Energy Conversion System (WECS), can be classified into the fixed speed WECS without power converter interface, the variable speed WECS using the reduced capacity converters and the variable speed full capacity converter operated WECS. In the VAWT, the orientation of the turbine's spinning axis is perpendicular to the ground. The generator and gearbox are normally placed at the base of the turbine on the ground. In the HAWT, the orientation of the spinning axis is parallel to the ground. The rotor blades and nacelle are elevated to a height with the tower to reach better wind conditions. The nacelle

houses the gearbox, the generator, and, in some designs, the power converters. Compared to the VAWT, the HAWT features higher wind energy conversion efficiency due to the blade design and access to the stronger wind, but needs a stronger tower to support the heavy weight of the nacelle thus its installation cost is higher. On the contrary, the VAWT has the advantage of lower installation costs and easier maintenance due to the ground level gearbox and generator installation, but its wind energy conversion efficiency is lower due to the weaker wind on the lower position of the blades and limited aerodynamic performance of the blades. In addition, the rotor shaft of VAWT is longer, making it prone to mechanical vibrations. These disadvantages hinder the practical application of VAWT for large scale wind energy conversion. HAWT dominate today's wind market, especially in large commercial wind farms.".

The four main types of wind turbines based on their rotor speed control strategies and WECS configurations in today's global market are described in the following sections. All of them are HAWT. The fixed speed wind turbine has the advantages of low manufacturing and maintenance costs as well as reliable operation, but they have the disadvantage of lower energy conversion efficiency. On the contrary, the variable speed wind turbine increases the energy conversion efficiency and reduces the mechanical stress caused by the wind gusts. It also reduces the wear and tear on the gearbox and bearings, expanding the lifetime and reducing the maintenance requirements. The main drawback of the variable speed wind turbine is the need for a power converter interface to control the generator speed, which adds cost and complexity to the system.[11],[12]

1.5 Horizontal and vertical axis wind turbines

From the physical setup viewpoint, there are horizontal axis wind turbines (HAWT) and vertical axis wind turbines (VAWT). In HAWT, the blade rotates about an axis parallel to the ground and wind flow. Common examples are the old-style Dutch windmill and modern wind turbine. For the VAWT, the blades rotate about an axis perpendicular to the ground. The most common design are the Darrieus (curved blades), Giromill (straight blades) and Savonius (scoop blades), as shown in Figure 21.

Most of the large turbines employed in modern wind farms are HAWT. One reason is that they are more suitable for harnessing the higher and smoother wind speed at higher altitude. In terms of blade loading and fatigue, HAWT are subject to reversing gravitational loads (structural load is reversed when the blade goes from upwards to downwards position) which imposes a limit on the size of such turbine. In terms of material, VAWT have

greater solidity (fraction of swept area that is solid) and hence are heavier. Presently, HAWT are the most commercially viable.[13] [9]

1.6 Drag and lift powered motion

The rotation of both HAWT and VAWT can be powered predominantly by lift or drag force depending on the design of the blade. In drag design, the wind pushes the blade out of the way. The rotational speed is typically slower. Due to their high torque capabilities, drag powered turbines are suitable for pumping, sawing or grinding. The typical example of such design is the old-style Dutch windmill. In lift design, the blade cross section has an airfoil shape so that when the wind passes by the blade, the pressure on the lower surface is higher and hence lifts the blade. The same principle allows airplanes and birds to fly. Lift powered turbines have much higher rotational speed than drag-powered turbine and are well suited for electricity generation. In general, lift machines are more efficient than their drag counterpart.

1.7 Number of blades

In order to extract a maximum amount of wind power, each blade should interact as much as possible with the wind passing through the swept area. Hence the lesser the blades the higher the rotational speed of the turbine, as the blades have to move faster to 'fill up' the swept area. In theory, the more blades a turbine has, the more efficient it should be. However, for larger number of blades there is more interference and a blade is more likely to pass in the disturbed weaker flow of the previous blade. In practice, low-solidity turbines tend to have a higher efficiency.

From a structural stability viewpoint, the number of blades of lift powered HAWT should be odd and greater or equal to 3, in which case the dynamic properties of the turbine rotor are similar to those of a disc. For an even number of blades, the structure is subject to more important bending forces because when a blade is in the uppermost position receiving most wind power, another blade is in the lowermost position in the shadow of the tower. Most commercialized modern wind turbines have three blades. Sometimes two-bladed or even single-bladed design are used to reduce the cost. However, these turbines require more complex structural design to avoid heavy shocks (two-bladed turbines require a teetering hub, one-bladed turbines require a counterweight on the hub) and are visually more intrusive due to their higher rotational speed.

1.8 Betz limit

An important operational characteristic of wind turbines is the Betz limit. It indicates the theoretical maximum amount of wind energy that can be extracted by a turbine. If turbines were 100% efficient all the airflow energy would be extracted and the flow speed after passing through the turbine would be zero, which is impossible. In 1928, Betz showed that under ideal assumptions (uniform rotor disk with infinite number of blades) the maximum efficiency of a turbine is 16/27 (59.3%). In practice, this coefficient is less due to non-idealities (wake rotation behind the rotor, finite number of blades, blade tip losses, frictional drag, etc.). Present turbines have efficiency around 30-40% .

1.9 Wind Turbine Components

The main components of a wind turbine generator are shown in Figure 2 (drawing not in scale). The turbine consists of the blades, the hub and the connecting components (bearings, pitching actuators). It transforms wind kinetic energy into mechanical energy. For multi-megawatt turbines, dimensions are larger with blade length ranging from 35-60 meters.

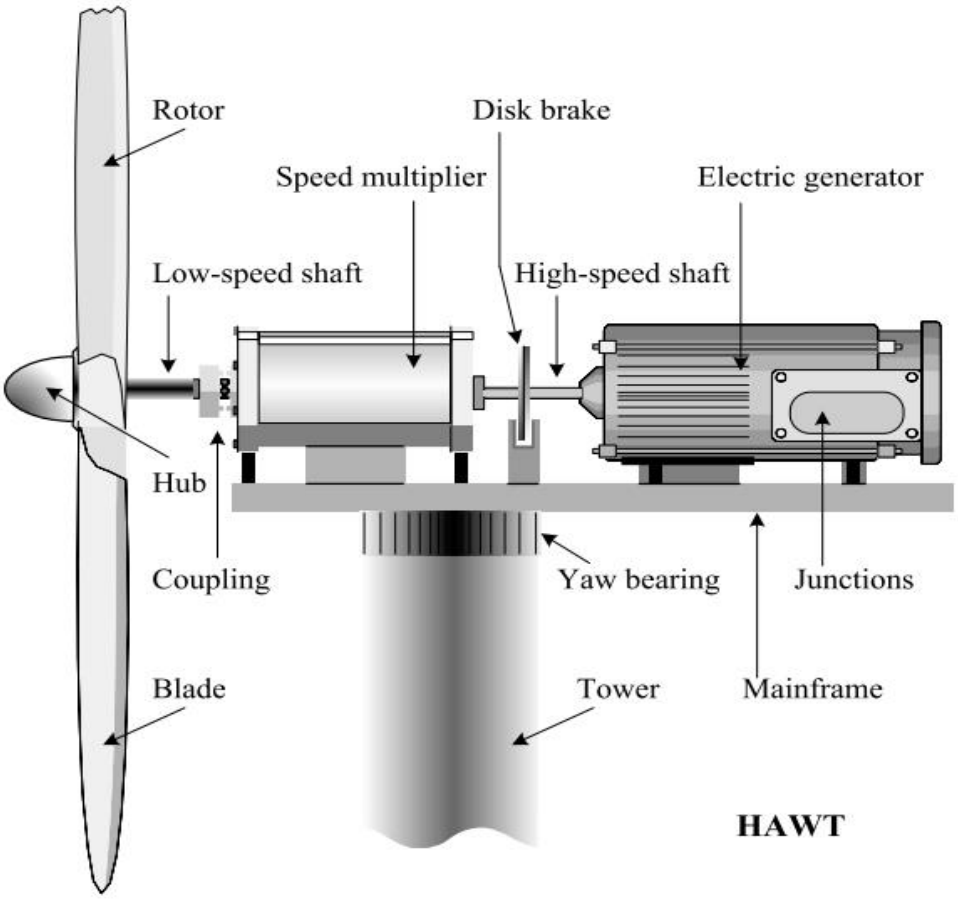

Figure 1. Main components of a wind turbine generator

The drive train is formed by the turbine rotating mass, low-speed shaft, gearbox, highspeed shaft and generator rotating mass. It transfers input power (turbine mechanical power) to the point where useful power (generator mechanical power) is used. In most cases, a gearbox is required because the rotating speed of the turbine is much lower than that of the generator. For multi-MW units the gearbox ratio is about 50-100 as the typical speed range of the turbine is 10-20 rpm while for the generator it is about 1000-2000 rpm. For smaller wind turbines, the speed is higher, hence the gearbox ratio may be less than 50. The low speed shaft contains pipes for the hydraulics system that operates the aerodynamic brake. The high-speed shaft is equipped with an emergency mechanical brake that is used in case of failure of the aerodynamic brake.

The *generator* converts mechanical power into electrical power. For variable speed generators, an ac-dc-ac converter is required. Usually the generator produces power at 690 V and a transformer steps up this voltage to 33 kV for underground cable transmission. The transformer may be placed at the bottom of the tower or in the nacelle to avoid losses. The power is then transmitted to the wind farm substation where a further voltage step-up may be done to 110»765 kV for long distance transmission.

Other components include the anemometer and vane which monitor the wind speed and direction respectively. Wind speed measurement is used to start and stop the turbine. Wind direction measurement is used by the yaw-control mechanism (see next subsection). Devices such as electric fans and oil coolers are used to cool the gearbox and generator.

1.10 Aerodynamic torque control

The mechanical input torque can be controlled in many ways. Figure 3 shows the tower yaw angle γ and blade pitch angle beta, which can be actively controlled for aerodynamic torque regulation.

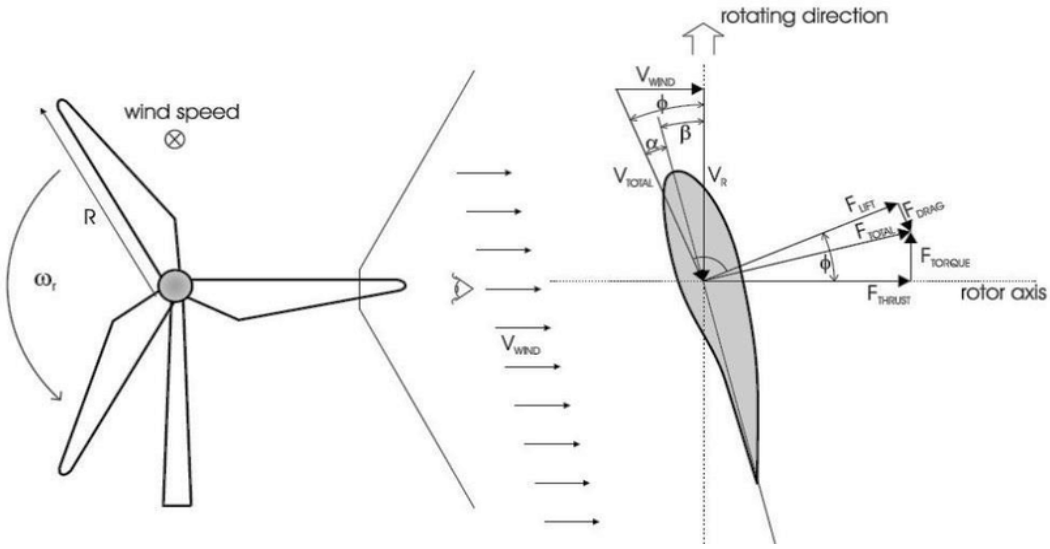

Figure 2 .Definition of aerodynamical angles forces and wind speeds.

The yaw angle is usually controlled to make sure that the turbine is facing the wind (γ = 0–). This is done by rotating the nacelle about the yaw axis (tower axis). In theory, it can also be used to reduce the captured power by turning the turbine out of the wind. However, this is only possible for very small turbines (• 1 kW) because the wind turbine's operation with yaw error increases fatigue loads (cyclical varying stresses, bending torques) which damage the structure.

Reduction of input mechanical power is usually done with the blades. In stall-controlled turbines, the aerofoil shape (blade cross-section) is designed so that above a certain speed the blade goes into stalling mode as shown in Figure 4. When the blade is stalled, the wind flow is partially eliminated on the upper surface, reducing the lift and hence performance. Stall-regulated turbine can be passive- or active-stall controlled. In the former case, the blades are bolted on the hub at a fix angle. In the latter case, a pitching mechanism twists the blade to stall (increases the angle of attack) when required.

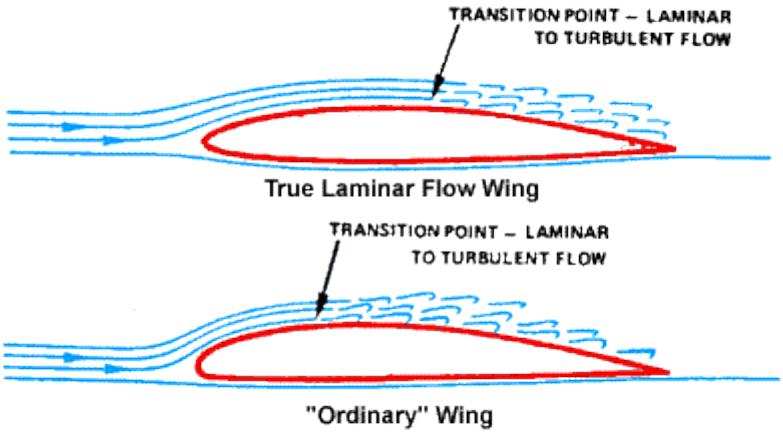

Figure 3. Laminar flow (left) and stalled flow(right)

The counterpart of stall-controlled turbines are pitch-controlled turbines. In these configurations, the windflow is always laminar and the aerodynamic torque is regulated by pitching the blade to feather (by reducing the angle of attack). Pitch regulated turbines can also be active- or passive-pitch controlled. In the former case, a pitching mechanism (usually hydraulics system) is in place. In the latter case, the blades are mounted on the hub so that the thrust force pitches the blade (i.e. the blades are “self-pitched”).

Rotation to feather (smaller angle of attack) gives quieter operation and easier control. Rotation to stall (larger angle of attack) is faster but gives more noise, bending loads, and less exact control due to the unsteady nature of stalled flow. The advantage of stall-regulation is that complex control for blade pitching is not required. The aerodynamic and structural design of the turbine are however more complex. In the early days, most wind turbines where fixed speed stall regulated, nowadays the trend is towards the use of variable-speed pitch regulated turbines because of increased performance (notable but not the main reason) and less mechanical loads (main reason) .

1.11 Generator concept

There are mainly four types of electrical generator used commercially Figure 26. Depending on the generator type, the turbine is referred to as fixed or variable speed.

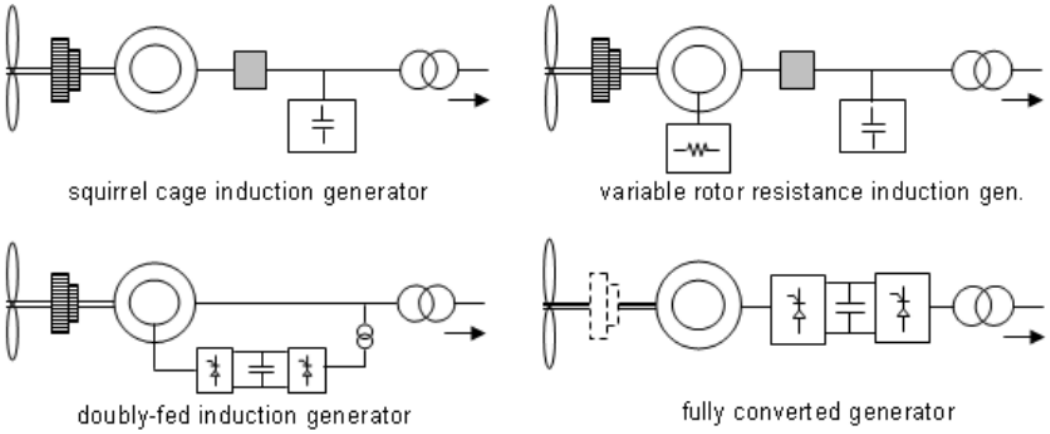

Figure 4. Electrical generator used in commercial wind turbines.

The simplest type is the fixed speed squirrel cage induction generator (SCIG) which makes up the largest share of the smaller wind turbines already installed and scattered on the network. The rotor consists of short-circuited bars (i.e. the rotor voltage is zero). The speed varies within a very narrow range (practically constant) and the mechanical torque is usually controlled by stalling the blades either actively or passively. The advantages of the Squirrel Cage Induction Generator (SCIG) are its simplicity and robustness. For small size turbines in a strong grid, this is arguably the most economical solution as the grid can provide reactive power and maintain a satisfactory voltage profile. Capacitor banks are installed to complement the reactive power consumption. The capacitors must be carefully sized to avoid self-excitation. Soft-starters are used to mitigate the high starting currents.

The second type of generator is a wounded rotor induction generator with variable rotor resistance (best known under the commercial brand name “opti-slip” from Vestas).

It is essentially a fixed-speed machine, where the speed range is increased to typically 2-10% by inserting an adjustable resistor bank in the rotor. The mechanical input is controlled by pitch regulation for optimal wind power capture. The advantage of this generator type is its larger slip range compared to the conventional SCIG and simpler control structure compared to the following two generator types. It has however the same problems as the SCIG. Reactive compensation and soft-starters are required and voltage quality is easily deteriorated in weak networks. Compared to the SCIG it has increased losses due to the larger rotor resistance.

The third type of generator is the Doubly-Fed Induction Generator (DFIG). which is a variable speed asynchronous generator where the rotor consists of conductors with slip-rings fed by an ac-dc-ac converter connected to the grid. The provision of non-zero rotor voltage at slip frequency results in speed variability. Modern transistor based back-to-back converters allow

bi-directional rotor power flows and hence operation at both sub- and super-synchronous speed. Typically, the slip range is §30% (determined by the size of the converters). The advantages of the DFIG are the speed variability which reduces mechanical stress, the possibility to optimize the power capture by regulating the electrical torque and control reactive power independently. Recent studies investigated have demonstrated further potential advantages such as frequency control and power system stabilizer capabilities. Both acquired and potential capabilities of the DFIG are achieved by appropriate control of the rotor voltage.

The last type of generator is the fully-converted SG or fully-converted SCIG. Synchronous generators are suitable for high power applications as they operate at unity power factor. Induction generators need reactive power compensation from the generator side converter or additional capacitor banks, hence are more suitable for small rating applications. For the SG which can be excited externally or with permanent magnet, using a multi-pole design removes the need for a gearbox. As the converter rating is the full rating of the generator, the slip range is not limited to 30%. The main advantage of the fully-converted generator is the complete decoupling of the generator from the grid which can facilitate the control of the system under severe disturbances from the wind or network. The main disadvantage is the higher cost of the large converter [3],[14].

The present trend in the industry is to use variable speed generators. Initially, the main reasons were the reduced mechanical stress (longer life-time), better wind capture, smoother power output (due to both variable speed and controllable electrical torque), and ability to operate at unity power factor. Nowadays, tighter grid connection requirements and advances in semi-conductors make converters economically justifiable. It is not yet clear which of the DFIG or fully converted generator will be the preferred choice in the future. It has been suggested that experienced manufacturers tend to propose the fully-converted design for new wind farm development. In the last decade, a significant share of the wind farms installed were based on the DFIG [15].

1.12 Doubly Fed Induction Generators (DFIG)

In recent years, Doubly Fed Induction Generators (DFIG) have been the most frequently deployed large grid-connected wind turbines and are becoming widely accepted due to their suitability in the context of variable speed wind power generating Aenergy production, improved power quality and the electronics equipment power are only carries a fraction of the total power (20-30%).[16][17]

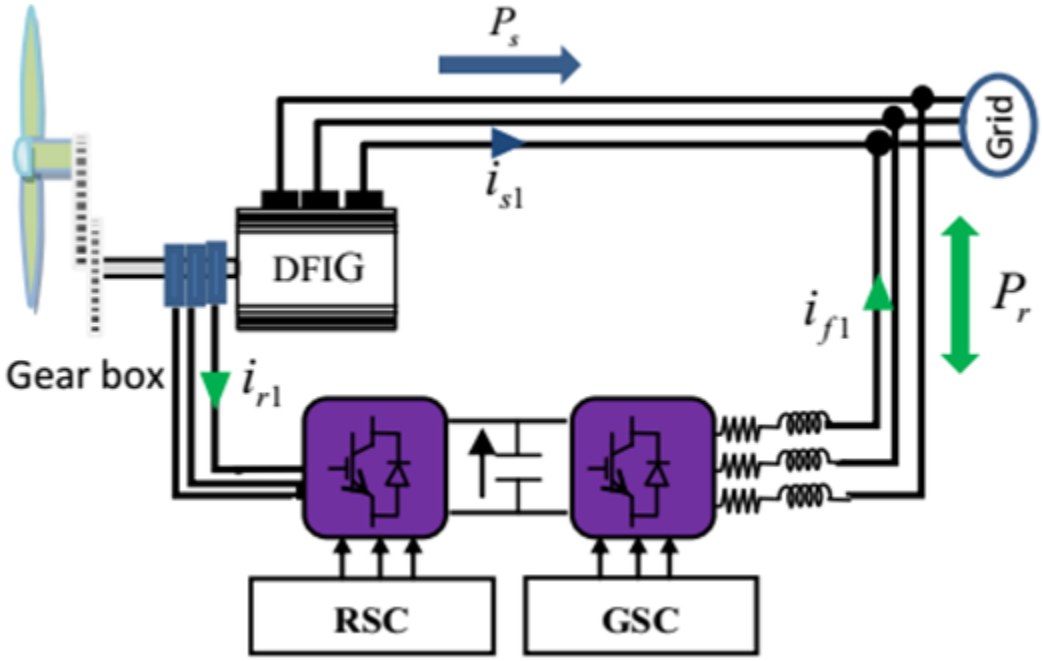

Figure 5. Schematic diagram of the DFIG.

1.12.1 Fixed speed wind turbine without power converter interface

As shown in Figure 6, the fixed speed wind turbine is based on the Squirrel Cage Induction Generator (SCIG) without a power converter interface. At different wind speeds, the generator speed varies in an extremely small range determined by the gear box ratio, the grid frequency and the number of poles of the generator. The maximum conversion efficiency can be achieved only at a given wind speed. A soft starter to limit high inrush currents during system start up is usually used, but the soft starter is bypassed by a switch after the system is started. A three-phase capacitor bank is required to compensate the reactive power drawn by the induction generator.

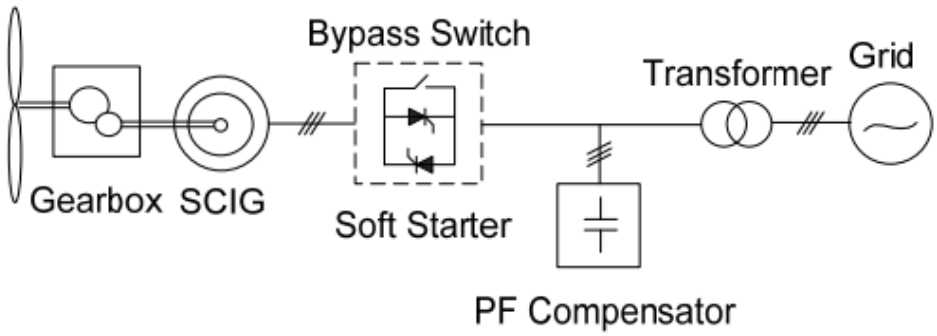

Figure 6 Fixed speed wind turbine without power converter interface.

This wind energy system features simplicity, low manufacturing/maintenance costs, and reliable operation. The main drawbacks include:

- The maximum conversion efficiency can be achieved only at a given wind speed, and the system efficiency degrades at other wind speeds.
- The highly fluctuating output power causes disturbances to the power system.

Despite its disadvantages, this wind energy system is still widely accepted in industry with a rated power up to several megawatts.

1.12.2 Variable rotor resistance based variable speed wind turbine with reduced capacity power converter

The variable speed wind turbine with reduced capacity converter is feasible with Wound Rotor Induction Generators (WRIG). One of the control diagrams for the WRIG wind turbine is shown in Figure 28. The rotor speed of the generator can be adjusted by changing the rotor resistance, which affects the torque/speed characteristic of the generator. Operating at variable speed, the energy conversion efficiency can be increased, with the power loss on the resistance. As the rotor speed is typically limited to about 10% above the synchronous speed of the generator. This configuration also requires a soft starter and reactive power compensation. The rotor resistance is normally made adjustable by a power converter.

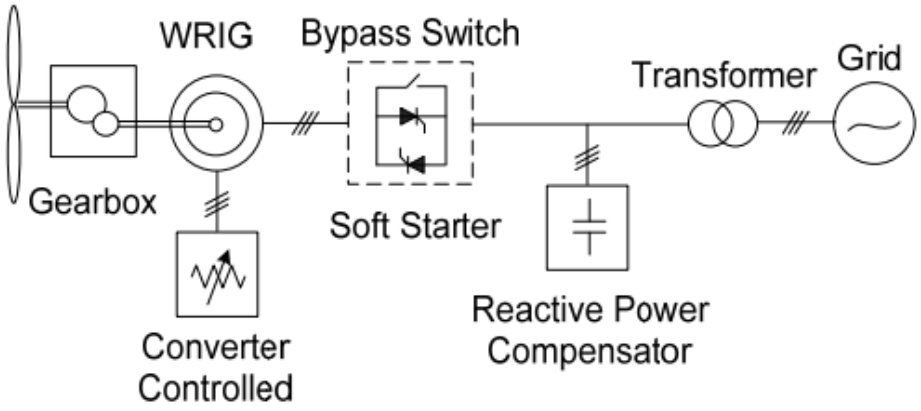

Figure 7 Variable rotor resistance based variable rotor speed wind turbine with reduced capacity power converter.

1.12.3 Doubly Fed Induction Generator (DFIG) based variable speed wind turbine with reduced capacity power converters

Another configuration for the variable speed wind turbine with reduced capacity power converters is the Doubly Fed Induction Generator (DFIG) based wind turbine, as shown in Figure 29. The rotor speed of the wind turbine is controlled by the four-quadrant power converter. The active power and the reactive power can be generated through both the stator side of the generator and rotor side of the generator. There is no need for the soft starter and the reactive power compensation. The power converters just need to process the slip power in the rotor circuit, which is approximate of 30% of the rated power, results in the reduced converter cost in comparison to the wind energy conversion system using full capacity converters.

"The use of the converters also allows bidirectional power flow in the rotor circuit and increases the speed range of the generator. This system features improved overall power conversion efficiency, extended generator speed range (±30%), and enhanced dynamic performance compared to the fixed speed WECS and the variable resistance configuration. These features have made the DFIG wind energy system widely accepted in today's market."

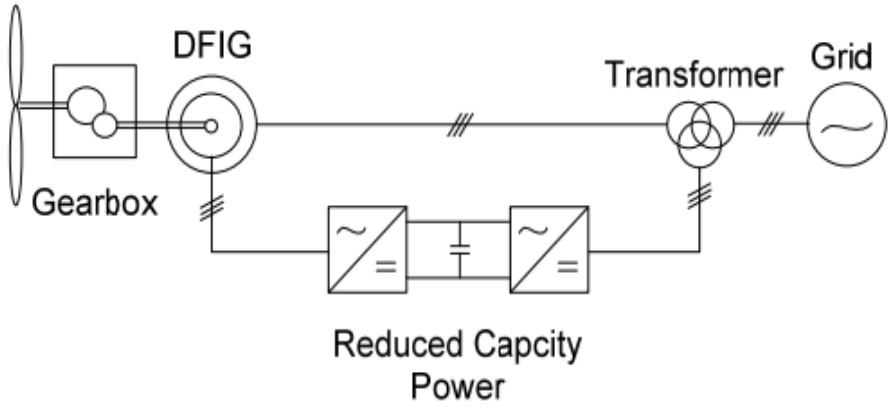

Figure 8. DFIG based variable speed wind turbine with reduced capacity power converters

1.12.4 Variable speed wind turbine with full capacity power converters

The configuration of the variable speed wind turbine with full capacity power converter is shown in Figure 30. Squirrel cage induction generators, wound rotor synchronous generators, and permanent magnet synchronous generators (PMSG)

have all found applications in this type of configuration with a rated power up to several megawatts. “As the wind turbine is connected to the grid via the power converters, the power rating of the converter is normally the same as that of the generator. With the use of the power converter, the generator is fully decoupled from the grid, and can be operated in full speed range. This also enables the system to perform reactive power compensation and smooth the grid connection. The main drawback is a more complex system with increased costs.” [18]

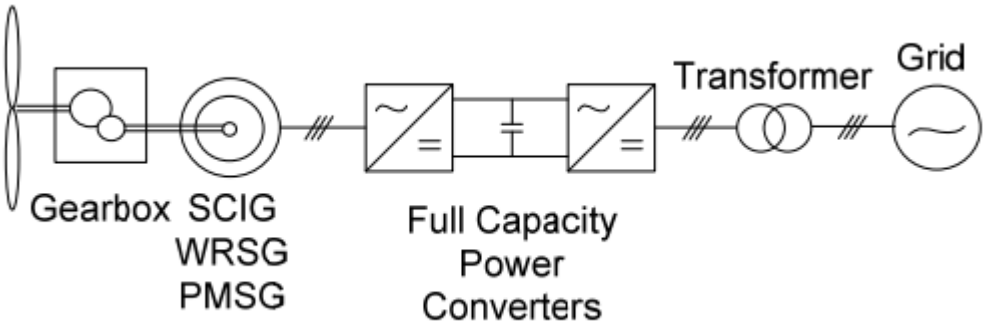

Figure 9 .Variable speed wind turbine with full capacity power converters.

“It is noted that this wind energy system can be operated without the need for a gearbox if a low speed synchronous generator with a large number of poles is used. The elimination of the gearbox improves the efficiency of the system and reduces initial costs and maintenance. However, a low speed generator has a substantially larger diameter to accommodate the large number of poles on the perimeter, which may lead to an increase in generator and installation costs.”

This PhD thesis focuses on the optimal control of the wind turbine to reduce the power loss due to the wake effect in the wind farm and to improve the lifetime of wind turbine. The wind farm equipped with the wildly installed DFIG wind turbines is studied. The optimization in the wind farm equipped with the PMSG wind turbines will be studied in the future work.[19]

1.13 Power System Stability

A power system comprises of generators, transformers, busbars, transmission lines and loads (devices which consume electrical energy). The basic aim of a power system is to deliver the electric power to the customers, fulfilling the power quality demands. It is assured that these demands are met in an economic manner and that the reliability is maintained. Generally, a power system is quite large with thousands of buses and transmission lines. The power system

is subjected to variety of severe disturbances such as faults (may be due to lightning or insulation failures) or sudden changes in the load conditions.

The ability of a power system or a part of a power system to maintain the voltages under normal conditions as well as during a disturbance is called power system stability. [20]

Power system stability can be further classified as angle stability and voltage stability. When the active power demand increases in a power system, then these demands are accommodated or met by the variations in the angular momentum of synchronous generators, feeding the grid. These variations in angular momentum are generally taken into account by the difference of the angle between the synchronous field and the rotor field. An increase in the active power demand increases this angle and this tends to reduce the synchronous machine speed. If the active power demand becomes greater than the machine ratings, then the generator can be pulled out of synchronism. The ability of a power system to maintain synchronism

during normal conditions as well as after a fault or sudden rise in the active power demand is known as angle stability.

From the knowledge of power systems, it is known that the flow of reactive power between two buses depends on the difference in magnitude of voltages at the buses. When the reactive power demand in a power system increases beyond the capability of generation sources (synchronous machines, capacitor banks), then it becomes difficult to keep the voltage profile within acceptable limits and the power system can become unstable. If after occurrence of a fault, the voltage magnitudes remain equal or close to their original values before the fault, then the power system is called voltage stable. [20]

Voltage stability can be defined as ‘‘ability of a power system to maintain steady acceptable voltages at all buses in the system at normal operating conditions and after being subjected to a disturbance’’.

Overloading, generators reactive power limits, capacity of reactive power compensation devices (capacitor banks, SVC etc), action of control devices and faults

are some factors, which contribute towards the voltage instability in a power system.

It is not only the severity of disturbance, which matters while discussing the voltage

or angle stability, but the duration of disturbance is also important. The time scale of stability criteria is divided into short-term and long-term time scale.

Angle stability is mainly associated with the synchronous generators and change in the angle between synchronous field and rotor field (due to any disturbance) can be

either in the form of undamped oscillations or may be in the form of gradual acceleration leading towards the loss of synchronism.

The undamped oscillations are often present due to small disturbances and stay for very short duration. This type of stability is referred as steady state or small signal stability, whereas the latter type of stability occurs mostly due to large disturbances and is referred as transient stability. Both small signal and transient stability fall into short-term time scale and last only a few seconds.

Long-term angle stability is also called frequency stability and it follows short-term dynamics after a large disturbance. Frequency stability is mainly about active power balance between the generators and the loads and relative transients last typically for several minutes.

Voltage stability is mainly considered as a load-driven phenomenon since it is the load dynamics, which decide the duration of voltage stability. Short-term voltage stability is mainly concerned with the loads, which are able to restore their consumed power within time frame, ranging in seconds e.g. induction motors, SVC etc.

The need for the analysis of long-term voltage stability arises mainly due to following factors:

• Load recovery due to action of OLTC
• Delayed shunt compensation switching (capacitor banks)
• Load shedding
• Outage of any major generator

Even though the duration of long-term voltage stability and angle stability is more or less same, the important aspect for voltage stability analysis is the need of detailed network representation.

Another important term which often appears when considering system stability is the voltage collapse. This occurs after voltage instability when system operator actions and automatic system controls fail to prevent the considerable decrease in the voltage profile of the system. A network can be considered more vulnerable or prone to voltage collapse, based on following indications:

• Low voltage profiles
• Heavy reactive power flows
• Inadequate reactive power support
• Heavily loaded systems

Voltage collapse may even lead to blackout, which leaves several customers without electric power supply and it may take quite a while before the system can be restored. Even though the magnitude of voltages in a network is generally attributed towards flow of reactive power, it is not the only factor affecting voltage stability but the active power affects this phenomenon equally. [20]

1.14 Factors Affecting the Capacity of Wind Generation

Wind generation is only possible in areas which are rich in wind resources. These areas can be situated either offshore or onshore. Such locations are often remote and open spaces, away from the load centres. The electric network in these areas is designed to supply the loads and may or may not accommodate generation. This results in the network becoming weak sometimes and imposes some restrictions on the capacity of generation that can be integrated through wind energy converters. These constraints are given as follows:

- Steady state voltage variations
- Reactive power and power factor
- Flicker
- Thermal capacity of lines and other components

1.15 Steady State Voltage Variation

Wind turbines are sources of fluctuating power and it is essential to ensure that the grid is capable of staying within the operational limits of frequency and voltage for all conditions of power production and load power consumption.

How does this fluctuating production of power affect the voltage in the network? This can be understood from an example given as follows:

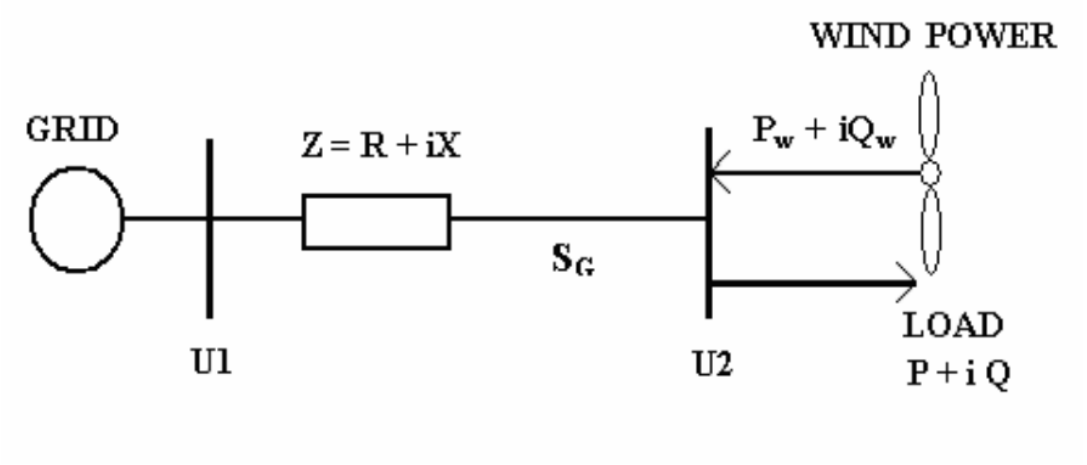

Figure 10. Simple arrangement with a wind turbine on grid describing the effect of fluctuating power on voltage.

Figure 31 shows a simple arrangement with a wind turbine connected to a bus, which is connected to the grid through an impedance Z . The load which is attached to bus 2 is $P+Q.i$ and the wind turbine is injecting both active and reactive powers, $P_w+Q_w.i$ to bus 2.

The voltage at bus 1 is denoted by U_1 and the voltage at bus 2 is denoted by U_2. Bus 1 is an infinite bus and thus voltage U_1 is constant.

Applying KVL to the circuit shown in Figure 11, gives:

$$U_1 = U_2 + \sqrt{3} I . Z \quad \text{(I,1)}$$

When the power production from a wind turbine is enough to meet the load demand, there will be no current drawn from the grid i.e. I = 0. Setting the current I to zero in Equation (1.1), gives:

$$U_1 = U_2 \quad \text{(I,2)}$$

When the power production from the wind turbine is more than the load demand or when the load decreases due to any reason then the voltage at bus 2 will be greater than the voltage at bus1.

$$U_1 \prec U_2 \quad \text{(I,3)}$$

When the power production from the wind turbine is low, then the difference between the power generated by the wind turbine and the load will be supplied by the grid. The current drawn from the grid, will pass through the impedance Z and the resulting voltage at bus 2 i.e. U_2 will be less than the voltage U_1.

$$U_1 \succ U_2 \quad \text{(I,4)}$$

In the literature regarding integration of wind turbines in the power system, the existing grid is often classified as weak or strong. Before looking at the effect of this ‘weakness’ or ‘strongness’ of the grid on the installation of wind power, let’s try to find the criteria, which makes a certain point of grid, fall into the specific categories of strong or weak.

There is not a clear and accurate method for distinguishing between a strong and a weak grid, these terms are relative, and that relativity has to do with the point of the grid that we are analyzing and the purpose of the grid assessment in that point. Generally, strength of the grid at a certain point is assessed by the available short circuit power or fault level or by the short circuit ratio to be more precise. In the case of wind power integration, short circuit ratio is calculated by dividing the available fault level at the point where the wind turbine is connected by the power rating of the wind turbine. The point of connection of wind turbine with existing system is called ‘Point of Common Coupling’ (PCC). Generally, if the value of the short circuit ratio is equal to or above 20, then the grid is considered as strong whereas the value of short circuit ratio below 20 represents a weak grid (the value of this parameter is subjected to change depending upon the different standards in different systems).

To see how the strength of grid at 'PCC' affects the wind power installed capacity, let's consider Figure 31 again. Suppose that S_G is the power or fault level available at bus 2. This power can be calculated as:

$$S = \frac{U_1^2}{Z} \tag{I,5}$$

As described earlier, the short circuit ratio is directly proportional to the fault level and relation given in (1.4) shows that the fault level is inversely proportional to the impedance between the source and the load. If the impedance is larger, than the fault level will be less, so will be the short circuit ratio and the grid will be considered weaker. This will restrict the possible installation of wind turbines because wind turbines are source of fluctuating of power and a sudden change in the power output from the wind turbine will cause the flow of current through impedance Z. Voltage fluctuations will take place and these will be more severe in the case of larger size wind turbine. The appropriate size of the wind turbine will be such that the value of the short circuit ratio is around 20.

1.16 Reactive Power and Power Factor

In a power system, the load is mostly inductive and it leads to the consumption of reactive power. These loads are connected to the generation sources by the transmission and distribution lines and the transformers. These components possess considerable inductive reactance and some resistance. It is often undesirable to transport all reactive power demand through these components mainly due to two reasons:

- Due to increased power losses
- Due to high voltage regulation

The most common way to meet with this reactive power demand is to use the shunt capacitors. These capacitors are connected (in the form of capacitor banks) at the buses where the load is connected, and their values is chosen so that they can provide the most of the reactive power demand by the load and keep the power factor close to unity. The power factor is defined as the ratio between active power and apparent power.

$$p.f = \frac{P}{S} \tag{I,6}$$

It is a unitless quantity and it describes how much apparent power is converted into active power. The values range between 0 and 1. The effect of load power factor and the presence of

inductive reactance in the lines and transformer is different for different types of wind power generators.

It is known that a directly connected induction generator draws reactive power from the grid and the consumption of reactive power increases with the active power production. The voltage at the bus is inversely proportional to the reactive power demand. To keep the voltage within the specified limits and to minimize the power losses, capacitors are generally installed at the terminals of induction generator. The value of these capacitors is selected such that it can provide the no-load reactive power to the induction generator. The installation of capacitors reduces the impact of X/R ratio of the line on the voltage. It should be noted that if the wind turbines are connected to the grid by the cables then these cables must be considered as producers of reactive power (due to presence of stray capacitance). Synchronous generators are mostly connected to the network by means of a frequency converter. The converter enables the synchronous generator to operate with a power factor which is either lagging, leading or one and these generators can keep the voltage within limits either by supplying reactive power (in the case of change in the load power factor) or by absorbing reactive power (in the case of lightly loaded line) at the expense of power losses. This type of generator is better as compared to the induction generator with switched capacitor banks in the sense that the control of reactive power is smooth

1.17 Flicker

The role of a power system is to supply power according to the customer demand when it is needed but also in a form (i.e. waveform and frequency), which is either equal or close to the specified standard. This requirement is often referred as 'Power Quality'. Flicker can be described as a power quality concern regarding the unsteadiness in the RMS value of the voltage. It can be defined as a physiological perception of modulation in the intensity of light. A dimensionless parameter called 'short time severity index, P_{st}' is normally used to assess the annoyance to voltage fluctuation. Its value is found to be most sensitive around 9 Hz (i.e. 8.8 Hz, being precise) where a voltage fluctuation of 0.25% will give a P_{st} value of 1. The problem of flicker is associated with both fixed and variable speed turbines and increases with the increase in wind speed. However, for fixed speed turbines, the flicker increases at increasing wind speeds whereas for variable speed turbines, the flicker level decreases at rated wind speed.

1.18 Thermal Capacity of Lines and Other Components

The thermal capacity of lines and transformers is a limiting factor for all power generation installations. Normally the generating voltages of wind turbines are below 1000V and in European countries the typical voltage level is 690 V. The voltage is stepped up to distribution level voltage by a transformer and the power rating of this transformer along with the rating of line decides the rating of wind turbines. This factor varies from one location to another since the power flow varies according to local conditions.[20]

CHAPTER 02

MATHEMATICAL MODEL OF WIND TURBINE

2.1 Introduction

This section presents a control for a DFIG in the healthy mode and faulty mode. The developed model allows the simulation of the inter-turn short circuit in the stator. First for the control of the DFIG we used the Field-Oriented Control (FOC) based on PI controllers and Sliding Mode controllers. This classical control considerably improved the performance and efficiency of our system. However, the control method was still sensitive to variations in the machine parameters and perturbations.

Three other methods of control have been developed to automatically switch to these controls when the fault occurs on the system. The first method is Direct Active and Reactive Power Control, the second method is based on Linear Quadratic Control (LQG) controllers and the third approach uses Sliding Mode Control.

2.2 Mathematical model of wind turbine

For the modeling of a wind turbine, it is important to understand airflow dynamics around the structure of the turbine because the resulting unsteady forces determine the turbine performance and improve the energy delevered,. Inaccurate predictions may lead to non-optimal design, larger capital investments and larger operation/maintenance costs.

From the mechanical viewpoint, the turbine while converting power is subjected to various kinds of stresses due to the surrounding air movement. Hence the detailed airflow dynamics are of interest to the turbine designer because they are key indicators of the soundness and fatigue of the structure.

From the electrical viewpoint, the turbine applies an input torque on the drive train and therefore any unbalance with respect to the load torque applied by the generator translates into acceleration or deceleration of the shaft and associated variation of electrical variables.

Hence for the electrical engineer, the interest is mainly in the dynamics of the input torque, while the complex airflow dynamics and associated mechanical vibrations and deformations may be ignored.[15] [21]

2.2.1 Wind turbine model

The mechanical power captured by the wind turbine is given as:

$$P_w = 0.5 C_p(\lambda, \beta) \rho \pi \mathrm{R}^2 V_w^2 \qquad \text{(II.1)}$$

Where V_w is the wind speed (m/s),R is the radius of the turbine disk, ρ is the air density,

$C_p(\lambda,\beta)$ is the power coefficient, λ is the tip speed ratio and β is the pitch angle.

$$\lambda = \frac{R.\Omega_t}{V_w} \tag{II.2}$$

The power coefficient C_p is expressed as a function of λ_i and β

$$C_p = 0.5776\left(\frac{116}{\lambda_i} - 0.4\beta - 5\right)\exp\left(-\frac{21}{\lambda_i}\right) + 0.0068\lambda \tag{II.3}$$

λ_i is given by

$$\frac{1}{\lambda_i} = \frac{1}{\lambda + 0.08\beta} - \frac{0.034}{\beta^3 + 1} \tag{II.4}$$

For the optimal extracted power $C_p = 0.48$, $\beta = 0$ and $\lambda = 8.1$.

The mechanical equation of the wind turbine and generator is written as:

$$J\frac{d\Omega_m}{dt} = T_m - T_{em} - f\,\Omega_m \tag{II.5}$$

Where J and f are the system moment of inertia and friction coefficient respectively.

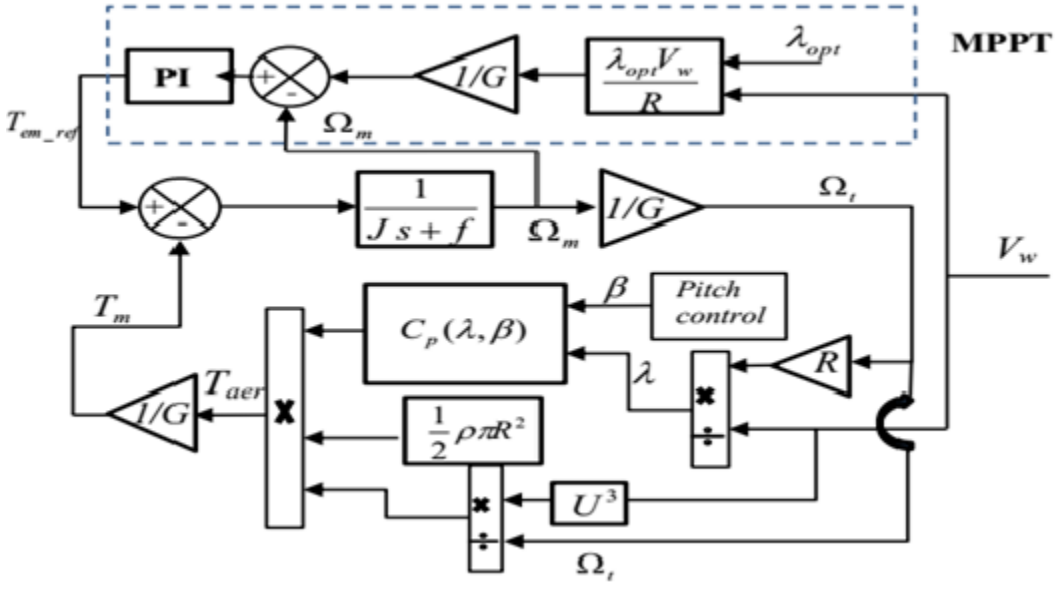

Figure 11. Wind turbine model with MPPT algorithm

2.2.2 Modeling of the DFIG

The following simplifying assumptions are made:

- The gap is of uniform thickness and the notching effect is neglected.
- The saturation of the magnetic circuit, hysteresis and eddy currents are negligible.
- The resistances of the windings do not vary with the temperature and the effect of water is neglected.
- The effect of inclination and the effect of the notches are neglected.
- It is further admitted that the magnetomotive force created by each of the phases of the two armatures is sinusoidally distributed. This hypothesis combined with that of the constancy of the permeability of the air gap leads to very simple expressions of the inductances of the machine [22], [23].

Figure 32 represents a simplified diagram of the location of the stator and rotor windings of a three-phase asynchronous motor with wound rotor, shifted relative to each other by an angle θ_r .

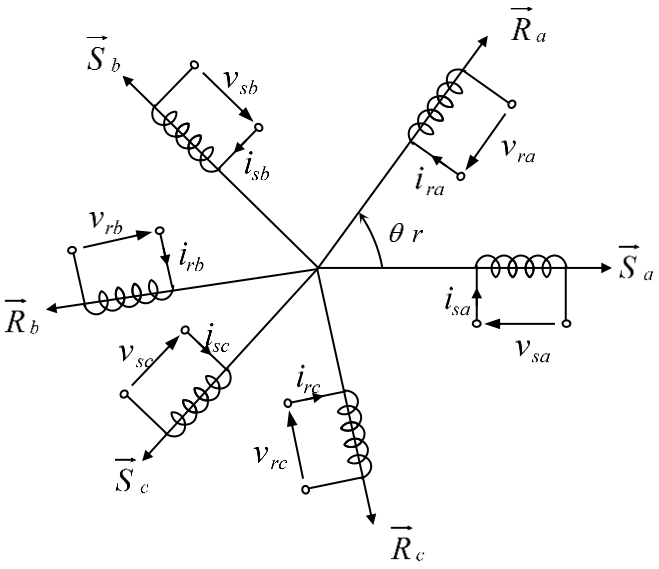

Figure 12. Représentation des phases statoriques et rotoriques

2.2.3 Machine equations system

For the stator phases, the voltage equations can be written in the following form:

$$v_{sa} = R_s\, i_{sa} + d\Phi_{sa}/dt$$
$$v_{sb} = R_s\, i_{sb} + d\Phi_{sb}/dt \qquad \text{(II.6)}$$
$$v_{sc} = R_s\, i_{sc} + d\Phi_{sc}/dt$$

For rotor phases, the voltage equations are:

$$v_{ra} = R_r\, i_{ra} + d\Phi_{ra}/dt$$

$$v_{rb} = R_r\, i_{rb} + d\Phi_{rb}/dt \qquad \text{(II.7)}$$

$$v_{rc} = R_r\, i_{rc} + d\Phi_{rc}/dt$$

$\Phi_{sa}, \Phi_{sb}, \Phi_{sc}, \Phi_{ra}, \Phi_{rb}, \Phi_{rc}$:The total fluxes specific to each stator and rotor winding respectively.

R_s : The resistance of a stator winding.

R_r : The resistance of a rotor winding.

$i_{sa}, i_{sb}, i_{sc}, i_{ra}, i_{rb}, i_{rc}$: Circulating currents in the different windings of the machine.

These equations can be rewritten in the following matrix form:

$$[v_{sabc}] = [R_s][i_{sabc}] + d[\Phi_{sabc}]/dt \qquad \text{(II.8)}$$

$$[v_{rabc}] = [R_r][i_{rabc}] + d[\Phi_{rabc}]/dt \qquad \text{(II.9)}$$

With

$[v_{sabc}] = [v_{sa}\ v_{sb}\ v_{sc}]^t$, $[v_{rabc}] = [v_{ra}\ v_{rb}\ v_{rc}]^t$

$[i_{sabc}] = [i_{sa}\ i_{sb}\ i_{sc}]^t$, $[i_{rabc}] = [i_{ra}\ i_{rb}\ i_{rc}]^t$

$[\Phi_{sabc}] = [\Phi_{sa}\ \Phi_{sb}\ \Phi_{sc}]^t$, $[\Phi_{rabc}] = [\Phi_{ra}\ \Phi_{rb}\ \Phi_{rc}]^t$

$[\Phi_{sabc}] = [\Phi_{sa}\ \Phi_{sb}\ \Phi_{sc}]^t$, $[\Phi_{rabc}] = [\Phi_{ra}\ \Phi_{rb}\ \Phi_{rc}]^t$

$[R_s] = R_s * [I_3]$, $[R_r] = R_r * [I_3]$

Knowing that:

$$[\psi_{sabc}] = \left[[L_s]\ [i_{sabc}] + [L_{sr}]\ [i_{rabc}] \right] \qquad \text{(II.9)}$$

$$[\psi_{rabc}] = \left[[L_r]\ [i_{rabc}] + [L_{rs}]\ [i_{sabc}] \right] \qquad \text{(II.10)}$$

with

$$[L_s] = \begin{bmatrix} L_{aa} & L_{ab} & L_{ac} \\ L_{ba} & L_{bb} & L_{bc} \\ L_{ca} & L_{cb} & L_{cc} \end{bmatrix} \quad [L_r] = \begin{bmatrix} L_{AA} & L_{AB} & L_{AC} \\ L_{BA} & L_{BB} & L_{BC} \\ L_{CA} & L_{CB} & L_{CC} \end{bmatrix} \qquad \text{(II.11)}$$

The inherent inductances in the gap due to the stator phase are designated by L_{aa} , L_{bb} et L_{cc} .

If the leakage induction of the windings in the gap is taken into consideration, the inductance specific to each phase is written as follows:

$$L_{xx} = L_x + L_{fx} \quad \text{(II.12)}$$

With $x = a, b$ ou c.

or :

L_x is the magnetizing inductance of each phase.

L_{fx} is the clean leakage inductance of each phase.

Since the stator windings are similar and have the same magnetising inductance and leakage inductance, then we can write:

$$L_{xx} = L_s + L_{fs} \quad \text{(II.13)}$$

L_s : The magnetising inductance of the stator winding.

L_{fs} : The leakage inductance of the stator winding.

2.2.4 Machine Inductances

The stator phases are separated in space by an angle of 2π / 3 radian electrical and the mutual inductances are calculated as follows [8]:

$$L_{ab} = L_{ba} = L_s \cos\frac{2\pi}{3} = -\frac{L_s}{2}$$

$$L_{bc} = L_{cb} = L_s \cos\frac{2\pi}{3} = -\frac{L_s}{2} \quad \text{(II.14)}$$

$$L_{ca} = L_{ac} = L_s \cos\frac{2\pi}{3} = -\frac{L_s}{2}$$

Using the same method to calculate the mutual inductances between the rotor windings, each specific inductance of these latter is written as follows: $L_{xx} = L_r + L_{fr}$

(II.15)

With Avec$x = A,B$ ou C.

Or :

L_r : The magnetising inductance of the rotor winding.

L_{fr} : The leakage inductance of the rotor winding.

And we have:

$$L_{AB} = L_{BA} = L_r \cos\frac{2\pi}{3} = -\frac{L_r}{2}$$

$$L_{BC} = L_{CB} = L_r \cos\frac{2\pi}{3} = -\frac{L_r}{2} \quad \text{(II.16)}$$

$$L_{CA} = L_{AC} = L_r \cos\frac{2\pi}{3} = -\frac{L_r}{2}$$

So the system (II.7)

$$[L_s] = \begin{bmatrix} L_s + L_{fs} & -\frac{L_s}{2} & -\frac{L_s}{2} \\ -\frac{L_s}{2} & L_s + L_{fs} & -\frac{L_s}{2} \\ -\frac{L_s}{2} & -\frac{L_s}{2} & L_s + L_{fs} \end{bmatrix} [L_r] = \begin{bmatrix} L_r + L_{fr} & -\frac{L_r}{2} & -\frac{L_r}{2} \\ -\frac{L_r}{2} & L_r + L_{fr} & -\frac{L_r}{2} \\ -\frac{L_r}{2} & -\frac{L_r}{2} & L_r + L_{fr} \end{bmatrix} \quad \text{(II.17)}$$

The matrix of mutual inductances between the stator and rotor windings is written as follows:

$$[L_{sr}] = l_{sr} \begin{bmatrix} \cos(\theta_r) & \cos\left(\theta_r + \frac{2\pi}{3}\right) & \cos\left(\theta_r + \frac{4\pi}{3}\right) \\ \cos\left(\theta_r + \frac{4\pi}{3}\right) & \cos(\theta_r) & \cos\left(\theta_r + \frac{2\pi}{3}\right) \\ \cos\left(\theta_r + \frac{2\pi}{3}\right) & \cos\left(\theta_r + \frac{4\pi}{3}\right) & \cos(\theta_r) \end{bmatrix} \quad \text{(II.18)}$$

Knowing that $L_{rs} = L_{sr}^{T}$

l_{sr}:The mutual inductance between stator and rotor.

2.2.5 Electromagnetic torque

The mechanical equation of motion depends on the characteristics of the load which can differ widely from one application to another.

This equation is expressed as:

$$J\frac{d^2\theta_{rm}}{dt^2} + T_c = T_e \quad \text{(II.19)}$$

Where θ_{rm} is the angular displacement of the rotor, Tc is the load torque and Te is the electromagnetic of the machine.

The electromagnetic torque can be written in terms of the magnetic co-energy Wco as follows:

$$T_e = \left[\frac{\partial W_{co}}{\partial \theta_{rm}}\right] \quad (I_s, I_r : \text{constant}) \quad \text{(II.20)}$$

In the case of a linear magnetic system, the co-energy is equal to the energy stored so that:

$$W_{co} = \frac{1}{2} I_s^t L_{ss} I_s + \frac{1}{2} I_s^t L_{sr} I_r + \frac{1}{2} I_r^t L_{sr}^t I_s + \frac{1}{2} I_r^t L_{rr} I_r \quad \text{(II.21)}$$

Since L_{ss} and L_{rr} contain only constant elements, equation (II.20) is easily reduced to:

$$T_e = \frac{1}{2} I_s^t \frac{\partial L_{sr}}{\partial \theta_{rm}} I_r + \frac{1}{2} I_r^t \frac{\partial L_{sr}^t}{\partial \theta_{rm}} I_s \quad \text{(II.22)}$$

Since Te is a scalar, therefore the two terms in (II.22) must also be scalar quantities,

$$I_r^t \frac{\partial L_{sr}^t}{\partial \theta_{rm}} I_s = \left[I_r^t \frac{\partial L_{sr}^t}{\partial \theta_{rm}} I_s \right]^t \quad \text{(II.23)}$$

From matrix algebra, we have the following result:

$(A^t B^t C) = (C^t B A)$

Then (II.23) is rewritten as follows:

$$I_r^t \frac{\partial L_{sr}^t}{\partial \theta_{rm}} I_s = I_s^t \frac{\partial L_{sr}}{\partial \theta_{rm}} I_r \quad \text{(II.24)}$$

Therefore, the first term of equation (II.22) is equal to the second, the torque equation reduces to the following final form:

$$T_e = I_s^t \frac{\partial L_{sr}}{\partial \theta_{rm}} I_r \quad \text{(II.25)}$$

So far, we have assumed that the machine has only two pairs of poles. In general, we have "*p*" which designates the number of pairs of generator poles. It is clear that any inductance that is a function of angular deviation undergoes "*p*/2" complete cycles while θ_{rm} varies from 0 to 2π.

$$\theta_r = p \theta_{rm} \quad \text{(II.26)}$$

θ_r is the electric angle of displacement of the generator which is expressed in radians.

The electromagnetic torque expressed in terms of θ_r is written:

$$T_e = p I_s^t \frac{\partial L_{sr}}{\partial \theta_r} I_r \quad \text{(II.27)}$$

Finally, equation (II.15) expressed in terms of θ_r gives:

$$\frac{d\omega_r}{dt} = \left(\frac{p}{J} \right) (T_e - T_c) \quad \text{(II.28)}$$

Introducing the coefficient of friction, gives:

$$\frac{d\omega_r}{dt} = \left(\frac{p}{J} \right) \left(T_e - T_c - \frac{K_f}{p} \omega_r \right) \quad \text{(II.29)}$$

With

$$\omega_r = \frac{d\theta_r}{dt} \tag{II.30}$$

Where:

J : the inertia of the machine. [Kg/m^2].

K_f : the coefficient of friction. [Kgm^2/s].

T_e : Electromagnetic torque [N.m].

T_c : Load torque. [N.m].

2.2.6 Mathematical model of the DFIG

The DFIG is described in the park dq frame by the following set of equations [2]

The stator dq voltage equations are given as bellow

$$v_{ds} = R_s i_{ds} + \frac{d\varphi_{ds}}{dt} - \omega_s \varphi_{qs} \tag{II.31}$$

$$v_{qs} = R_s i_{qs} + \frac{d\varphi_{qs}}{dt} + \omega_s \varphi_{ds} \tag{II.32}$$

The rotor dq voltage equations are given as bellow

$$v_{dr} = R_r i_{dr} + \frac{d\varphi_{dr}}{dt} - \omega_r \varphi_{qr} \tag{II.33}$$

$$v_{qr} = R_r i_{qr} + \frac{d\varphi_{qr}}{dt} + \omega_r \varphi_{dr} \tag{II.34}$$

The stator dq flux equations are given as bellow

$$\varphi_{ds} = L_s i_{ds} + L_m i_{dr} \tag{II.35}$$

$$\varphi_{qs} = L_s i_{qs} + L_m i_{qr} \tag{II.36}$$

The rotor dq flux equations are given as bellow

$$\varphi_{dr} = L_m i_{ds} + L_r i_{dr} \tag{II.37}$$

$$\varphi_{qr} = L_m i_{qs} + L_r i_{qr} \quad \text{(II.38)}$$

The mechanical power in the shaft P_m minus the cupper losses in the stator and rotor is equal to the sum of the stator active power P_s and the rotor active power P_r as follows

$$Ps + Pr = Pm + Pcu\_r + Pcu\_s \quad \text{(II.39)}$$

While

$$Pcu_s = 3Rs|Is|^2 \quad \text{(II.40)}$$

And

$$Pcu_r = 3Rr|Ir|^2 \quad \text{(II.41)}$$

By neglecting the power losses in the stator and rotor resistances the stator active and reactive powers can be given as follows:

$$Ps = \frac{3}{2}(VdsIds + VqsIqs) \quad \text{(II.42)}$$

$$Qs = \frac{3}{2}(VqsIds + VdsIqs) \quad \text{(II.43)}$$

The rotor active and reactive powers can be given as follows:

$$Pr = \frac{3}{2}(VdrIdr + VqrIqr) \quad \text{(II.44)}$$

$$Qr = \frac{3}{2}(VqrIdr + VdrIqr) \quad \text{(II.45)}$$

The efficiency of the machine particular to motor or generator operation can be given as:

$$\eta = \frac{Pm}{Ps + Pr} \ , Pm < 0 \quad \text{or} \quad \eta = \frac{Ps + Pr}{Pm} \ , Pm > 0 \quad \text{(II.46)}$$

2.3 Modeling of the DFIG with Fault

Using the fundamental magnetic concept, the DFIG will be represented by two coupled circuits stator and rotor. For a DFIG, a simple circuit model can be given by considering individual stator, rotor coils (abc) and their links. The methodology of inter-turn short circuit fault

modelling consists in considering the turn itself as a separate coil in series with the phase (a) of the stator or the rotor. The parameters of this coil are denoted by a d subscript. Taking into account the distributed nature of the windings, the stator and rotor equivalent circuits can be represented on a conductor-by-conductor basis. The resistive and inductive effects are only taken into account and the capacitive effect is neglected to remain in the low frequency range. For this study, the variations of the resistances with currents for all stator and rotor coils are represented separately.[24] [16]

The three-phase stator and rotor windings are sinusoidally distributed circuits as shown in Figure35. In the following equations, the stator voltages equations in terms of the machine quantities can be expressed as:

$$[v_s] = [R_s][i_s] + \frac{d[\Phi_s]}{dt} \tag{II.47}$$

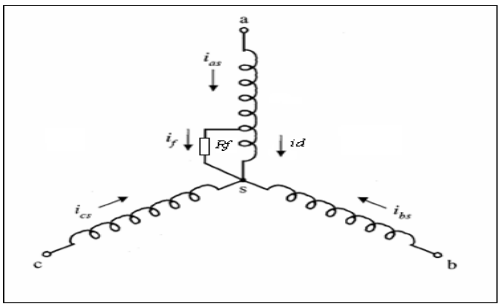

Figure 13. Inter-turn short circuit fault on phase 'a'.

$$[v_s] = \begin{bmatrix} v_{sa} \\ v_{sb} \\ v_{sc} \\ v_{sd} \end{bmatrix}, \quad [i_s] = \begin{bmatrix} i_{sa} \\ i_{sb} \\ i_{sc} \\ i_{sd} \end{bmatrix}, \quad [\Phi_s] = \begin{bmatrix} \Phi_{sa} \\ \Phi_{sb} \\ \Phi_{sc} \\ \Phi_{sd} \end{bmatrix} \tag{II.48}$$

$$[R_s] = \begin{bmatrix} (1-cc).R_s & 0 & 0 & cc.R_s \\ 0 & R_s & 0 & 0 \\ 0 & 0 & R_s & 0 \\ 0 & 0 & 0 & cc.R_s \end{bmatrix} \tag{II.49}$$

$$L_s = l_{fs} diag\left[(1-cc)\ 1\ 1\ cc\right] + L_{ms} \begin{bmatrix} (1-cc)^2 & -\frac{1-cc}{2} & -\frac{1-cc}{2} & cc(1-cc) \\ -\frac{1-cc}{2} & 1 & -\frac{1}{2} & -\frac{cc}{2} \\ -\frac{1-cc}{2} & -\frac{1}{2} & 1 & -\frac{cc}{2} \\ cc(1-cc) & -\frac{cc}{2} & -\frac{cc}{2} & cc^2 \end{bmatrix} \tag{II.50}$$

$$L_{sr} = l_{sr}\begin{bmatrix} (1-cc)\cos\theta_r & (1-cc)\cos\left(\theta_r+\frac{2\pi}{3}\right) & (1-cc)\cos\left(\theta_r-\frac{2\pi}{3}\right) \\ \cos\left(\theta_r-\frac{2\pi}{3}\right) & \cos\theta_r & \cos\left(\theta_r+\frac{2\pi}{3}\right) \\ \cos\left(\theta_r+\frac{2\pi}{3}\right) & \cos\left(\theta_r-\frac{2\pi}{3}\right) & \cos\theta_r \\ cc\cos\theta_r & cc\cos\left(\theta_r+\frac{2\pi}{3}\right) & cc\cos\left(\theta_r-\frac{2\pi}{3}\right) \end{bmatrix} \quad \text{(II.51)}$$

$$[L_r] = \begin{bmatrix} L_r+L_{fr} & \frac{L_r}{2} & \frac{L_r}{2} \\ \frac{L_r}{2} & L_r+L_{fr} & \frac{L_r}{2} \\ \frac{L_r}{2} & \frac{L_r}{2} & L_r+L_{fr} \end{bmatrix} \quad \text{(II.52)}$$

2.4 DOUBLE FLUX ORIENTATION STRATEGY

This methodology consists on aligning the rotor flux and stator flux along the d axis and q axis respectively. Figure 35 shows the orientation of stator and rotor fluxes [25].

Consequently, the two fluxes become orthogonal and we can write [26]:

$$\begin{aligned} \phi_{sq} &= \phi_s \\ \phi_{rd} &= \phi_r \\ \phi_{sd} &= \phi_{rq} = 0 \end{aligned} \quad \text{(II.53)}$$

If the resistance is neglected, we have:

$$\begin{aligned} V_{sd} &= V_s \\ V_{sq} &= \frac{d\phi_{sq}}{dt} = 0 \end{aligned} \quad \text{(II.54)}$$

Using equation (II.54), the developed active and reactive powers can be rewritten as follows:

$$\begin{aligned} P &= V_s i_{sd} \\ Q &= -V_s i_{sq} \end{aligned} \quad \text{(II.55)}$$

Where

$$\begin{aligned} i_{sd} &= -\frac{M_{sr}}{L_s} i_{rd} \\ i_{sq} &= -\frac{L_s}{M_{sr}} i_{rq} \end{aligned} \quad \text{(II.56)}$$

Therefore,

$$P = -V_s \frac{M_{sr}}{L_s} i_{rd} \qquad (II.57)$$
$$Q = V_s \frac{L_s}{M_{sr}} i_{rq}$$

For the calculation of PI gains we used the pole compensation method. The block diagram of the power control loop is shown in Figure 36.

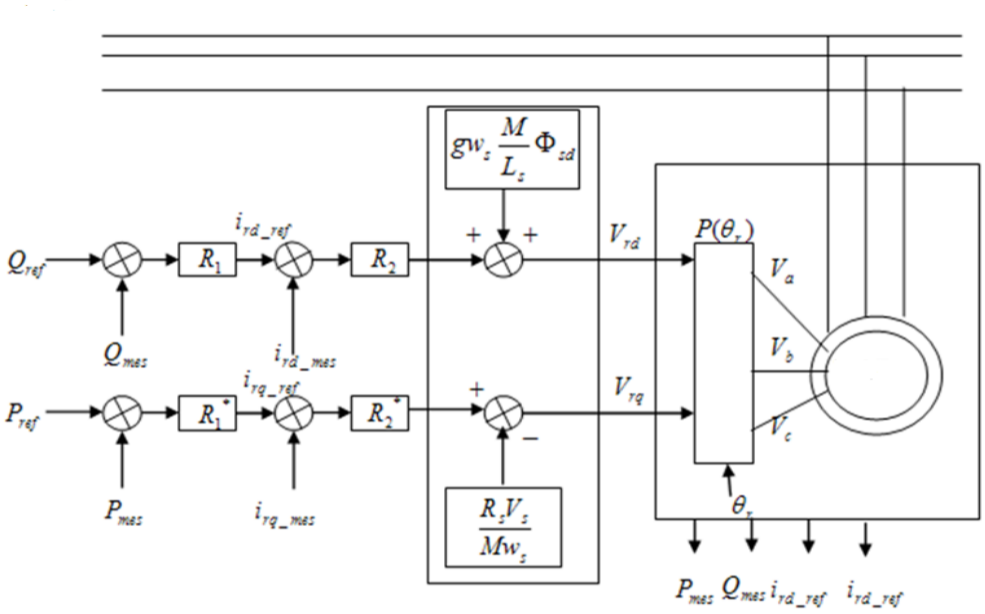

Figure 14. DFIG Powers control

2.4.1 PI regulator synthesis

Figure 37 shows the block diagram of the system implemented with a PI controller. [27],[28]

Where K_p and K_i represent the proportional and integral gains respectively.

The quotient B/A represents the transfer function to be controlled, where A and B are defined as follows:

$$A = L_s R_r + pL_s (L_r - \frac{M^2}{L_s}) \quad \text{and} \quad B = MV_s \qquad (II.58)$$

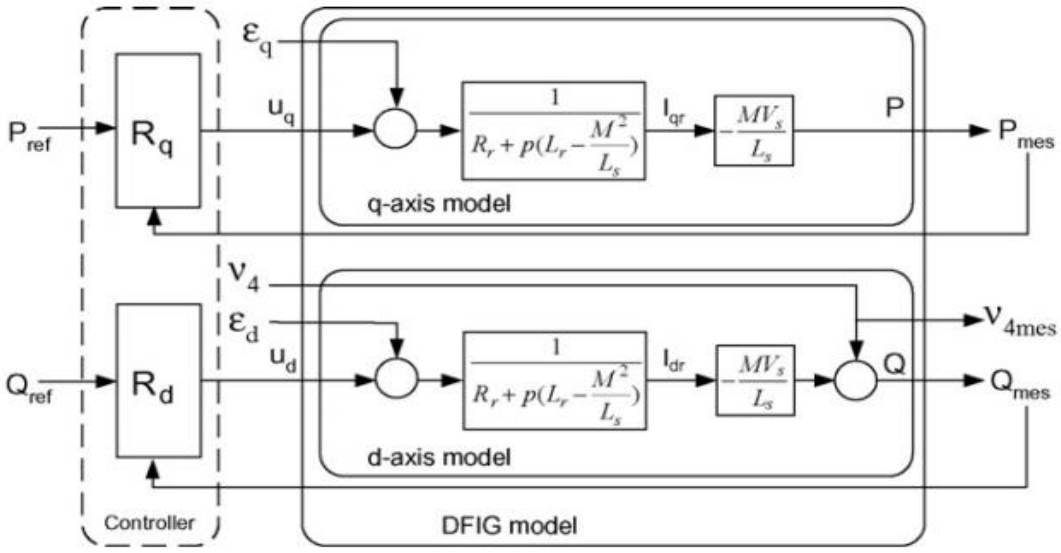

Figure 15 Simplified model of the DFIG with controller.

The controller gains are calculated using a pole-placement method. The time response of the controlled system will be fixed at 10 ms. This value is sufficient for our application and a smaller value may results in large transients with important overshoots.

The calculated terms are:

$$K_p = \frac{1}{5\times10^{-3}} \frac{L_s(L_r - \frac{M^2}{L_s})}{MV_s} \tag{II.59}$$

$$K_i = \frac{1}{5\times10^{-3}} \frac{L_s^2 R_r (L_r - \frac{M^2}{L_s})}{MV_s L_s (L_r - \frac{M^2}{L_s})} \tag{II.60}$$

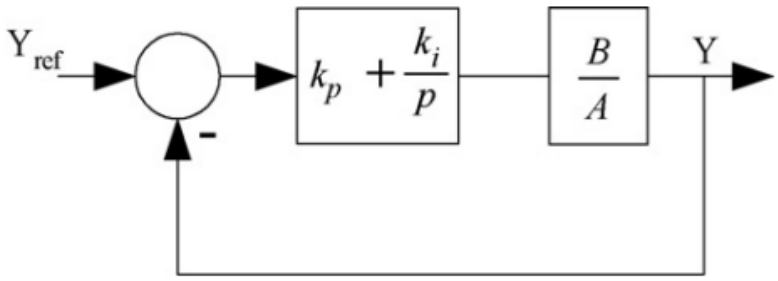

Figure 16. System with PI controller

It is important to specify that the pole-compensation is not the only method to calculate a PI regulator gains but it is simple to elaborate with a first-order transfer-function and it is sufficient in our case to compare with other regulators. We can also note that this regulator presents several disadvantages: [27]

- A zero is present in the numerator of the transfer-function.

- The integrator introduces a phase difference which can induce instability.
- The regulator is directly calculated with the parameters of the machine, if these parameters vary then the performance of the overall system can be affected.
- The perturbations are not considered, and the system has few degrees of freedom to be tuned.

2.5 Simulation Results

Our system described is simulated using MATLAB, Figures 39and 40 show the dynamic responses for both PI controllers, The active and reactive powers generated follow their references signals applied at 0.2 and 0.5 sec . These show that the references have been well followed and the time response is good which show the effectiveness of the proposed control strategy for the power production in normal conditions.

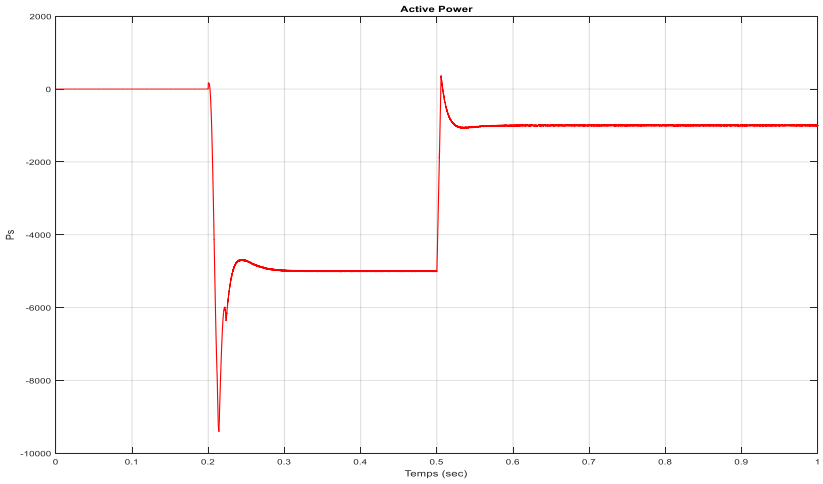

Figure 17. Active power using PI controller

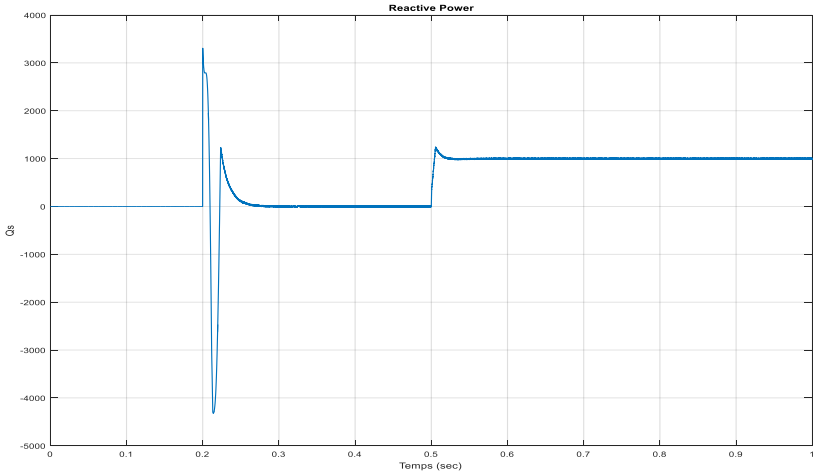

Figure 18. Reactive power using PI controller

At 1 sec We vary the following parameters Rs=2*Rs ;Rr=2*Rr ;Ls=0.5*Ls ;Lr=0.5*Lr figure(40)

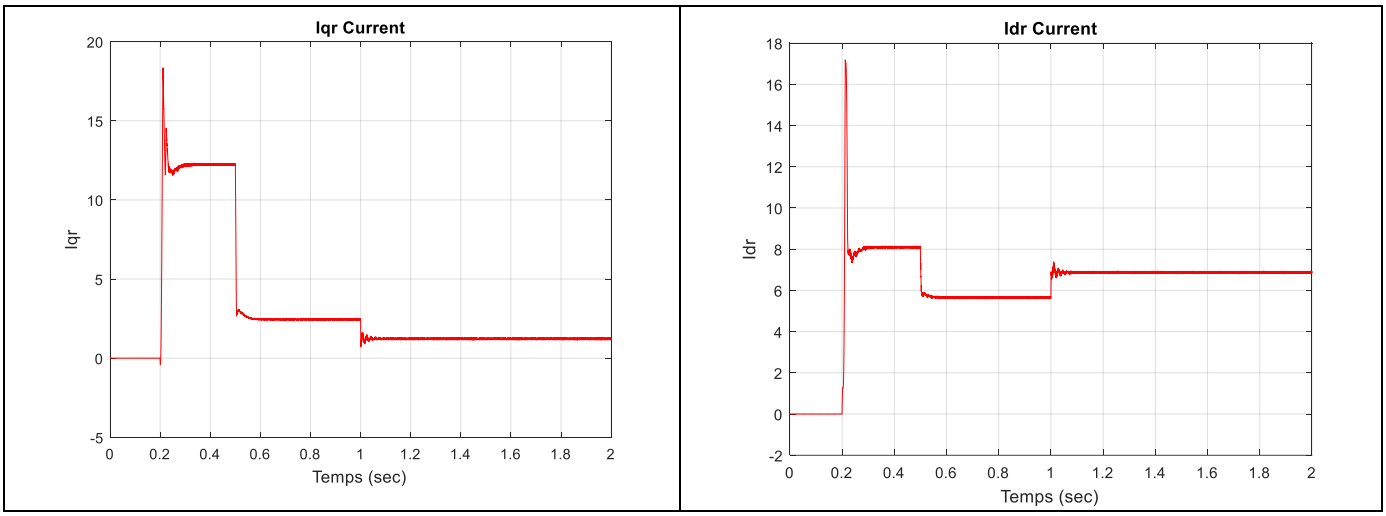

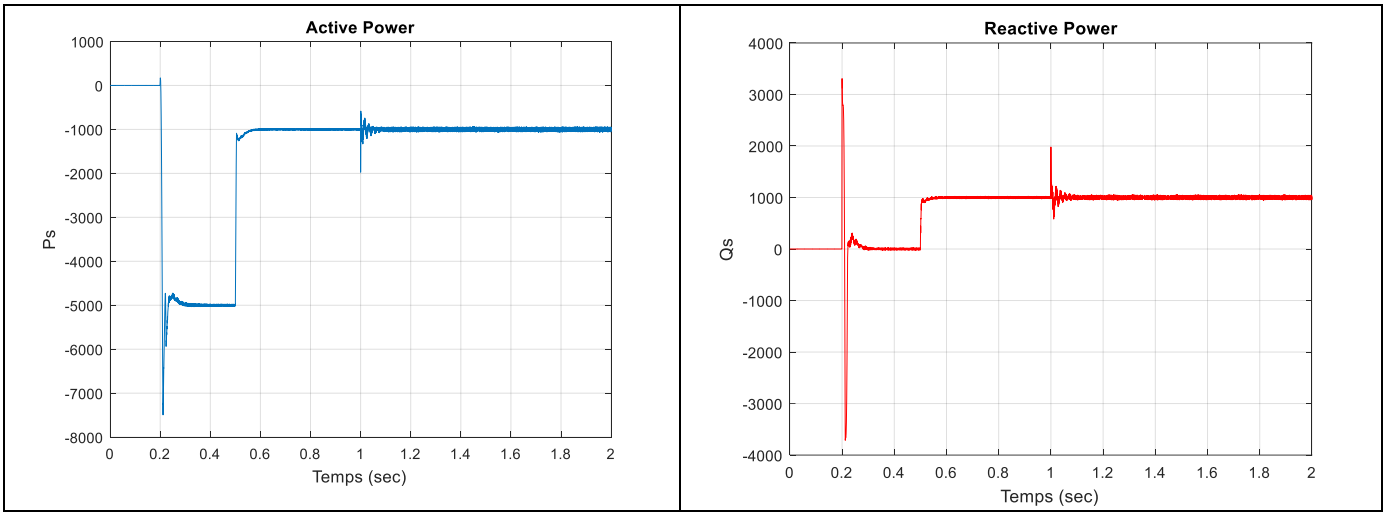

Figure 19.Tests de Robustesse PI

2.6 Sliding mode controllers based on flux orientation

This control approach is based on choosing a sliding surface to elaborate a law of regulation that controls the system in this zone. The system state variables determine the non-linear sliding surface, the variables that are going to be controlled to be inside the sliding zone.

The design of the sliding mode control strategy takes into consideration both stability and good performance issues in a systematic way, that is accomplished, essentially in three complementary steps: (i) Selection of the sliding surfaces, (ii) Definition of the sliding regime's, its existence and convergence, (iii) Determination of the control law. In this part the selected sliding surfaces are both the direct and quadrature rotor current, because of the rotor currents being the image of the stator powers. [29] [30]

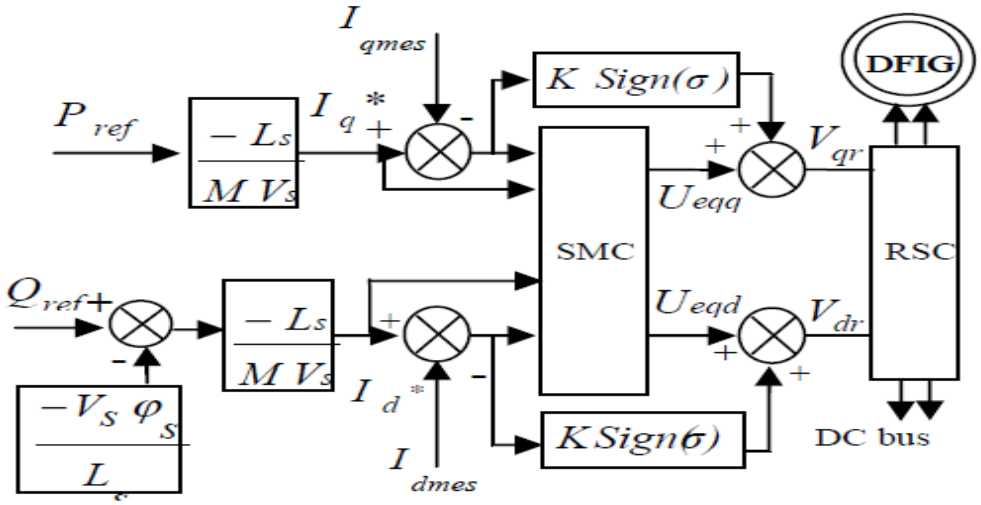

Figure 20. Global diagram of simulation and control of DFIG the by SMC

2.6.1 Active power control (Ps)

In the following, an indirect control of the active power of the DFIG is performed by acting on the current. The error of the i_{rq} quadrature rotor current is given by:[16]

$$e = \mathbf{i}_{rq\_ref} - \mathbf{i}_{rq} \tag{II.61}$$

For n = 1, the surface of the quadrature rotor current can be defined by the following equation:

$$S(\mathbf{i}_{rq}) = e = \mathbf{i}_{rq\_ref} - \mathbf{i}_{rq} \tag{II.62}$$

By replacing $\mathbf{i}_{rq}$ with its expression according to the term control law, one obtains:

$$\dot{S}(\mathbf{i}_{rq}) = \dot{\mathbf{i}}_{rq\_ref} - \left(-\frac{1}{\sigma}\left(\frac{1}{T_r} + \frac{M^2}{L_r L_s T_s}\right) i_{rq} - g\omega_s i_{rd} + \frac{1}{\sigma L_r} V_{rq} \right) \tag{II.63}$$

Replacing V_{rq} by:

$$V_{rq} = V_{rq}^{eq} + V_{rq}^{n} \tag{II.64}$$

During the sliding mode and in steady state:

$$S(\mathbf{i}_{rq}) = 0; \dot{S}(\mathbf{i}_{rq}) = 0, V_{rq}^{n} = 0. \tag{II.65}$$

$$V_{rq}^{eq} = \left(i_{rq\_\mathrm{ref}} + \frac{1}{\sigma}\left(\frac{1}{T_r} + \frac{M^2}{L_r L_s T_s}\right) i_{rq} - g\omega_s i_{rd} \right) \sigma L_r \tag{II.66}$$

Consequently:

$$V_{rq}^{n} = K_{V_{rq}} sat(S(\mathbf{i}_{rq})) \tag{II.67}$$

Where $K_{V_{rq}}$ is a positive constant.

2.6.2 Reactive power control

The reactive power generated is regulated by controlling the direct rotor current $\mathbf{i}_{rd}$. The error of the direct rotor current is defined as: [16],[31]

$$e = \mathbf{i}_{rd\_ref} - \mathbf{i}_{rd} \tag{II.68}$$

For n = 1, the surface of the direct rotor current is defined by the following equation.

$$S(\mathbf{i}_{rd}) = e = \mathbf{i}_{rd\_ref} - \mathbf{i}_{rd} \tag{II.69}$$

And its derivative is given by:

$$\dot{S}(i_{rd}) = \dot{i}_{rd\_ref} - \dot{i}_{rd} \tag{II.70}$$

Replacing i_{rd} with its expression gives:

$$\dot{S}(i_{rd}) = \dot{i}_{rd\_ref} - \left(\frac{1}{\sigma T_r} i_{rd} + g\omega_s i_{rq} + \frac{1}{\sigma L_r} V_{rd} \right) \tag{II.71}$$

Where V_{rd} can be expressed as:

$$V_{rd} = V_{rd}^{eq} + V_{rd}^{n} \tag{II.72}$$

During the sliding mode and in-steady state:

$$S(i_{rd}) = 0; \dot{S}(i_{rd}) = 0, V_{rd}^{n} = 0. \tag{II.73}$$

$$V_{rd}^{eq} = \left(i_{rd\_ref} + \frac{1}{\sigma T_r} i_{rd} + g\omega_s i_{rq} \right) \sigma L_r \tag{II.74}$$

Consequently:

$$V_{rd}^{n} = K_{V_{rd}} sat(S(i_{rd})) \tag{II.75}$$

Where $K_{V_{rd}}$ is a positive constant.

2.7 Conclusion

First a flux orientation control based on PI controllers and Sliding Mode Controllers was presented. The main idea behind all flux orientation control strategies is that the machine flux position or vector flux components are computed from the direct measurements of the machine quantities. In DFIG, both stator and rotor currents are easily measured, since the fluxes are used like control variables, the machine fluxes must be maintained at acceptable level especially during the transient regimes. This strategy of control leads to an optimal developed torque.

In the second part.

The aims of the control system are the control of the reactive power exchange between the generator and the grid and the control of the power drawn from the wind turbine in order to track the wind turbine optimum operation point.

CHAPTER 03

ADVANCED CONTROL

3.1 Introduction

In this chapter, we explore advanced control techniques known as Sliding Mode Control (SMC) and Linear Quadratic Regulator (LQR) and how we can use them with wind energy turbines. These methods provide smart solutions to make wind turbines work better and more reliably, especially when the wind keeps changing. We'll show you how SMC and LQR can help generate more power, keep the system stable, and deal with problems caused by changes in the wind. By the end, you'll see how these advanced controls can make wind energy more efficient and dependable.

3.2 Sliding-Mode Control

This section introduces Variable Structure Control (VSC) theory and its extension to the so-called Sliding-Mode Control (SMC). Note that the presentation is not intended as a comprehensive survey of the state-of-the-art in the field, but to merely present the basic concepts on SMC required to understand the derivation of the control algorithms introduced in this chapter. [35]

3.3 Variable Structure Control Preliminaries

The VSC and associated SMC strategies were first proposed and developed by Stanislav Emelyanov and Vadim Utkin in the early 1950s in the ex. Soviet Union. The most important feature of SMC is its robustness which can be defined as the ability to remain invariant under certain operating conditions. In brief, the concept of invariance indicates that the system remains completely insensitive to certain types of disturbances and uncertainties.

Since the 1990s, the control of systems subject to external disturbances and model uncertainty has been the focus of increasing interest. Among the different existing alternatives, the SMC has proven to be an attractive control scheme for different classes of nonlinear systems, due to its robustness and insensitivity against certain system uncertainty and perturbations. The feasibility and benefits of SMC applied to electronically controlled actuators have been extensively demonstrated in the literature.

In addition, the design of SMC is relatively simple design even when dealing with nonlinear systems. SMC can also be successfully combined with other nonlinear control techniques such as energy shaping and model predictive control. As a result, the research and development of SMC design methods have been extensively investigated both in theoretical and practical fields.

One of the most distinctive aspects of the SMC is the discontinuous nature of its control action. Its primary function consists in performing a switching between two different structures in order to get desired new dynamics in the system, known as sliding-mode dynamics. This feature allows the system to have an enhanced performance, including insensitivity to parametric uncertainties and rejection to disturbances that verify the so-called matching condition. When the concept of parametric uncertainties is considered, it is referred to both external and internal uncertainties in the parameters as the product of the process of model reduction used in control design.

However, a great deal of the success to fulfil the control objectives depends on the capability of the SMC design to reduce chattering which can be described as a phenomenon of finite-frequency, finite-amplitude oscillations appearing in many sliding-mode implementations. These oscillations are caused by the high-frequency switching of a SMC under practical (non-ideal) operating conditions, such as unmodelled dynamics in the closed-loop or finite switching frequency.[35],[36]

A successful alternative to reduce this undesired phenomenon, currently addressed by many control researchers and engineers, is to use the so-called Higher Order Sliding-Mode control. In this case, from the definition of a continuous control action, the HOSM generalizes the concept of sliding surface or manifold while keeping the main advantages of the original approach of SM under Lipschitz continuous uncertainty/perturbations. In particular, there are several promising results related to Second-Order Sliding-Mode control and several approaches have been proposed to solve the robust stabilization of nonlinear uncertain systems, while guaranteeing a finite-time convergence of the sliding variable.

3.3.1 Fundamentals of Sliding-Mode Control

Sliding Mode Control is a strategy based on output feedback and a high-frequency switching control action which, in ideal conditions, is infinite. Essentially, this high-speed control law can lead the system trajectories to a subspace of the state space (commonly associated to a sliding surface or manifold). If a system is forced to constrain its evolution on a given manifold, the static relationships result in a dynamical behavior determined by the design parameters and equations that define the surface . On average, the controlled dynamics may be considered as ideally constrained to the surface while adopting all its desirable geometrical features. Thus, making an appropriate design of the sliding surface (i.e. embedding the control objectives into

the control function that gives rise to such manifold), it is possible to achieve conventional control goals such as global stability, optimization, tracking, regulation, etc.

In the sequel, the basics of the theory of classical sliding-mode control are introduced, focusing on Single-Input Single-Output (SISO) systems. Note that in this chapter, the possible explicit dependence on time of the dynamical system has been omitted for the sake of clarity and simplification of the equations. In the present approach, this compacted notation can be used without loss of generality, provided that in the case of a non-autonomous system, it could be rewritten as autonomous by treating t as an additional dependent variable, with its trivial evolution given by the fictitious equation $t^{\cdot} = 1$ (obviously, at the expense of increasing the dimension by one).

3.3.2 Diffeomorphisms, Lie Derivative and Relative Degree

Firstly, it is useful to review some mathematical tools and procedures that will be necessary later. Let a control affine nonlinear system be given by

$$\begin{aligned} \dot{x} &= f(x) + g(x)u \\ y &= h(x) \end{aligned} \tag{III.1}$$

with $x \in X \subset R^n$, $f : R^n \to R^n$ and $g : R^n \to R^n$ smooth vector fields (infinitely differentiable) with $g(x) \neq 0$, $h(x)$ smooth scalar field and $u : R^n \to R$ possibly discontinuous. These systems are linear in the control , so they are called control affine systems or analytical linear systems.

A diffeomorphism is defined as coordinate transformation of the form $z = \phi(x)$ with $\phi : R^n \to R^n$ vector field with inverse ϕ^{-1}.In particular, we only consider transformations such that ϕ and ϕ^{-1} are ζ^n (i.e.with n continuous derivatives)

This last condition ensures that the transformed system preserves its original structure. After making the proposed change of coordinates, the dynamical system (III.1) becomes:

$$\dot{z} = \dot{\phi}(x) = \frac{\partial \phi}{\partial x}\dot{x} = \frac{\partial \phi}{\partial x} f(x) + \frac{\partial \phi}{\partial x} g(x)u \tag{III.2}$$

Not That $\frac{\partial \phi}{\partial x} = \left[\frac{\partial \phi}{\partial x_1} \frac{\partial \phi}{\partial x_2} .... \frac{\partial \phi}{\partial x_n} \right]$ gives the direction of the gradient vector of $\phi(x)$, $\nabla\phi(x)$.So the system (III.1) can be written in terms of the new variable Z.

$$\begin{aligned} \dot{z} &= \tilde{f}(z) + \tilde{g}(z)u \\ y &= \tilde{h}(z) \end{aligned} \tag{III.3}$$

Where

$$\begin{aligned} \tilde{f}(z) &= \frac{\partial \phi}{\partial x} f(x)\Big\|_{x=\phi^{-1}(z)} \\ \tilde{g}(z) &= \frac{\partial \phi}{\partial x} g(x)\Big\|_{x=\phi^{-1}(z)} \\ \tilde{h}(x) &= h(x)\Big\|_{x=\phi^{-1}(z)} \end{aligned} \tag{III.4}$$

To simplify the notation, it is necessary to define the concept of directional derivative or Lie derivative, which is expressed as

$$(L_f h)(x) = L_f h(x) : R^n \rightarrow R \tag{III.5}$$

And represents the derivative of a scalar field $h(x): R^n \rightarrow R^n$ in the direction of vector field $f(x): R^n \rightarrow R^n$

$$L_f h(x) = \frac{\delta h}{\delta x} f(x) \tag{III.6}$$

L_f is a first-order diffirential operator, while the composition $L_f \circ L_g$, which is usually written as $L_f L_g$, is a second-order operator. Moreover, the directional derivative can be applied recursively :

$$L_f^k h(x) = \frac{\partial}{\partial x}(L_f^{k-1} h(x))\, f(x) \tag{III.7}$$

In this way, a compact notation for the derivatives of scalar functions in the direction of vector fields is obtained. Either in the direction of a single vector field (*f*) or more (*f* and *g*):

$$L_g L_f h(x) = \frac{\partial}{\partial x}(L_f h(x))\, g(x) \tag{III.8}$$

Finally, assuming a smooth output $h(x)$ of the system given by equation (III.1), the relative degree of $h(x)$ in the vicinity of a given point *x* is defined as the smallest positive integer *r*, if one exists, having the following property:

$$\begin{aligned} &\mathrm{L}_g\, L_f^i\, h = 0 \\ &\forall 0 \le i \le r-2 \end{aligned} \tag{III.9}$$

And

$$L_g L_f^{r-1} h \neq 0 \tag{III.10}$$

Therefore, a system output $h(\mathrm{x})$ with relative degree *r* implies, in a simplified way, that *u* explicitly appears for the first time at t0 the time derivative of $h(\mathrm{x})$. In short, *r* gives an idea about how directly the control influences the output.

3.3.3 First-Order Sliding Mode

Consider the nonlinear dynamical system (III.1) with the control action $u:\mathrm{R}^m \to \mathrm{R}$ (possibly discontinuous), f and g are smooth vector fields with $g(x) \neq 0, \forall x \in X$ be defined as a smooth constraint function $s: X \to R,$ designed according to the desired as a smooth constraints function designed according to the desired control objectives (i.e. the specifications are fulfilled when s is constrained to zero), with gradient $\nabla s = \dfrac{\partial s}{\partial x}$ non-null on X .then the set

$$\zeta = \left\{ x \in X \subset R^n : s(\mathrm{x}) = 0 \right\} \tag{III.11}$$

defines a locally regular manifold in *X* (of dimension *n* - 1 in the case of a SISO system), called sliding manifold or, simply, switching surface. This order reduction feature is a characteristic of SM control systems (first and HOSM) and indicates that the subspace on which the sliding movements occur have "non-zero co-dimension", meaning that after reaching the sliding regime, the trajectories of the system will remain within a subspace of lower dimension than the space generated by *n* states.
The results obtained below are of a local nature, restricted to an open neighborhood of $X \subset R^n$,having a non-empty intersection with sliding manifold ζ .
In order to reach the sliding motion in such manifold, a variable structure control law can be proposed by imposing a discontinuous control action *u*, which takes one of two possible feedback values, depending on the sign of *s(x)*. For example,

$$u = \begin{cases} u^+(\mathrm{x}) & if\, s(\mathrm{x}) \succ 0 \\ u^-(\mathrm{x}) & if\, s(\mathrm{x}) \prec 0 \end{cases} \tag{III.12}$$

With $u^+ \neq u^-$

The upper and lower levels of u ($u^+(\mathrm{x})$ and $u^-(\mathrm{x})$, respectively) are smooth functions of x. Moreover, without loss of generality , it can be assumed that $u^+(\mathrm{x}) \succ u^-(\mathrm{x})$ holds locally in X . Note that if $u^+(\mathrm{x}) \succ u^-(\mathrm{x})$ for any point of x , then the inequality holds for every x , given that the functions are smooth and do not intersect.

Assuming that, as a result of the control law (III.12), the constraint function locally satisfies the following inequalities in the neighborhood of ζ :

$$\begin{cases} \dot{S}(\mathrm{x}) \prec 0 & if s(\mathrm{x}) \succ 0 \\ \dot{S}(\mathrm{x}) \succ 0 & if s(\mathrm{x}) \prec 0 \end{cases}$$
$$\dot{S}(\mathrm{x}) = L_{f+gu} s = L_f s + L_g s u$$
$$f + gu \qquad \text{(III.13)}$$
$$\nabla s$$
$$\dot{S}(\mathrm{x}) S(\mathrm{x}) \prec 0$$

Under these conditions, the system will reach the sliding manifold ζ and thereafter will remain confined in a vicinity of ζ as illustrated in Figure 45. Then, it is considered that a sliding regime is established on ζ whenever (III.13) holds.

$$\dot{S}(\mathrm{x}) = L_{f+gu} s = L_f s + L_g s u \qquad \text{(III.13)}$$

Using the notation of the directional derivative, s(x) ˙ can be expressed as follows:

Note that the output $s(\mathrm{x})$ must have relative degree of 1, i.e. $L_g s \neq 0$, to ensure that the discontinuous control action is able to change the sign of $\dot{s}(\mathrm{x})$.

Equation (III.13) can also be written as follows:

$$\begin{cases} \lim\limits_{s \to +0} & L_{f+gu^+} s \prec 0 \\ \lim\limits_{s \to -0} & L_{f+gu^-} s \succ 0 \end{cases} \qquad \text{(III.14)}$$

This means that the rate of change of the constraint or SM function $s(\mathrm{x})$, evaluated in the direction of the control field, is such that a crossing of the surface is guaranteed

from each side of the surface, by using the switching law (III.12). This can be graphically interpreted with the help of Figure.21. analyzing the projection of the controlled field $f + gu$ onto the gradient vector ∇s at both sides of S .

To conclude this subsection, a succinct final remark regarding the SM control

finite reaching time is pertinent. Note then that the explicit condition (III.13) can be

condensed as $\dot{S}(x)S(x) \prec 0$. From this it is simple to understand that, to achieve finite reaching time, the control law (III.12) must be designed to fulfil the previous inequality, but in a more strict way, that is according to the scalar sufficient condition $\dot{S}(x)S(x) \prec k\,|s(x)|0$ with $k \succ 0$ (or, similarly, $\dot{S}(x)\operatorname{sing}S(x) \prec k$). This means that the system should always be moving toward the switching surface with non-zero speed. This can be straightforwardly proven by taking $V = \frac{1}{2}S^2(x)$ as a Lyapunov function.[35].

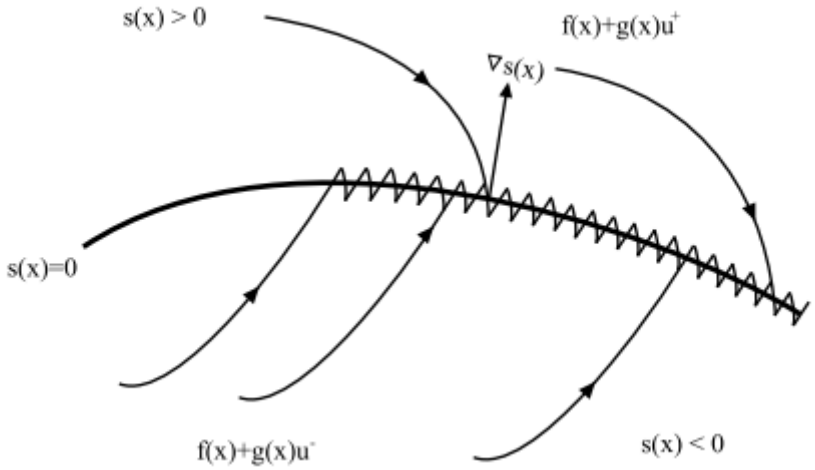

Figure.21. Sliding manifold and system trajectories

3.3.4 Sliding Mode controller design

The SM controller has been very successful in many applications in the past decades. This is due to the simplicity of its implementation and its robustness against the uncertainties of the system and external disturbances in the process. Sliding mode control is to bring back the state trajectory to the sliding surface and to advance on it with a certain dynamic point balance Figure 22. This trajectory determination consists of three parts. [37]

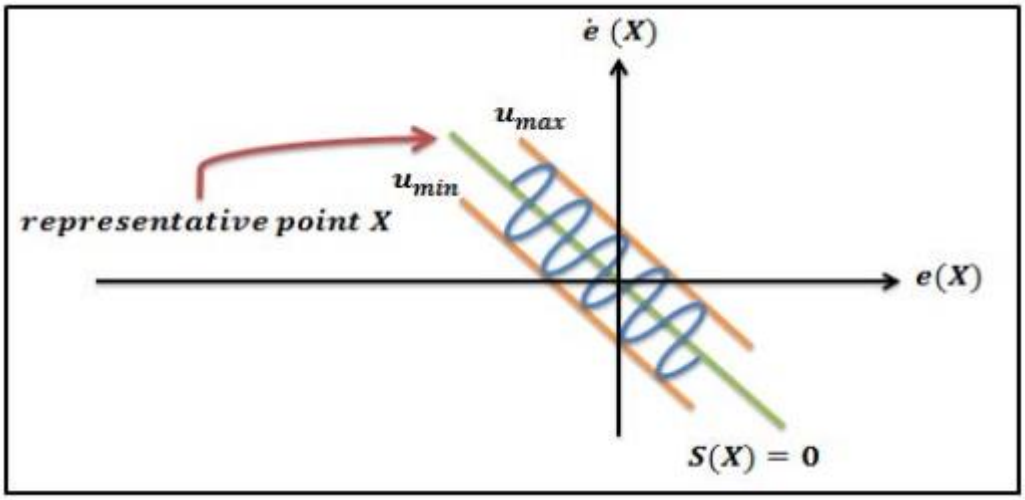

Figure.22. Trajectory mode in the phase plane

Choice of the sliding surface

For a nonlinear system presented in the following form:

$$\begin{aligned} \dot{X} &= f(\mathrm{X},\mathrm{t}) + \mathrm{g}(\mathrm{X},\mathrm{t})\,\mathrm{u}(\mathrm{X},\mathrm{t}) \\ \mathrm{X} &\in \mathrm{R}^n, u \in R \end{aligned} \tag{III.15}$$

Where $f(\mathrm{X},\mathrm{t}), \mathrm{g}(\mathrm{X},\mathrm{t})$ are two non-linear continuous functions and uncertain assumed bounded. It takes the form of the general equation proposed by J. J. Slotine to determine the sliding surface:

$$\begin{cases} S(\mathrm{X}) = (\dfrac{d}{dt} + \lambda)^{n-1} e \\ e = X^{d} - X \end{cases} \tag{III.16}$$

Where e is the error, λ is a positive coefficient, n is relative degree, X^{d} is the desired greatness:

$$X^{d} = \left[x^{d}, \dot{x}^{d}, \ddot{x}^{d} \ldots\right]^{T} \tag{II.17}$$

X is the state variable:

$$X = \left[x, \dot{x}, \ldots, \mathrm{x}^{n-1}\right]^{T} \tag{III.18}$$

2) The convergence condition

The convergence condition is defined by the equation of Lyapunov. It makes the surface attractive and invariant:

$$S(X)(\dot{S}(X)) \leq 0 \tag{III.19}$$

Computation of the control

The control law is defined by:

$$u = u^{eq} + u^{n} \tag{III.20}$$

Where u :is the control signal, u^{eq} :is the equivalent control signal, u^{n} represents the switching control term.

$$u^{n} = u^{\max} sat(S(X)/\phi) \tag{III.21}$$

$$sat(S(X)/\phi) = \begin{cases} sign(s) si \ |s| \succ \phi \\ s/\phi \quad si \ |s| \prec \phi \end{cases} \tag{III.23}$$

$sat(S(X)/\phi)$ denotes the saturation function, ϕ is the width of the threshold saturation function.

The simplest solution satisfying this condition has the form:

$$\begin{cases} u^{n} = Ksign(S(X)) \\ K \succ 0 \end{cases} \tag{III.24}$$

Applying this to our system, the derivative of the sliding surface for the active and reactive powers are given by:

$$\begin{cases} \dot{S}(P) = (\dot{P}_{s-ref} - \dot{P}_{s-mes}) \\ \dot{S}(Q) = (\dot{Q}_{s-ref} - \dot{Q}_{s-mes}) \end{cases} \tag{III.25}$$

$$\begin{cases} \dot{S}(P) = (\dot{P}_{s-ref} - V_s \frac{L_m}{L_s} i_{rq}) \\ \dot{S}(Q) = (\dot{Q}_{s-ref} - V_s \frac{L_m}{L_s} i_{rd}) \end{cases} \tag{III.26}$$

$$\begin{cases} \dot{S}(P) = (\dot{P}_{s-ref} - V_s \frac{L_m}{L_s L_r \sigma}(V_{rq} - R_r i_{rq})) \\ \dot{S}(Q) = (\dot{Q}_{s-ref} - V_s \frac{L_m}{L_s L_r \sigma}(V_{rd} - R_r i_{rd})) \end{cases} \tag{III.27}$$

Replacing V_{rq} by $V_{rq}^{eq} + V_{rq}^{n}$,and V_{rd} by $V_{rd}^{eq} + V_{rd}^{n}$

$$\begin{cases} \dot{S}(\mathrm{P}) = (\dot{\mathrm{P}}_{s-ref} - V_s \dfrac{L_m}{L_s L_r \sigma}(V_{rq}^{eq} + V_{rq}^{n} - \mathrm{R}_r\, i_{rq})) \\ \dot{S}(Q) = (\dot{\mathrm{Q}}_{s-ref} - V_s \dfrac{L_m}{L_s L_r \sigma}(V_{rd}^{eq} + V_{rd}^{n} - \mathrm{R}_r\, i_{rd})) \end{cases} \quad \text{(III.28)}$$

the equivalent controls V_{rq}^{eq} and V_{rd}^{eq} can be written as:

$$\begin{aligned} V_{rq}^{eq} &= (-\dot{\mathrm{P}}_{s-ref} \frac{L_s L_r \sigma}{L_m V_s} + \mathrm{R}_r\, i_{rq}) \\ V_{rd}^{eq} &= (-\dot{Q}_{s-ref} \frac{L_s L_r \sigma}{L_m V_s} + \mathrm{R}_r\, i_{rd}) \end{aligned} \quad \text{(III.29)}$$

During the sliding mode and under steady state conditions, we have:

$$\begin{cases} S(\mathrm{P}) = 0 \quad and \quad S(\mathrm{Q}) = 0 \\ \dot{S}(\mathrm{P}) = 0 \quad and \quad \dot{S}(\mathrm{Q}) = 0 \\ V_{rd}^{eq} = 0 \quad and \quad V_{rq}^{eq} = 0 \end{cases} \quad \text{(III.30)}$$

During the convergence mode, the condition for $S(\mathrm{P})(\dot{\mathrm{S}}(\mathrm{P})) \le 0$ and $S(\mathrm{Q})(\dot{\mathrm{S}}(\mathrm{Q})) \le 0$ is verified by setting:

$$\begin{cases} \dot{S}(\mathrm{P}) = (V_s \dfrac{L_m}{L_s L_r \sigma} V_{rq}^{n}) \\ \dot{S}(Q) = (V_s \dfrac{L_m}{L_s L_r \sigma} V_{rd}^{n})) \end{cases} \quad \text{(III.31)}$$

Therefore, the switching term is given by:

$$\begin{cases} V_{rq}^{n} = K_1 sign(\mathrm{S}(\mathrm{P})) \\ V_{rd}^{n} = K_2 sign(\mathrm{S}(Q)) \end{cases} \quad \text{(III.32)}$$

To verify the condition of stability of the system, parameters K_1 and K_2 must be positive. To mitigate the overshoot of the reference voltage V_{rq} and V_{rd}, it is often useful to add a voltage limiter.

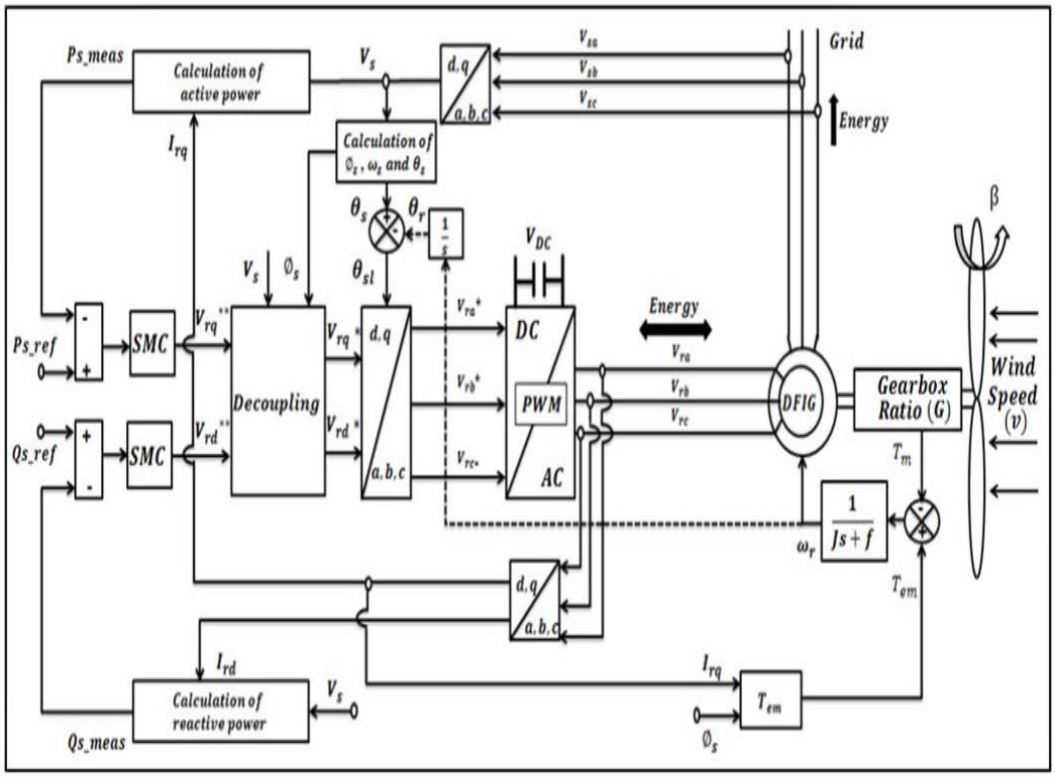

Figure.23. Direct control loop of DFIG using Sliding Mode

3.3.5 Simulations Results

Our system is simulated using under MATLAB environment. Figures 48 and 49 show the dynamic responses with both PI controllers. The power reference signal is stepped at 0 and 0.5 sec. The results show that the references have been well tracked and a good transient response is achieved which shows the effectiveness of the proposed control strategy for the power production in normal conditions.

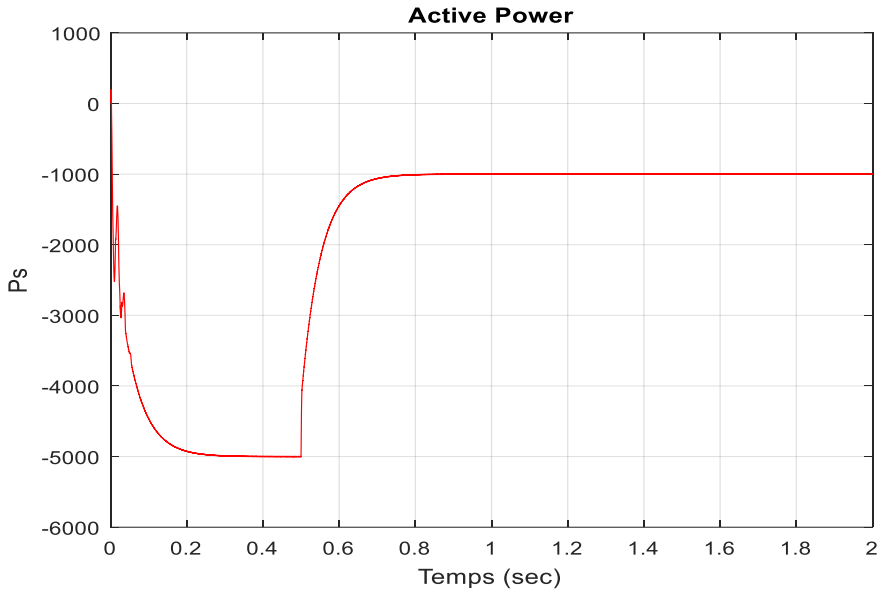

Figure 24. Direct control loop of of Active Power using Sliding Mode

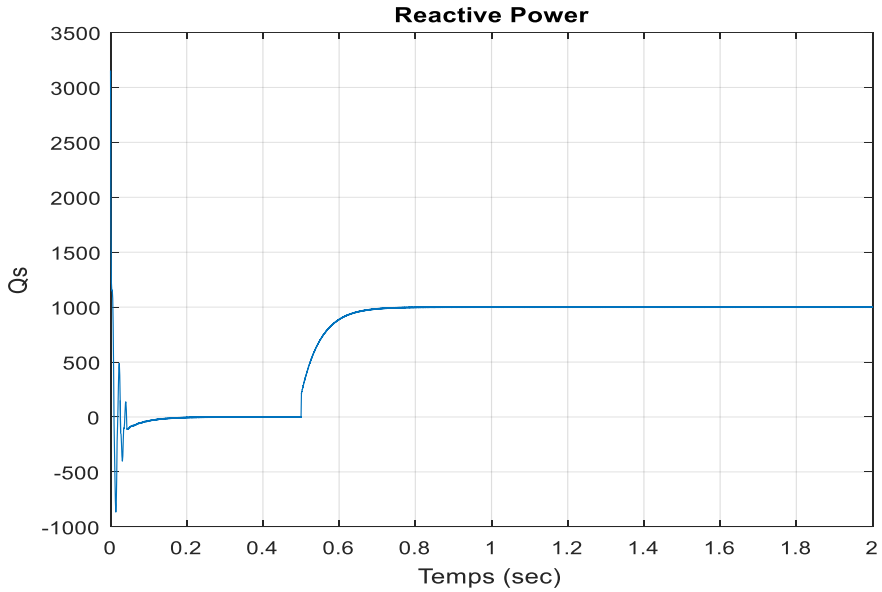

Figure 25.Direct control loop of of Reactive Power using Sliding Mode

3.4 LQG CONTROLLER DESIGN

3.4.1 Introduction LQR

An advantage of linear quadratic regulator (LQR) design is that it gives a robust system by guaranteeing stability margins. This property is used to develop an algorithm for placing robust poles. The algorithm chooses the positive semidefinite weighting matrix *Q* and positive definite weighting matrix R by attempting to place closed loop poles at selected positions. If the desired poles lie outside the allowable LQR region, the algorithm finds the achievable poles inside the region that are closest to the desired poles. The solution requires using a gradient search technique to minimize a weighted eigenvalue difference cost *function.* The weighting of the eigenvalue difference establishes the relative importance between the poles. In a multi-input multi-output system, the placement of one pole effects the allowable placement region of the other poles. Thus, the heavier weighted poles have precedence and are forced closer to their desired location.[38]

3.4.2 Problem Statement

Consider the state space representation of a linear time invariant system

$$\begin{aligned} \dot{x} &= Ax + Bu \\ y &= Cx \end{aligned} \tag{III.33}$$

where **x** is an n-dimensional state vector, u is an m-dimensional input vector and y is an 1-dimensional output vector. A, B, and C are constant matrices of the appropriate size.

Assuming (A, B) is controllable, a linear feedback of the state variables

$$u = -Kx \tag{III.34}$$

can be found that shifts the closed loop poles to the desired locations. A problem arises when a control is required to drive the plant output from a nonzero state to the zero state for a plant subjected to unwanted disturbances. The problem is to drive the system back to the zero state as fast as possible while trying to use the smallest control inputs. Anderson and Moore define this as the regulator problem.[39]

The optimal solution is to find the control input u to minimize the quadratic cost function

$$J = \int_0^\infty (\mathrm{x}^T \mathrm{Qx} + \mathrm{u}^T \mathrm{Ru}) dt \tag{III.35}$$

where **Q** and R are weighting matrices to be selected by the user. This is the classical linear quadratic regulator design problem. An advantage of using LQR design is that the system will always be stable and robust. The optimal solution is given by

$$K = R^{-1}B^T P \tag{III.36}$$

where P is found from the algebraic Riccati equation

$$PA + A^T P + Q - PBR^{-1}B^T P = 0 \tag{III.37}$$

LQR method guarantees robustness, but only allows pole placement in a specific region, and the poles that give the desired performance may or may not be in these regions. Therefore, it may not be possible to use this method to achieve both robustness and exact pole placement. In that case a choice would have to be made. This part takes the stance that robustness has higher priority over pole placement and hence uses the LQR technique to choose the poles. When the desired pole is outside the allowable LQR region, a gradient search is used to find the achievable pole inside the region that is the closest to the desired pole. This is done by minimizing the following cost function.

$$J^* = \sum_{i=l}^{u}\left[V_i\left(\lambda_{des\_i} - \lambda_{\text{ach}\_i}\right)^2\right] \tag{III.38}$$

V_i is a positive definite weighting parameter for the poles, λ_{des_i} is the i^{th} desired pole,

λ_{ach_i} is the i^{th} achievable pole from LQR.

Thus, when J is made small, convergence to the desired poles and robustness are simultaneously achieve.

Pole weighting is included in the cost function to give more priority to poles that need to be a specific value. Some poles may have limitations that prevent deviations from the desired locations. For example, an actuator may have characteristics that determine the location of the pole, and if a designer were to move the pole he would violate the physical model. To circumvent this, a high weighting is placed on that particular eigenvalue difference in the cost function.

For the linear, time-invariant system, the Linear–Quadratic Regulator (LQR) problem is, given an initial condition $x(0) = x_0$, to find a state feedback $u = Fx$

that minimizes the cost function[14]–[16]

$$J = \int_0^\infty (\mathrm{x}^T Qx + u^T Ru^T)dt \tag{III.39}$$

Where $Q,R > 0$. $R \succ 0$

The solution to this problem is well known and

$$u = -Fx = -R^{-1}B^T P \tag{III.40}$$

where $P > 0$ and solves the following Algebraic Riccati Equation:

$$A^T P + PA - PBR^{-1}B^T P + Q \prec 0 \tag{III.41}$$

Furthermore,

$$J_{\min} = \min \int_0^\infty (\mathrm{x}^T \mathrm{Qx} + \mathrm{u}^T \mathrm{Ru})dt \prec x_0^T P x_0 \tag{III.42}$$

The LQR problem can also be formulated as an LMI Problem. It can be shown by direct deductions that with a $P > 0$ satisfying the following matrix inequality:

$$A^T P + PA - PBR^{-1}B^T P + Q \prec 0 \tag{III.43}$$

and by setting the negative state feedback matrix $F = R^{-1}B^T P$ we have

$$J_{\min} = \min \int_0^\infty (\mathrm{x}^T \mathrm{Qx} + \mathrm{u}^T \mathrm{Ru})dt \prec x_0^T P x_0 \tag{III.44}$$

Hence we can reduce the cost function J if we can find smaller P .

However, is not a linear inequality in P . We need a few “tricks” here.

First, we define $L = P^{-1}$ and pre- and post-multiply L on both sides of the inequality , which changes it into

$$LA^T + AL - BR^{-1}B^T + LQL \prec 0 \tag{III.45}$$

Next, we use the following Schur Complement Formula to transform equivalently into linear inequalities.

Schur Complement Formula For a symmetric matrix

$$M = \begin{bmatrix} M_{11} & M_{12} \\ M_{21}^T & M_{22} \end{bmatrix} \tag{III.47}$$

$M \prec 0$ if and only if $M_{22} \prec 0$ and $M_{11} - M_{12}M_{22}^{-1}M_{12}^T \prec 0$. (III.48)

Complement Formula can be verified by pre- and post-multiplying

$$\begin{bmatrix} I & -M_{12}M_{22}^{-1} \\ 0 & I \end{bmatrix} \tag{III.49}$$

and

$$\begin{bmatrix} I & 0 \\ -M_{22}^{-1}M_{12}^{T} & I \end{bmatrix} \tag{III.50}$$

respectively, on both sides of the inequality $M \prec 0$

Now by defining $M_{11} = LA^T + AL - B^{-1}RB^T$, $M_{12} = L$ and $M_{22} = -Q^{-1}$

and using the Schur Complement Formula, solving the quadratic matrix inequality is equivalent to solving the following linear matrix inequality:¨

$$\begin{bmatrix} LA^T + AL - B^{-1}RB^T & L \\ L & -Q^{-1} \end{bmatrix} \tag{III.51}$$

Further, in order to find the minimal cost function, we may minimize γ, $\gamma \succ x_0^T P x_0$ is required,i.e. $\gamma - x_0^T P x_0 = 0$. To write this inequality in terms of L, the Schur Complement Formula can be used again. By defining $M_{11} = -\gamma, M_{12} = x_0^T$ and $M_{22} = -L = (-P^{-1})$,it is equivalent to

$$\begin{bmatrix} -\gamma & x_0^T \\ x_0 & -L \end{bmatrix} \prec 0 \tag{III.52}$$

Therefore, the state feedback matrix F , in u = -Fx, which leads to the minimal cost function J can be found by solving the following LMI optimization problem for L > 0 and γ > 0:

$$\begin{aligned} &\min \gamma \\ &s.t. \begin{bmatrix} -\gamma & x_0^T \\ x_0 & -L \end{bmatrix} \prec 0 \end{aligned} \tag{III.53}$$

$$\begin{bmatrix} LA^T + AL - B^{-1}RB^T & L \\ L & -Q^{-1} \end{bmatrix} \prec 0 \tag{III.54}$$

And

$$F = R^{-1}B^T L^{-1} \tag{III.55}$$

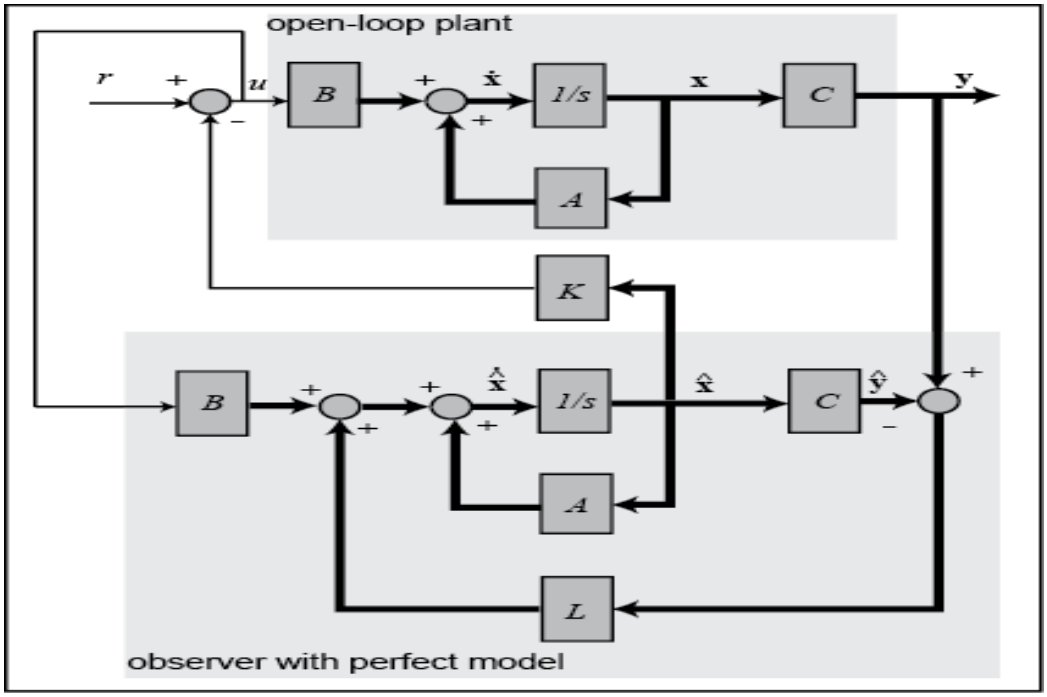

Figure 26 System with LQR controller with Estimator

Figure 49 shows the representation of the Regulation system using LQR controlls and Estimator which estimate the state feedback

3.4.3 Simulation Results

The first test consists of performing active and reactive power steps while the machine is driven at a fixed speed.

Conditions of the test:

at t = 0.2 s and t=0.5 s : active reference power (Pref from 0 to -5000W than to -1000)

at t = 0.2 s: reactive reference power (Qref from 0 to 1000 VAR)

Figure 50 shows the results obtained in the case of direct control.

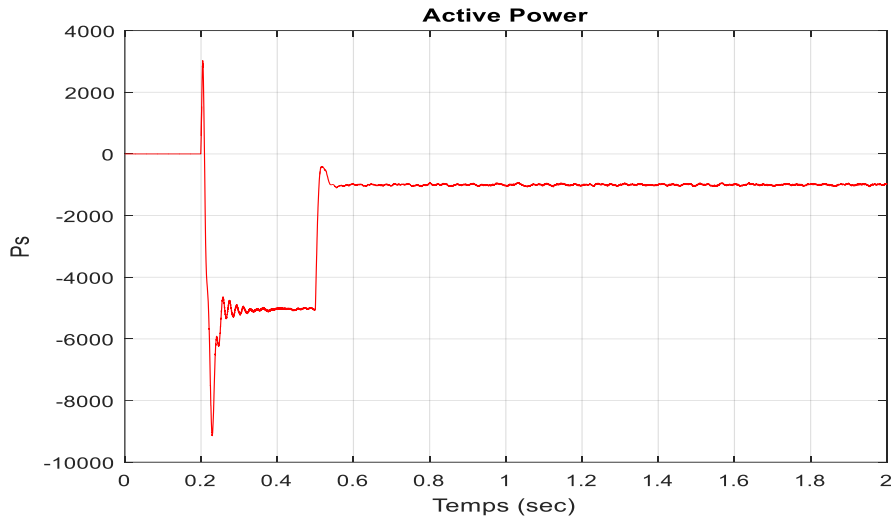

Figure 27 Active Power using LQR controllers

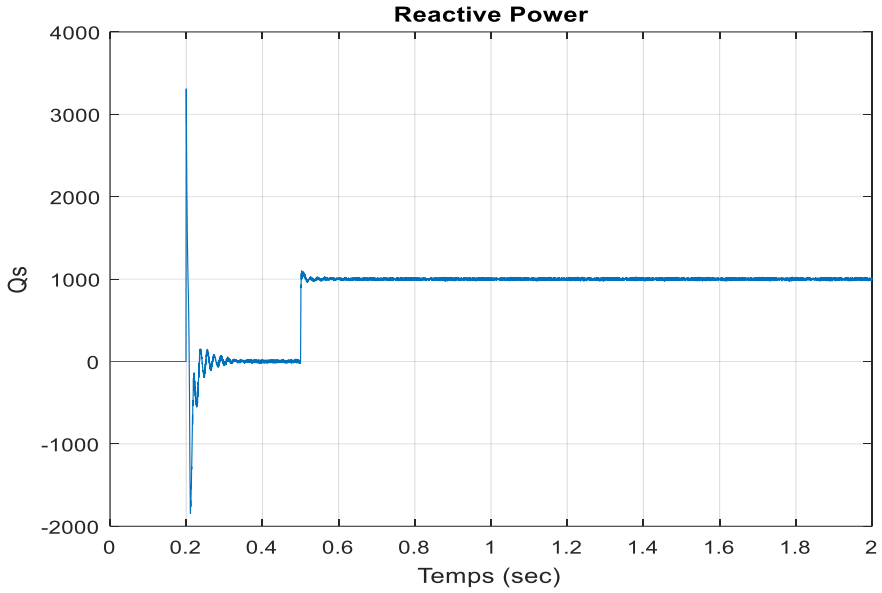

Figure 28. Reactive Power using LQR controllers

Robustesse test of LMI-LQR

At 1 sec We vary the following parameters Rs=2*Rs; Rr=2*Rr ;Ls=0.5*Ls ;Lr=0.5*Lr

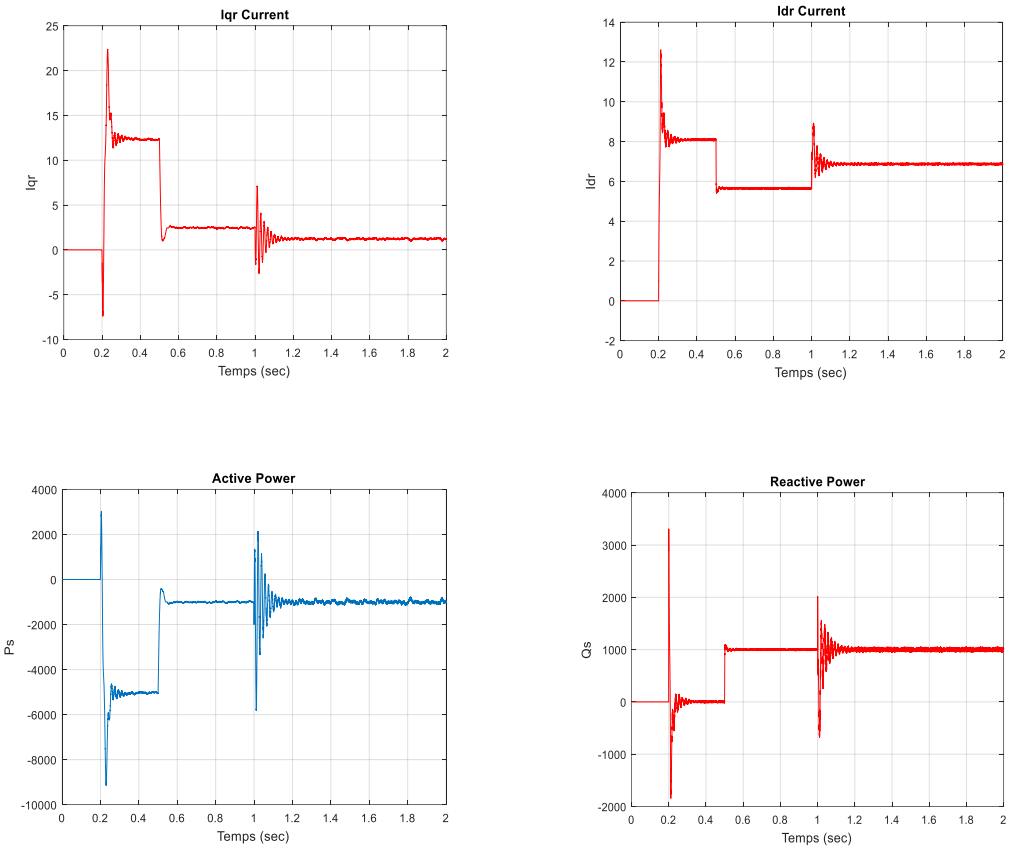

3.4.4 Linear Quadratic Gaussian

If a linear time invariant system is completely controllable, the poles can be placed anywhere in the complex plane using full state feedback. It makes sense to place all the poles in the left half plane for stability, but it is also desirable to place the poles far to the left to make the transients die out quickly. By doing this the system would converge quickly to its steady state, but the control inputs may be excessively large. The control input amplitudes are physically limited which puts a constraint on the speed of the system or how far left the poles can be shifted. The relative importance of system speed to control input amplitude naturally leads to an optimization problem.

To formulate the linear quadratic regulator problem, first consider the state space representation of a completely controllable linear time-invariant system

$$\dot{x} = Ax + Bu \tag{III.56}$$

with the full state feedback law $u = -Kx$. Then the closed loop system poles

$$\dot{x} = (A + BK)\,\mathrm{x} \tag{III.57}$$

are the eigenvalues of:

$$\det(\lambda \mathrm{I} - \mathrm{A} + \mathrm{BK}) \tag{III.58}$$

With the appropriate feedback gains, these poles can be shifted to any desired location. The problem is to place the poles such that the system comes to its steady state as fast as possible with the least control inputs. With this in mind, a criterion to measure the speed at which an initial state is returned to the zero state (which is the desired steady state) is given by:

$$\int_{t_0}^{t_1} x^T Q x dx \tag{III.59}$$

where the state weighting matrix Q is a positive-definite symmetric real matrix.

The matrix Q is chosen to indicate the relative importance of each state component. The integral in equation (II.42) measures the deviation of x from its steady state value during the time $(t_1 - t_0)$.

By minimizing this criterion, the states will now be driven to the steady state as fast as possible, but the system will experience large control amplitudes. To prevent the large control amplitudes, a term must be added to equation (II.42) to include the input. Thus, the criterion to be optimized is defined by

$$J = \int_{t_0}^{t_1} (\mathrm{x}^T \mathrm{Qx} + \mathrm{u}^T \mathrm{Ru}) dt \tag{III.60}$$

Where the controls weighting matrix R is a positive-definite symmetric real matrix which determines the relative importance of the control inputs. This integral is called the linear quadratic regulator cost function or performance index. The problem now lies in finding the input u that minimizes the performance index J.

From optimization theory, the feedback law $\mathrm{u} = -\mathrm{kx}$ that minimizes equation (III.60) as $t_1 \to \infty$

$$K = R^{-1} B^T P \tag{III.61}$$

The matrix P is the positive-definite solution (which is unique) of the algebraic Riccati equation:

$$PA + A^T P + Q - PBR^{-1} B^T P = 0 \tag{III.62}$$

By requiring the matrix Q to be positive definite, all the states will appear in the

$x^T Qx$ term.

This ensures that all initially unstable poles are observable (which is a requirement for stability).

By defining $H^T H = Q$ and requiring **[A,H]** to be detectable, the closed loop system will be always stable.

As mentioned before, the designer has the freedom to choose the weighting matrices **Q** and R. Equation (III.45) shows that the choice of **Q** and R will influence P, the solution of the algebraic Riccati equation. Note that, from equation (III.45), the matrices **P** and **R** play an important role in determining the feedback matrix K. Since the feedback matrix **K** shifts the poles of the system, the elements of **Q** and **R** become the design parameters for pole placement.

3.4.5 LQG CONTROLLER DESIGN

Linear Quadratic Gaussian (LQG) is a system formed by gathering linear equation with quadratic one. A merger between LQ controller and Kalman estimator prescribe LQG methodology. A cost function could be optimized by loop system as LQG approach determines state-feedback gain. As a matter of fact, LQG is deduced from LQR technique. In order to obtain the weighting matrices in LQR design artificial intelligence technique have been applied.

Linear state space model of the LQG controller and Kalman filter, which estimate state vector from the sensors measurements and the control model by the multivariable state feedback.[40] [41]

$$\begin{cases} \dot{x} = Ax + Bu + Gw \\ y = Cx + Du + \mu \end{cases} \quad \text{(III.63)}$$

The Kalman filter and the state feedback are designed taking into account measurements noises and plant disturbances, The Kalman filter and the state feedback take into consideration measurements noises and plant disturbances, using w and μ to express the model uncertainty and measured output noise while w and μ are white noise

$$E\left[ww^t\right] = \Xi \geq 0, E\left[\mu\mu^t\right] = \Theta \succ 0 \quad \text{(III.64)}$$

Assuming w and u are independent of each other then:

$$E\left[w\,\mu^t\right] = 0 \quad \text{(III.65)}$$

The cost function is chosen as follows:

$$J = E\left(\int_0^{\infty}\left[z^t Qz + u^t Ru\right]dt\right) \quad \text{(III.66)}$$

where z Mx is a combination of the state variable, weighted matrix Q is a symmetric semi-definite positive matrix, R is a symmetric definite positive matrix, i.e.

$Q = Q^t \geq 0, R = R^t \succ 0$, In practice, considering the random measured noise, the system states derived from the state-space equation getting from Kalman filter. This

requires the determination of the optimal state estimation $\hat{x}(t)$ that minimize $E\left[(x-\hat{x})(x-\hat{x})^t\right]$

. Then using $\hat{x}(t)$ substitute the state variables.[38]

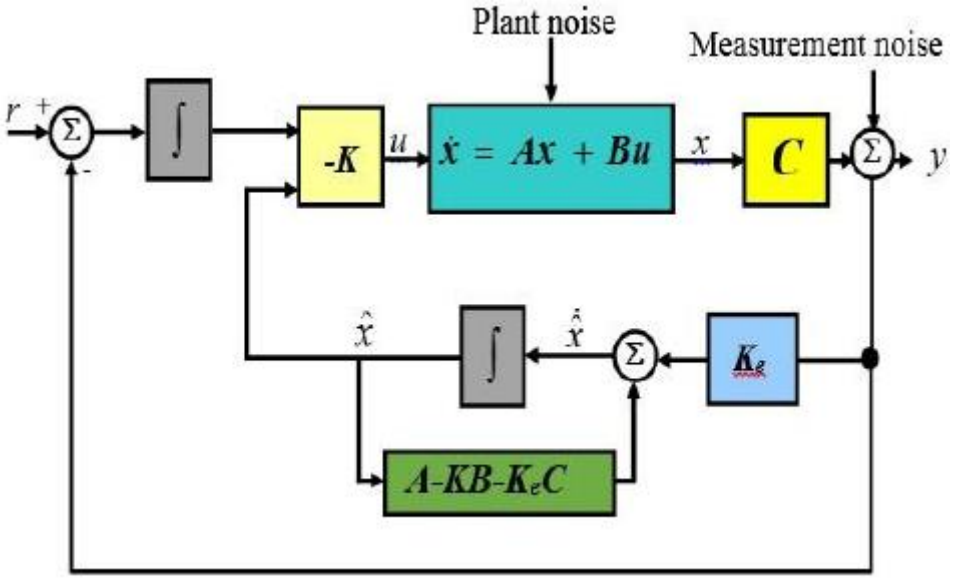

Figure.29. Basic Structure of a LQG controller

3.4.6 Simulations Results

The DFIG model associated with turbine emulator which is now controlled with MPPT.
Our system described is simulated using MATLAB Script Program. Figure 54 shows the dynamic responses of the active and reactive powers with both LQG and the SM controllers. The powers generated follow their reference signals. Figure 53 shows the corresponding currents and flux residues. These results demonstrate the effectiveness of the proposed control strategy for the wind energy conversion system.

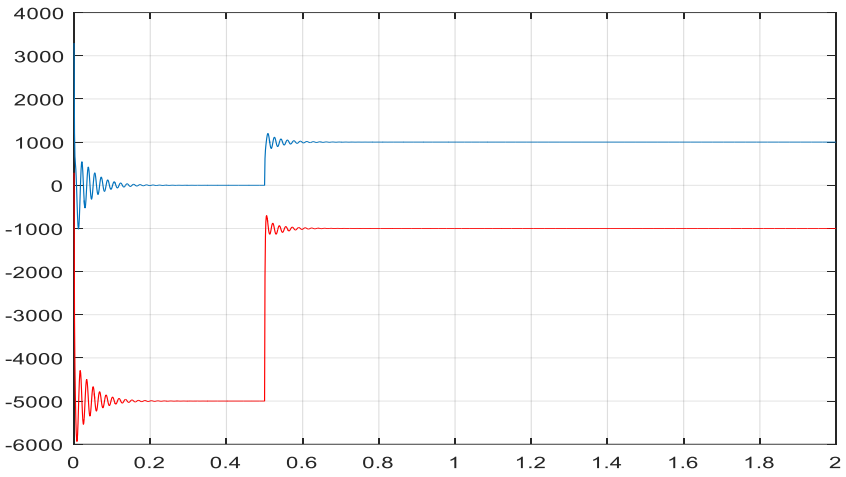

Figure 30.Acitive and Reactive Powers LQG control

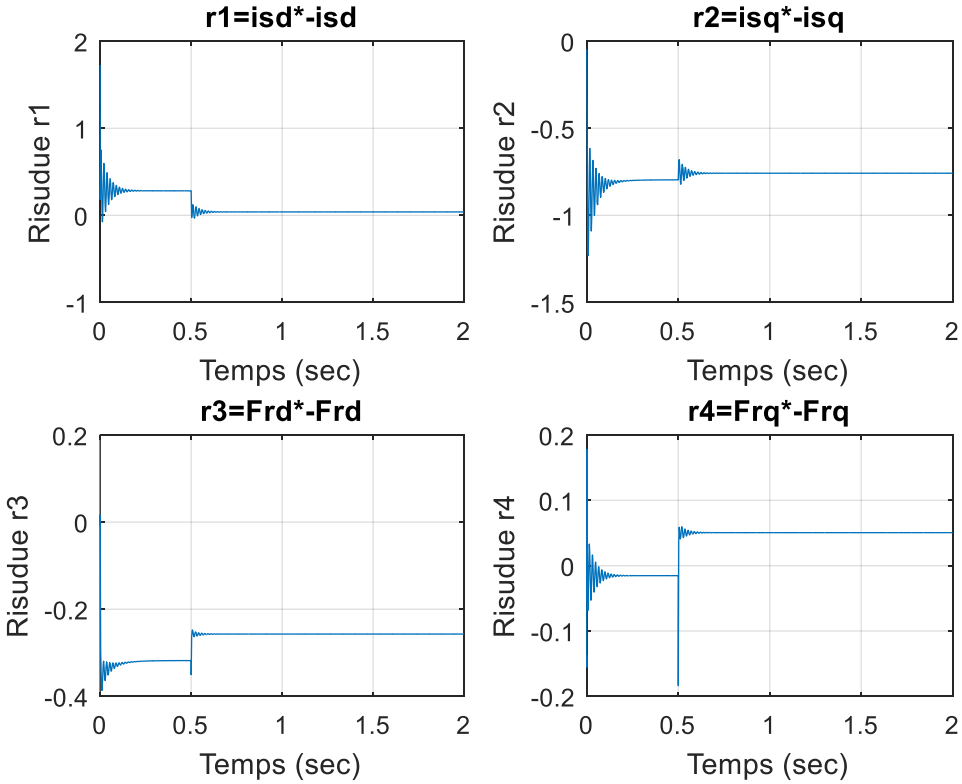

Figure 31 Currents and flux residues

3.5 CONCLUSION

This chapter allowed us to establish the synthesis of three different approaches for the control of the Double Feed Induction Generator. A Proportional-Integral regulator that served as a comparison reference, Sliding Mode Control and an LQG controller based on the minimization of a quadratic criterion. The purpose of these regulators is to control the active and reactive power exchange between the stator of the machine and the network by modifying the amplitude and the frequency of the rotor voltages.

The differences between the three regulators are not very significant with regard to the setpoint tracking and robustness, although the LQG regulator and SM controllers seem to yield relatively better results. In the face of disturbances, the PI regulator, which does not take them into account in its synthesis, is less efficient than the LQG and SM Controllers

CHAPTER 04

FAULT TOLERANT CONTROL SYSTEMS

4.1 Introduction

The performance of the designed controller can be easily interrupted by possible faults and failures in different parts of the system. Therefore, looking for fault-tolerant controller designs with early fault detection, isolation and successful controller reconfiguration would be very beneficial in wind turbine operation. This chapter provides a review of fault-tolerant control designs for wind turbine systems and provides a framework for further research topics in this important and rapidly growing field of research. [42] [43] [44]

For the fault detection and state estimation we used a Bank of four Observers and for r the control reconfiguration we used four type of machine controls.

4.2 Structure and Approaches to FTC Systems

Generally the nominal controller (sometimes referred to as the 'baseline' controller, aims to stabilize and achieve the required closed-loop performance during normal operating conditions. To give the controlled system the ability to tolerate fault effects, additional inherent ability of the controller and/or extra assistant blocks should be inserted in the control loop. Figure 56 illustrates the main structure of the fault tolerant system. Generally, two steps are required to provide the system with the capability to tolerate faults:

• Equip the system with some mechanism to make it able to detect the fault once it occurs, provide information about the location, identification of faulty component and decide the required remedial action in order to maintain acceptable operation performance (Supervision level).

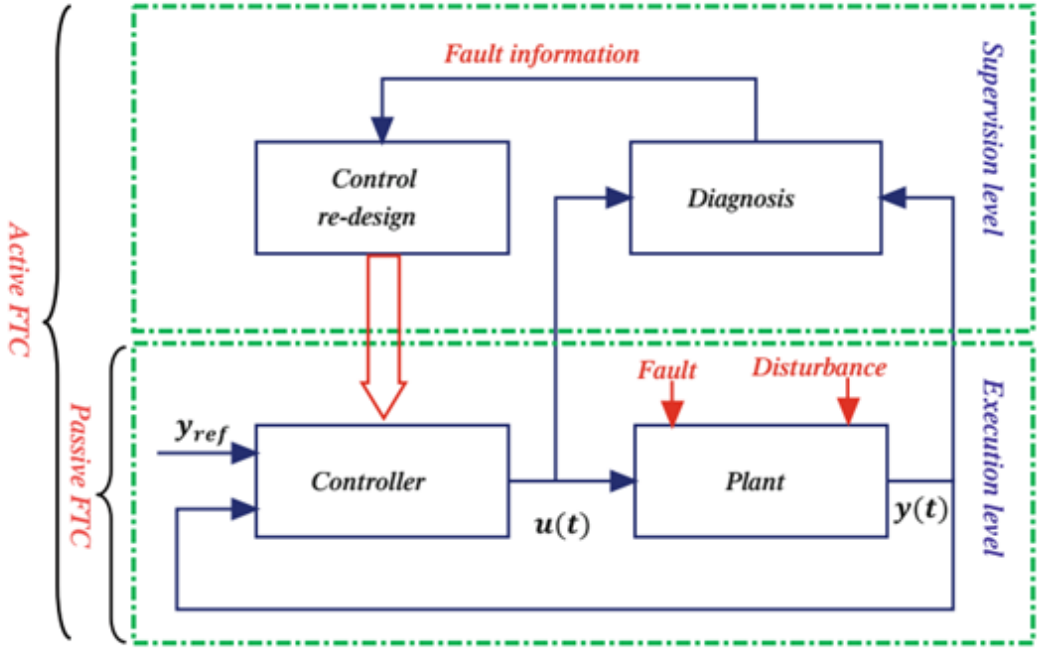

Figure 32. Schematic of the Fault Tolerant System

Make use of the information obtained from the supervision level and adapt the controller parameters and/or reconfigure the structure of the controller so that the required remedial activity can be achieved (Execution level). Hence, the FTC loop extends the usual feedback controller by a supervision level. In the absence of a fault, the system matches its nominal response so that the nominal controller attenuates the disturbance and ensures good reference following and other requirements on the closed-loop system. In this situation, the diagnostic block recognizes that the closed-loop system is fault-free and no change of the control law is necessary.

If a fault occurs, the supervision level makes the control loop fault-tolerant. The diagnosis block identifies the fault and the control re-design block adjusts the controller to the new controller parameter set. Following this, the reconfigured system continues to satisfy the control target. Thus, FTC is the control loop that has the ability to fulfil the required system performances even if faults occur through utilizing the help provided by the supervision level. Approaches for synthesizing the FTC loop are classified as either a passive FTC (PFTC) or active FTC (AFTC). In the PFTC approach, the control loop is designed to tolerate some anticipated types of faults. The effectiveness of this strategy, that usually handles anticipated faults scenarios, depends upon the robustness of the nominal closed-loop system. Additionally, since the robustness of the closed-loop system to the fault is considered during the design cycle of the

nominal controller, this may lead to post-fault degraded performance of the closed-loop system. However; it is interesting to note that the PFTC system

does not require the FDD and controller reconfiguration and hence it has the ability to avoid the time delay due to online diagnosis of the faults and reconfiguration of the controller. In fact, this is very important in practice where the time windows during which the system remains stabilizable in the presence of faults are very short. Most of the PFTC methods have been proposed mainly based on robust control theory.

However, the fundamental difference between the traditional robust control and the PFTC lies in the fact that robust control deals with small parameter variations or model uncertainties, whilst PFTC deals with more drastic changes in system configuration caused by faults. It should be noted that in the early literature the PFTC approach was referred to as 'reliable control'. In order to improve the post-fault control performance and cope with severe faults that break the control loop, it is commonly advantageous to switch to a new controller that is on-line or designed off-line to control the faulty plant. In the AFTC approach, two conceptual steps are required: FDD and controller adjustment so that the control law is reconfigured to achieve performance requirements, subsequent to faults. An AFTC system compensates for faults either by selecting a pre-computed control law (projection-based approaches) or by synthesizing a new control strategy online (online automatic controller redesign approaches). Another widely studied method is the fault compensation approach, where a fault compensation input is superimposed on the nominal control input. It should be noted that owing to the ability of the traditional adaptive control methods to automatically adapt controller parameters to changes in system parameters, adaptive control has been considered as a special case of AFTC that obviates the need for diagnosis and controller re-design steps . Figure 57 shows a general overview of the main approaches used to achieve FTC for each class .[45] [46] [47]

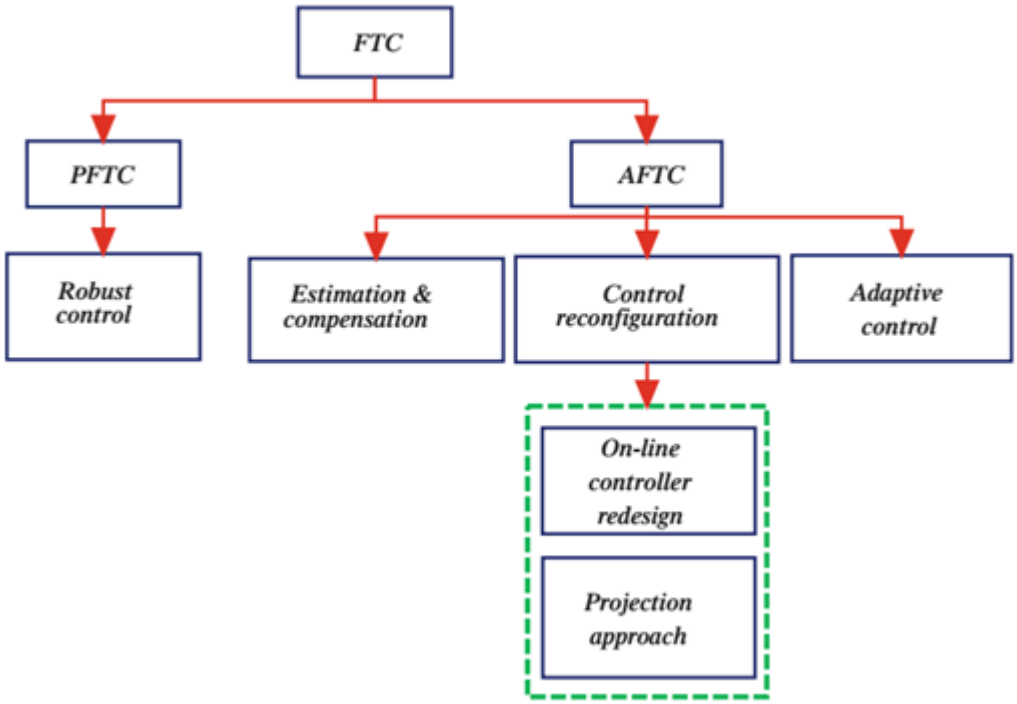

Figure 33. General Classification Of FTC Methods

4.3 Physical and Analytical Redundancies

For systems whose failure involves human life and high economic costs, such as transportation aircraft, highly reliable architectures must be adopted for their control. [45], [48]

4.3.1 Physical redundancy:

This technique consists in disposing in parallel of identical subsystems or components to diminish the probability of their overall failure. Redundant actuators will allow to continue to act on a process while redundant sensors will allow to detect the failure of one of them and adopt the correct signal. High order physical redundancy can be of interest for critical components. Then subsystems which develop a critical function whose failure should be proven to be extremely improbable may present a duplex, triplex or even quadruplex architecture. Figure 58 displays main redundancies in the roll control channel of past generation transportation aircraft (A300). [48]

4.3.2 Analytical redundancy:

The concept of analytical redundancy is based on the use of a mathematical model of the controlled system which displays analytical relationships between different physical parameters. Then the measure of some physical parameters provides indirect information about

others which may be no more accessible to measurement when the sensors in charge of their direct measure fail. Analytical redundancy is mainly used for fault detection and identification. There residuals can be computed from the comparison of measurements with expected values from mathematical models, leading when threshold levels are exceeded to detect possible faults.

For example, roll, pitch and yaw rates of an aircraft can be either estimated from attitude angles measures through the Euler or measured directly with gyrometers. Since modern transportation aircraft make use of three gyro lasers, the failure of one of them will be detected by majority voting and the triplex redundancy will be maintained by replacing the measure of the failed gyro laser by the estimation from the Euler equations and the attitude measurements. This can be done simultaneously for the three body axis. Also, to feed the longitudinal normal law of modern transportation aircraft, Airbus uses analytical redundancy to validate the pitch rate information when provided by a single inertial reference unit. The load factor is estimated through the pitch rate information and compared to the available accelerometric measurements in order to validate the Inertial Reference System (IRS) data. [48]

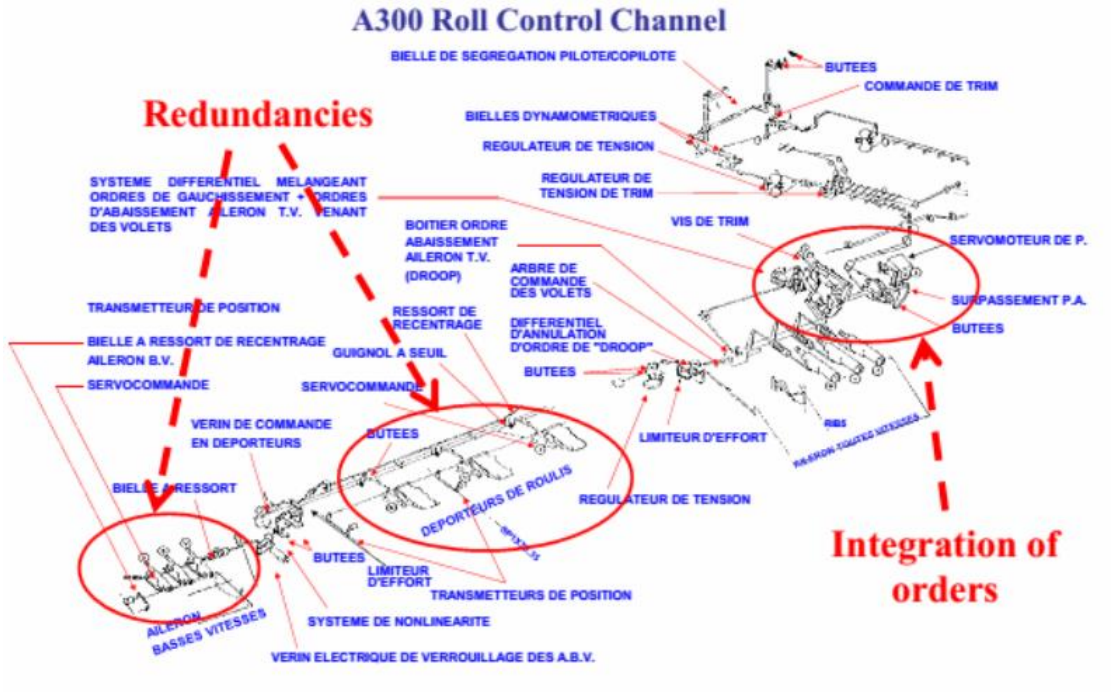

Figure 34. Main physical redundancy in A300 roll control channel

The adoption of analytical redundancy techniques can also to reduce the overall weight of the resulting fault tolerant critical system and to limit its maintenance needs. In many situations, it appears that a combination of the two forms of redundancy provides better solutions.[49]

The general structure of a fault tolerant flight control system is shown in Figure 57 where physical redundancies of actuators, sensors and control computers are colored in red. Of course, the circuits between actuators, sensors and control computers present also an adequate degree of physical redundancy. Observe that since the failure of actuators or sensors may break critical control loops, redundancy is commonly introduced at their level. In Figure 58, information flows resulting from analytical redundancy are colored in blue.

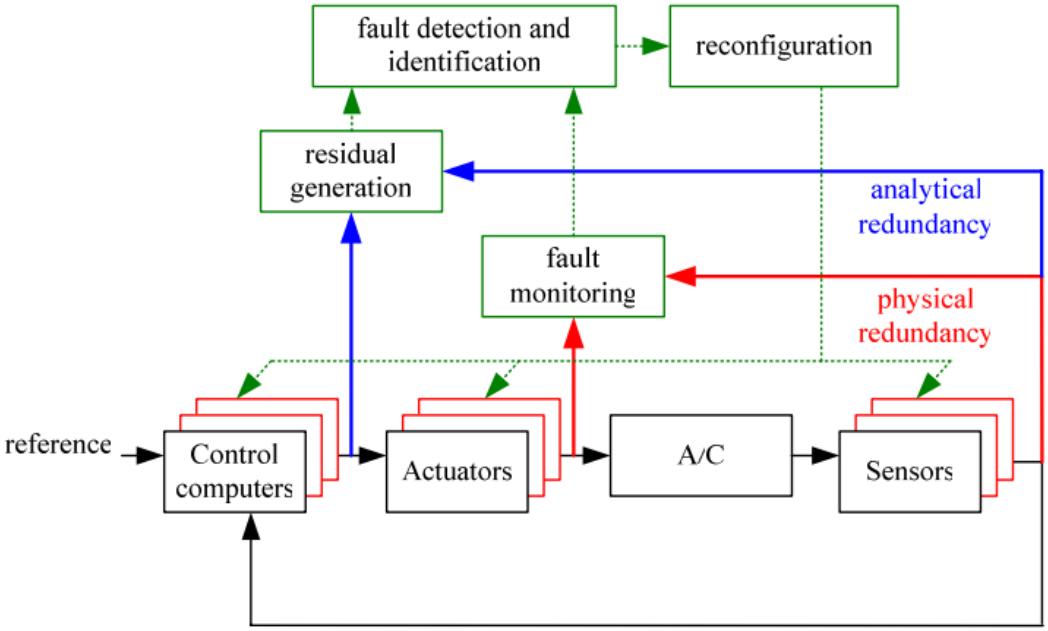

Figure 35. General view of a fault tolerant flight control system

4.4 Fault Detection and Identification

Faults leading to failures of a controlled physical process can appear either at the level of the control channels, at the level of the controlled process itself or at the level of the data channels Figure 59. An efficient fault detection and identification (FDI) scheme is essential to guarantee safety of a critical system by allowing the activation of automatic protections and reconfiguration mechanisms resulting in fault tolerance.

Fault detection and identification is composed of three main activities:

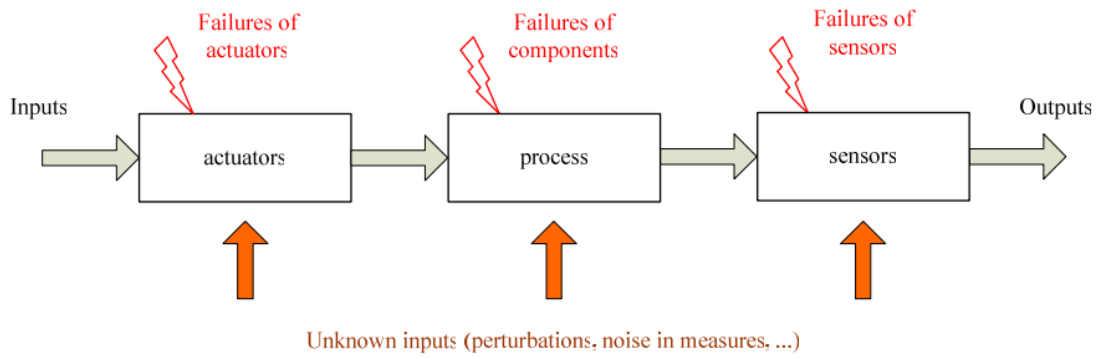

Figure 36. Fault localization in physical processes

4.4.1 Detection

A fault is detected in the system. If there is a nominal model of the fault free system, a fault will be characterized by the existing distance of the process parameters to those of the nominal model.

4.4.2 Location

It allows to trace the origin of the fault when a fault has been detected . In general an original fault may generate a sequence of failures in a system and these cascading failures may mask their real cause.

4.4.3 Identification

It determines the time the fault occurred, its duration and its amplitude. The main technical performance criteria for fault detection and identification are: detectability, isolability, sensibility and robustness.

4.4.4 The detectability

It is the ability of the diagnostic system to detect the presence of a failure in the process. It is closely related to the notion of fault indicators (residuals): the residual generator must, somehow, be sensitive to the failure to be detected. It will actually set a compromise between the false alarm rate and the non-detection.

4.4.5 The isolability

It is the ability of the diagnostic system to directly trace back the origin of the fault. Failure often causes a sequence of cascading alarms and it can be difficult to trace the original faulty

component. The degree of fault isolation is related to the structure of the generated residuals and to the detection technique.

4.4.6 The sensitivity

Is characterized by the ability of the FDI system to detect faults of a certain amplitude. It depends not only on the structure of the residuals but also of the relationship between the measuring noise and the fault.

4.4.7 The robustness

Characterizes the ability of the FDI system to detect faults regardless of modeling errors (sensitivity to residual faults and insensitivity to disturbances). Most studies about the development of new fault detection and identification devices have concentrated on the generation of residuals based on analytical redundancy which allow probabilistic tests to decide about the presence of a fault or not. Figure 61 displays the data processing sequence in a model based FDI technique.

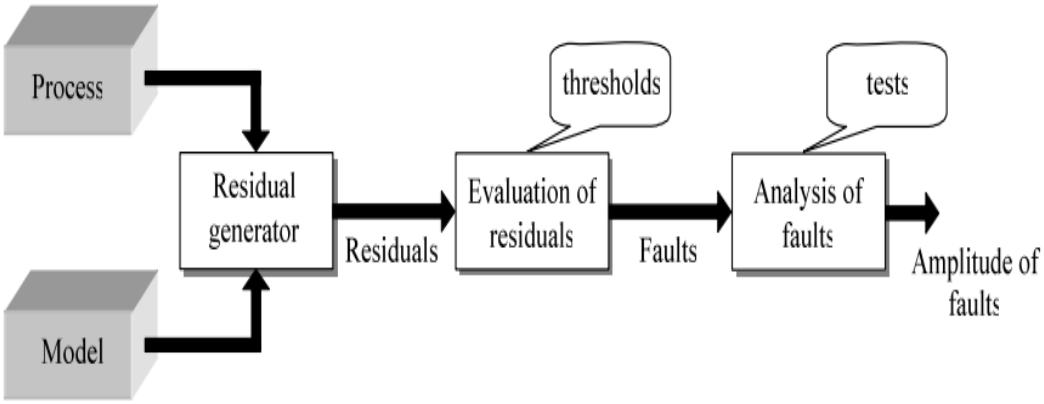

Figure 37. FDI based on residuals analysis

To have an overview of FDI techniques including advanced methods based on mathematical properties of flight dynamics models which allows to perform FDI on highly nonlinear systems. Figure 61 displays the general architecture of a FDI system for a physical process. Going back to transportation aircraft, multiple air and inertia data channels (ADIRUs) are used to provide online redundant data for the flight control system. Voting schemes ensure that the transmitted signal is correct while faulty sensors can be detected. Fault detection is mainly performed by cross checks, consistency tests, voting mechanisms and built-in test techniques of varying sophistication . For example, threshold logics are often used for actuator and sensor monitoring.

If a measurement signal exceeds a given limit threshold, then the failure of this measurement unit is declared. Besides these classical fault detection techniques, modern fault detection and identification approaches start to be used onboard aircraft. For example, analytical redundancy techniques are already used on A340 and A380, though it is not used widely.[50] [51]

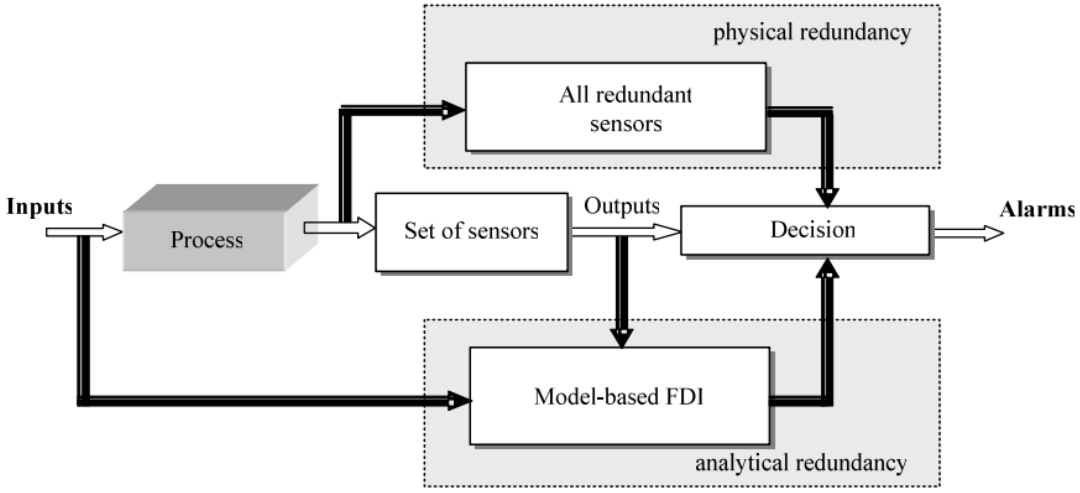

Figure 38. General architecture of a FDI system

4.5 Fault Tolerant Control

As stated above, to meet the stringent requirement of airworthiness regulations, flight control systems are extremely redundant, resulting in safe fault tolerant systems. However, increased physical redundancy not only supposes higher production and maintenance costs, but also is the cause of larger weight. Moreover, even with this redundancy level it seems that the performance of conventional control techniques is hardly able to tackle efficiently unexpected or novel failure situations. So, new control laws are being developed to maintain system performance and stability in the event of failure. Fault tolerant control laws are expected to help to reduce the redundancy degree of the control system while improving its safety level. It has been argued that several air transportation accidents could have been avoided if fault tolerant control techniques have been in use.[52] [53]

A fault tolerant control system has the ability to deal with its faults automatically so that it is able to achieve its control objectives.

In general, the fault tolerant control system must guarantee at least stability and/or acceptable degraded performance in the presence of major failures (failures of sensors and actuators, physical changes of the controlled process).

Over the last three decades, the growing demand for safety, reliability, maintainability, and survivability in safety-critical systems has motivated significant research in fault tolerant control [54]. Both classes of FTC approaches integrate the FDI capability while the active FTC techniques include also fault accommodation and control system reconfiguration capabilities. [55] The main ideas related to the design and development of a reconfigurable control system were initially proposed by Blanke[56][50].

An efficient implementation of a reconfigurable fault tolerant control system will depend on the ability of the FDI subsystem to identify the fault timely and accurately. Figure 63 displays the general structure of a fault tolerant flight control system implementing automatic reconfiguration.

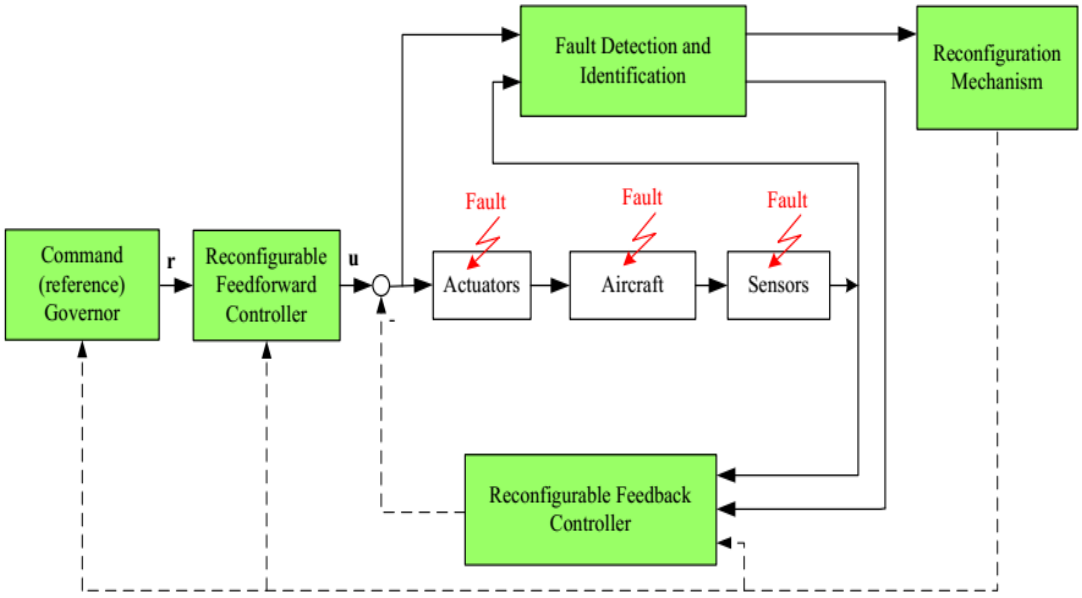

Figure 39. General scheme of a fault tolerant control system

It consists of fault detection and identification module, a reconfigurable control module designed to activate fault free redundant components and a flight control law reconfiguration module to adapt the control law to the new control situation (active actuators and sensors, operational state of the controlled process). There, the solid lines represent the main signals (control, instructions, estimates, measures) while the dotted lines represent adaptation (adjusting, programming, reconfiguration or restructuring).
It appears opportune to include in a fault tolerant control structure, next to an FDI module, a supervision module associated to the knowledge base and whose main function is to decide if the fault situation can be managed as a fail-operational or a fail-passive situation. In the first case, through an actuator reassignment module.[48] [57]

The current flight condition (manual or auto flight modes) at the occurrence of the fault will be maintained as well as the nominal handling performances of the aircraft, since the remaining active actuators are found able to produce timely the required moments to perform nominal maneuvers [48].

Figure 64 (a) displays the fail-operational case with a running autopilot. Otherwise, Figure 64 (b), to insure a fail-passive situation, flight control will return to manual mode through the actuator reassignment module and with the help of a flight director. The flight director modes which provide tendency information to the pilot will take into account the identified downgraded handling capability of the aircraft under the

current actuator failure situation. [58], [28]

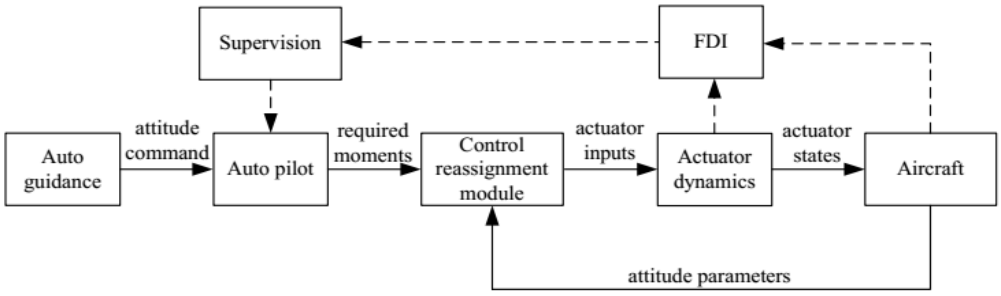

(a) fail-operational mode

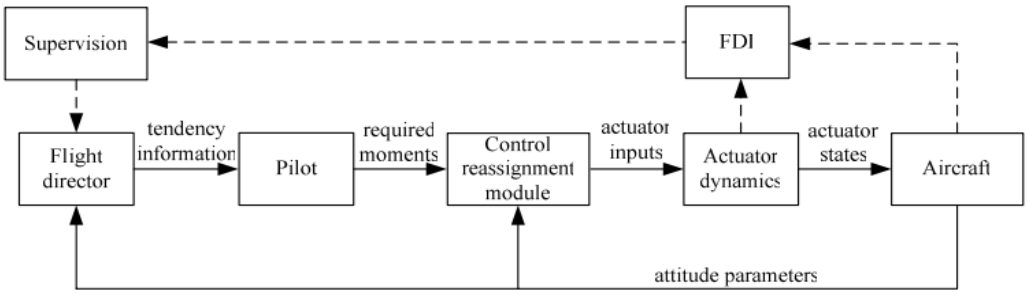

(b) fail-passive mode

Figure 40. Possible fail modes for a fault tolerant control structure

4.6 Different Type of Faults

Fault tolerance is the ability of a control system to maintain control objectives, despite the occurrence of a fault. Dynamic systems can be subjected to various faults as caused by actuators, sensor or component failures. To understand the difference between fault and failure, the exact definitions are provided at the following.

4.6.1 Failure

Inability of a system or a component to accomplish its function. Note that faults can be overcome using fault-tolerant control. But failure leads to system or component shut off since it's an irrecoverable event.

From control engineering point of view there are three different types of faults as shown in Figure 65.

4.6.2 Fault

A fault in dynamical systems is a deviation of the system structure or the system parameters from the nominal situation.

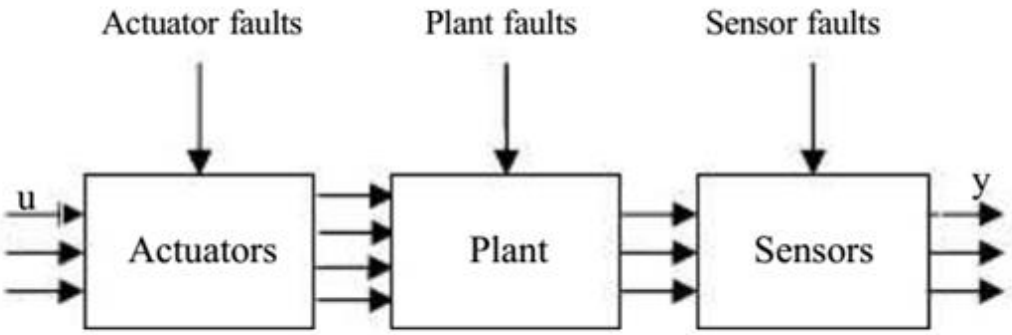

Figure 41. Different types of faults

4.6.2.1 Sensor faults

plant properties are not affected, but sensor readings have substantial errors.

4.6.2.2 Actuator faults

Plant properties are not affected, but the influence of the controller on the plant is interrupted or modified.

4.6.2.3 Plant (system) faults

dynamical I/O properties of the plant are changed.

Note that faults can occur both in component level and overall system level. For example in Figure 66, it is shown how a component level fault propagates in the system and influences all other components.

The effects of a fault in a single component may be of minor importance to the component itself. However, due to fault propagation throughout the overall system, the fault may eventually cause to system failure. It would be very beneficial if fault-tolerant control is applied in component level wherever possible.

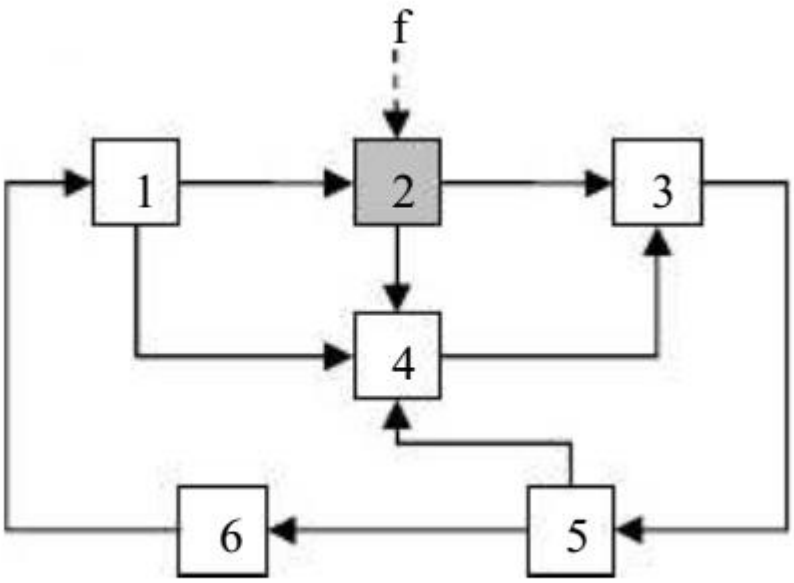

42. Fault propagation in overall system

4.6.3 Fault Detection

Decide whether a fault has occurred. This step determines the time at which the system is subjected to some faults.

There are four types of fault detection schemes [31]:

2 hardware redundancy

3 plausibility test

4 signal-based approaches

5 model-based approaches

The core of the first scheme consists in the reconstruction of the process components using the identical (redundant) hardware components. A fault in the process component is then detected if the output of the process component is different from the one of its redundancy. The plausibility test is based on the check of some simple physical laws under which a process component works. On the assumption that a fault will lead to the loss of the plausibility, checking the plausibility will reveal fault occurrence.

Under the assumption that certain process signals carry information about the faults of interest and this information is presented in form of symptoms, a fault detection can be achieved by a suitable signal processing. Typical symptoms are time domain functions like magnitudes, arithmetic or quadratic mean values, trends, or frequency domain functions like spectral power densities, frequency spectral lines, and etc.

The intuitive idea of the model-based fault diagnosis technique is to replace the hardware redundancy by a process model which is implemented in the software form on a computer. A process model is a quantitative or a qualitative description of the process dynamic and steady behavior. The difference between the measured process variables and their estimates is called residual.[59]

4.6.4 Fault Isolation

Determine in which components fault has occurred. Fault Identification: determine the type of fault and its severity.[60]

4.7 Estimator (observers)

The state of a dynamical system are variables that provide a complete representation of the internal condition or status of the system at a given instant of time. When the state is known, the evolution of the system can be predicted if the excitations are known.[26], Another way to say the same is that the state consists of variables that prescribe the initial condition. When a model of the structure is available, its dynamic behavior can be estimated for a given input by solving the equations of motion. However if the structure is subjected to unknown disturbances and is partially instrumented, the response at the unmeasured degrees of freedom is obtained using state estimation.
The basic idea in state estimation theory is to obtain approximations of the state of a system which is not directly observable by using information from a model and from any available measurements. There are three estimation problems, namely:

6 Estimate the current state, x_n given all the data including y_n ; this is called *filtering*.

7 Estimate some past value of x_k , $k \prec n$ given all the data including y_n ; this is called *smoothing*.

8 Estimate some past value of x_k , $k \succ n$ given all the data including y_n ; this is called *prediction*.

State estimation can be viewed as a blend of information from the analytical model of the system and measurements to make predictions about present and future states of the system. Uncertainty in estimating the state of a dynamical system arises from three sources:

9 Stochastic disturbances,

10 (2) Discrepancies between the real system and the model used to represent it (model uncertainty),

11 (3) Unknown initial conditions.

The theory of state estimation originated with least squares method essentially established by the early 1800s with the work of Gauss. The mathematical framework of modern theory of state estimation originated with the work of Wiener in the late 1940s. The field began to mature in the 1960's and 1970's after a milestone contribution was offered by R. E. Kalman in 1960 , which is very well-known as the *Kalman filter* (KF). The KF is a recursive data processing algorithm, which gives the optimal state estimate of the systems that are subjected stationary stochastic disturbances with known covariances.

4.7.1 Controllability and Observability

The concepts of controllability and observability are fundamental to state estimation theory, which were introduced by Kalman [61]. The following definitions of these concepts are adapted from the texts that cover the material.

A continuous-time system is *controllable* if for any initial state *x*(0) and any final time $t > 0$ there exists a control force that transfers the state to any desired value at time *t*. A discrete-time system is controllable if for any initial state *x*0 and some final time step *k* there exists a control force that transfers the state to any desired value at time *k*. A simple test of controllability for linear systems in the both the continuous-time and discrete time cases involves using the controllability matrix, namely

$$S = \begin{bmatrix} B & AB & A^2B \ldots & A^{n-1}B \end{bmatrix} \qquad \text{(IV.1)}$$

where n is order of the state. The system is controllable if and only if rank of S is equal to the n . A continuous-time system is *observable* if for any initial state $x(0)$ and any final time

$T \succ 0$ the initial state $x(0)$ can be uniquely determined by information of the input $u(t)$ and output $y(t)$ for all up time $t \in [0 \quad T]$ A discrete-time system is observable if for any initial state x_0 and some final time step k the initial state x_0 can be uniquely determined by knowledge of the input u_j and output y_i for all $j \in [0 \quad k]$.A simple test of observability for linear systems in the both continuous-time and discrete time cases involves using the observability matrix namely.

$$O = \begin{bmatrix} C \\ CA \\ CA^2 \\ CA^3 \\ \vdots \\ CA^{n-1} \end{bmatrix} \qquad \text{(IV.2)}$$

The system is observable if and only if rank of *O* is equal to the *n*.

The concepts of *stabilizability* and *detectability* are also closely related to the controllability, observability and modes of the system. A system is *stabilizable* if its unstable modes are controllable. A system is *detectable* if its unstable modes are observable.

4.7.2 Observers Synthesis

The observer operates in two phases. The first is an estimation step and the second is a correction step. Estimation is accomplished by calculating state quantities using a model, which is a copy of the system. The correction is done by adding the difference between the estimated states and those measured (estimation error) that is multiplied by the gain K. This gain governs the dynamics and the robustness of the observer. So his choice is important and must be adapted to the properties of the system whose states are to be observed.

Two approaches are used The linearization around operating point: this is the case of the Luenberger observer.

The gain construction based on the nonlinearity of the system: These observers are synthesized taking into account the nonlinear modelling of the system. This is the case of observers with sliding or high gain mode.

4.8 Sliding Mode Observer

In this part, the intention is to design a current-flux sliding observer based on a general class of manifold S_c the basic sliding mode observer design procedure is performed in two steps. Firstly, an attractive manifold $S_c(y,t) \in R^p$ is designed so that the output estimation error trajectories restricted to $S_c(y,t)$ will have a desired stable dynamics. In the second step, the observer gain, to stabilize the equivalent dynamic on $S_c(y,t)$ determined.[36],[63]

The statoric currents the rotoric speed $i_{s\alpha}, i_{s\beta}$, the rotor speed ω_r and input vector (u1, u2) are measurable. Adding, the speed dynamic ω_r is slower than the statoric currents. In the following, $\hat{i}_{s\alpha}, \hat{i}_{s\beta}$ are observed currents, $\tilde{\varphi}_{r\alpha}, \tilde{\varphi}_{r\beta}$ re observed flux, $\tilde{i}_{s\alpha}, \tilde{i}_{s\beta}$ are currents error observation and $\tilde{\varphi}_{r\alpha}, \tilde{\varphi}_{r\beta}$ are flux errors observations. De plus, we consider that the real flow is bounded as follows: $|\varphi_{r\alpha}| < \rho_1; |\varphi_{r\beta}| < \rho_2$

We propose the observer of the stator current $i_{s\alpha}, i_{s\beta}$:

$$\begin{pmatrix} \dot{\hat{i}}_{s\alpha} \\ \dot{\hat{i}}_{s\beta} \end{pmatrix} = -a_1 \begin{pmatrix} \hat{i}_{s\alpha} \\ \hat{i}_{s\beta} \end{pmatrix} + A_o . \begin{pmatrix} \hat{\varphi}_{r\alpha} \\ \hat{\varphi}_{r\beta} \end{pmatrix} - L_1 \begin{pmatrix} sign(S_{c1}) \\ sign(S_{c2}) \end{pmatrix} \tag{IV.3}$$

With

$$A_o = \begin{pmatrix} b_1 & c_1\omega_r \\ -c_1\omega_r & b_1 \end{pmatrix}; L_1 = \begin{pmatrix} L_{11} & 0 \\ 0 & L_{12} \end{pmatrix}; \tag{IV.4}$$

$$a_1 = \frac{R_s}{L_d}; a_2 = \frac{L_q}{L_d}; a_3 = \frac{1}{L_d}; \tag{IV.5}$$

$$b_1 = \frac{R_s}{L_q}; b_2 = \frac{L_d}{L_q}; c_1 = \frac{3.(P)^2}{2J}. \tag{IV.6}$$

The dynamic of the observation error $\hat{i}_{s\alpha}, \hat{i}_{s\beta}$:

$$\begin{pmatrix} \dot{\tilde{i}}_{s\alpha} \\ \dot{\tilde{i}}_{s\beta} \end{pmatrix} = -a_3 \begin{pmatrix} \tilde{i}_{s\alpha} \\ \tilde{i}_{s\beta} \end{pmatrix} + A_o . \begin{pmatrix} \tilde{\varphi}_{r\alpha} \\ \tilde{\varphi}_{r\beta} \end{pmatrix} - L_1 \begin{pmatrix} sign(S_{c1}) \\ sign(S_{c2}) \end{pmatrix} \tag{IV.7}$$

With

$$L_1 = \begin{pmatrix} L_{11} & 0 \\ 0 & L_{12} \end{pmatrix} \tag{IV.8}$$

$$L_{11} \geq a_1 \left|\tilde{i}_s\right| + b_1(\rho_1 + \left|\hat{\varphi}_{r\alpha}\right|) + c_1\omega_r(\rho_2 + \left|\hat{\varphi}_{r\beta}\right|) \tag{IV.9}$$

$$L_{12} \geq a_1 \left|\tilde{i}_s\right| + b_1(\rho_2 + \left|\hat{\varphi}_{r\beta}\right|) + c_1\omega_r(\rho_1 + \left|\hat{\varphi}_{r\alpha}\right|) \tag{IV.10}$$

We propose the flux observer $\varphi_{r\alpha}, \varphi_{r\beta}$ as below:

$$\begin{pmatrix} \dot{\hat{\varphi}}_{r\alpha} \\ \dot{\hat{\varphi}}_{r\beta} \end{pmatrix} = a_3 \begin{pmatrix} \dot{i}_{s\alpha} \\ \dot{i}_{s\beta} \end{pmatrix} + B_o \cdot \begin{pmatrix} \dot{\hat{\varphi}}_{r\alpha} \\ \dot{\hat{\varphi}}_{r\beta} \end{pmatrix} - L_1 \begin{pmatrix} sign(S_{c1}) \\ sign(S_{c2}) \end{pmatrix} \tag{IV.11}$$

With

$$B_o = \begin{pmatrix} -b_3 & -\omega_r \\ \omega_r & -b_3 \end{pmatrix} \tag{IV.12}$$

and the dynamics of the errors $\left(\tilde{\varphi}_{r\alpha}, \quad \tilde{\varphi}_{r\beta}\right)$

$$\begin{pmatrix} \dot{\tilde{\varphi}}_{r\alpha} \\ \dot{\tilde{\varphi}}_{r\beta} \end{pmatrix} = a_3 \begin{pmatrix} \tilde{i}_{s\alpha} \\ \tilde{i}_{s\beta} \end{pmatrix} + B_o \cdot \begin{pmatrix} \tilde{\varphi}_{r\alpha} \\ \tilde{\varphi}_{r\beta} \end{pmatrix} - L_1 \begin{pmatrix} sign(S_{c1}) \\ sign(S_{c2}) \end{pmatrix} \tag{IV.13}$$

When the observer of the current is in sliding mode, the dynamics of the errors $\left(\tilde{\varphi}_{r\alpha}, \quad \tilde{\varphi}_{r\beta}\right)$ become

$$\begin{pmatrix} \dot{\tilde{\varphi}}_{r\alpha} \\ \dot{\tilde{\varphi}}_{r\beta} \end{pmatrix} = \left(B_o - L_2(L_1)^{-1}A_o\right) \begin{pmatrix} \tilde{\varphi}_{r\alpha} \\ \tilde{\varphi}_{r\beta} \end{pmatrix} \tag{IV.14}$$

If the gain Matrix L2 imposed as :

$$L_2 = (\Pi + B_o)(A_o)^{-1}.L_1 \tag{IV.15}$$

The dynamics of the flux observation error is exponentially stable:

$$\begin{pmatrix} \dot{er}_3 \\ \dot{er}_4 \end{pmatrix} = -\Pi \begin{pmatrix} er_3 \\ er_4 \end{pmatrix} \tag{IV.16}$$

Where

$$\Pi = \begin{pmatrix} \pi_1 & 0 \\ 0 & \pi_2 \end{pmatrix}; \pi_1, \pi_2 > 0 \qquad \text{(IV.17)}$$

4.8.1 SIMULATION

Our system described is simulated using Matlab Script Program, the Figure 36 shows the current residues and flux residues.

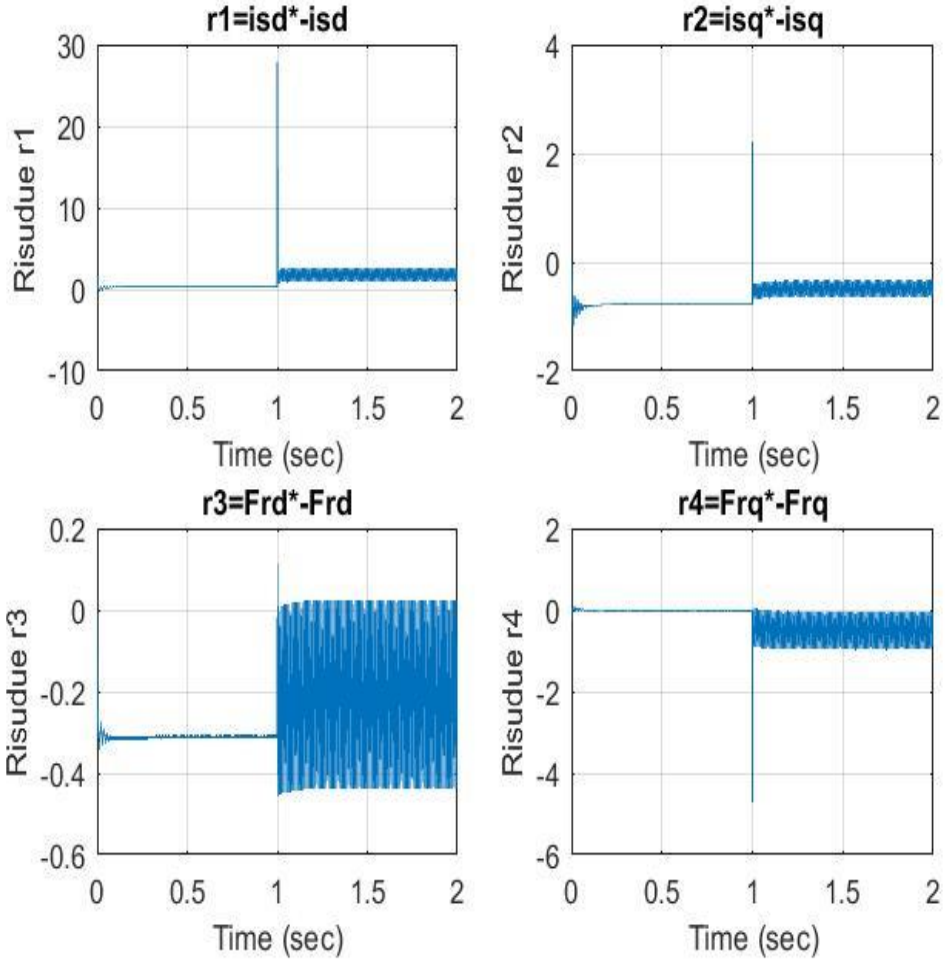

Figure 43. Sliding Mode Observator

4.9 Kalman Filter

The gain matrix of Kalman filter is derived from

$$K_f = P_f C^t \Theta^{-1} \qquad \text{(IV.18)}$$

Where K_f satisfy the following Riccati equation:

$$P_f A^t + A P_f - P_f C^t \Theta^{-1} P_f + G \Xi G^t = 0 \qquad \text{(IV.19)}$$

Using MATLAB lqe command we can obtain K_f after obtain the optimal filtering signal; we can constitute LQG controller structure as shown in Figure.37.

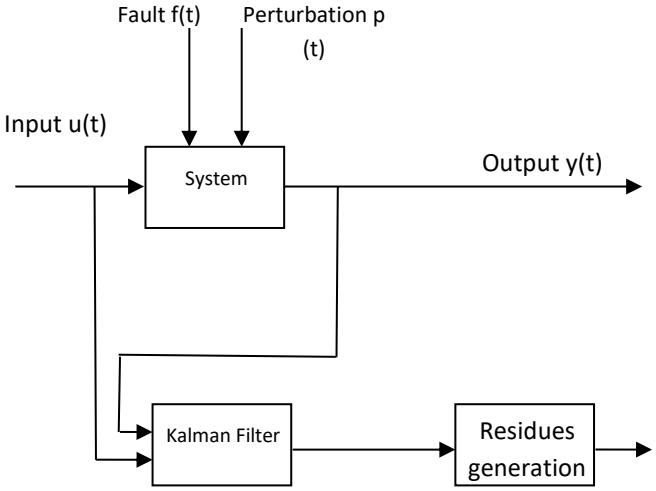

Figure 44 .Kalman filter structure

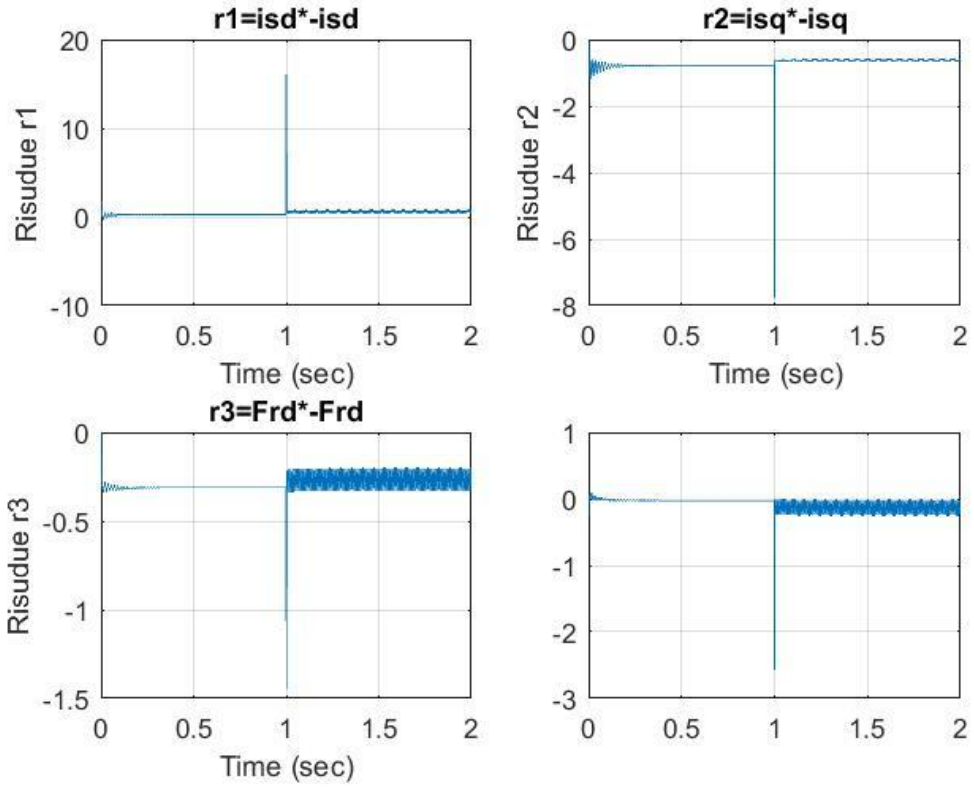

Figure 45. Kalman Estimator errors

4.10 High gain observer

Consider the nonlinear system: [64]

$$\begin{cases} \dot{x} = f(x) + g(x)u \\ y = h(x) \end{cases} \qquad \text{(IV.20)}$$

$x \in R^n, u \in R^m, y \in R^s$

The system (IV.20) must be uniformly observable. Then, it is possible to apply a change of variable $z = \Gamma(x)$ which will transform the system (IV.18) to the following forms: [64]

$$\begin{cases} \dot{z} = Az + \varphi(u, z) \\ y = Cz \end{cases} \qquad \text{(IV.21)}$$

The Function φ is globally Lipschitzienne compared to x and uniformly Lipschitzienne compared to u .

Supposed

$$K = \begin{bmatrix} K_1 & & & \\ & \ddots & & \\ & & \ddots & \\ & & & K_p \end{bmatrix}$$

That matrix must have the adequate size for each block K, where

$A_k - K_k C_k$ all eigenvalue of that matrix has a negative eigenvalue real part.

Suppose that exist two sets of integers $\{\sigma_1, ..., \sigma_n \in Z\}$ et $\{\delta_1 > 0, ..., \delta_p > 0 \in N^*\}$

Such as

$$\sigma_{\mu_k + v} = \sigma_{\mu_k + v - 1} + \delta_r \qquad k = 1, ..., n; v = 1, ..., \mu_k - 1,$$

$$\frac{\partial \varphi_i}{\partial z_i} = 0 \Rightarrow \sigma_i \geq \sigma_j \qquad i, j = 1, ..., n; j \neq \mu_k, k = 1, ..., p.$$

(IV.22)

So $\dot{\hat{z}} = A\hat{z} + \varphi(\hat{z}, u) - S_\theta^{-1}.K(C\dot{z} - y)$.

Is an exponential observer is an exponential observer for the system (II.21).

it exists T_0 such that for all $0 < T < T_0$ with

$$S(S,\delta) = \begin{bmatrix} S^{\delta_1}\Delta(S^{\delta_1}) & & & \\ & \ddots & & \\ & & \ddots & \\ & & & S^{\delta_p}\Delta(S^{\delta_p}) \end{bmatrix}, \Delta_\theta(S) = \begin{bmatrix} 1 & & & \\ & S & & \\ & & \ddots & \\ & & & S^{\mu_0 - 1} \end{bmatrix} \quad \text{(IV.23)}$$

By making an inverse variable change to return to the initial non-linear system, the observer for the system (II.20) is given by:

$$\dot{\hat{x}} = f(\hat{x}) + g(\hat{x})u - \left(\frac{\partial \Gamma}{\partial \hat{x}}(\hat{x}(t))\right)^{-1} S_\theta^{-1} C^T (h(\hat{x}) - y) \quad \text{(IV.24)}$$

$\hat{x}$: observed value of x.

Γ : an application on $R^n \to R^n$

So

$$\Gamma = \left[h_1, L_f h_1, L_f^2 h_1, ..., L_f^{\delta_1} h, h_2, L_f h_2, L_f^2 h_2, ..., L_f^{\delta_2} h_2, ..., h_p, L_f h_p, L_f^2 h_p, ..., L_f^{\delta_p} h_p \right]^T \quad \text{(IV.25)}$$

And $L_f^{\delta_k}$ is a derived δ_k^i de Lie.

p : output numbers.

And S_θ satisfied the lyaponov theorem

$$\dot{S}_\theta = -\theta S_\theta A^T S_\theta A + C^T C = 0 \quad \text{(IV.26)}$$

There are two steps to build the observer, First one is predection $f(\hat{x}) + g(\hat{x})u$

And the second one is for correction $\left(\frac{\partial \Gamma}{\partial \hat{x}}(\hat{x}(t))\right)^{-1} S_\theta^{-1}(h(\hat{x}) - y)$.

The adjustment of the observer's dynamics is done with the parameters θ_k called gains. These are chosen randomly. Their effect and as follows:

A value of θ has to be enough big to stabilize a linear part and guaranty a stability of non linear part using the fact that φ is imposed globally Lipschitzienne compared to x.

If θ is big enough, the convergence time is reduced but the observer becomes sensitive to the measurement noises. For small value of θ will leads to inverse effect.

4.11 Application to the DFIG

The synthesis of the Grand Gain observer to the system of equations of states consists in constructing the two parts of the gain: $\left(\frac{\partial \Gamma}{\partial \hat{x}}(\hat{x}(t))\right)$ et S_θ^{-1}

So, we have: $\dot{\hat{x}} = \begin{bmatrix} \dot{\hat{i}}_{ds} \\ \dot{\hat{i}}_{qs} \\ \dot{\hat{\phi}}_{ds} \\ \dot{\hat{\phi}}_{qs} \\ \dot{\hat{w}}_r \end{bmatrix}$; $h(\hat{x}) = \begin{bmatrix} \hat{i}_{ds} \\ \hat{i}_{qs} \end{bmatrix}$; $y = \begin{bmatrix} i_{ds} \\ i_{qs} \end{bmatrix}$; (IV.27)

$$\frac{\partial \Gamma}{\partial t}(\hat{x}(t)) = \begin{bmatrix} 1 & 0 & 0 & 0 & 0 \\ -\gamma & w_s & \frac{k}{T_r} & k\hat{w}_r & k\hat{\phi}_{qr} \\ 0 & 1 & 0 & 0 & 0 \\ -w_s & -\gamma & k\hat{w}_r & \frac{k}{T_r} & k\hat{\phi}_{dr} \\ 0 & 0 & 0 & 0 & 1 \end{bmatrix}; \quad \text{(IV.28)}$$

$$S_\theta^{-1}(\theta)C^T = \begin{bmatrix} 2\theta & 0 \\ 0 & 2\theta \\ 0 & 0 \\ 0 & 0 \\ 0 & 0 \end{bmatrix} \quad \text{(IV.29)}$$

Avec:

$$\gamma = \left(\frac{R_s}{L_s} + \frac{R_r(1-\sigma)}{L_r\sigma}\right); k = \frac{(1-\sigma)}{M_{sr}\sigma}; \sigma = \left(1 - \frac{M_{sr}^2}{L_s L_r}\right)$$

4.12 Luenberger Observer

In This section, we used a linear Luenberger observer to estimate the variables state of doubly fed induction generator.

First we developed a space stat representation of the DFIG

$$\begin{bmatrix} \dot{i}_{sd} \\ \dot{i}_{sq} \\ \dot{\Phi}_{rd} \\ \dot{\Phi}_{rq} \end{bmatrix} = \begin{bmatrix} k & \omega_{sp} & \frac{M_{sr}}{\sigma L_s L_r^2} R_r & \frac{M_{sr}}{\sigma L_s L_r} \omega \\ -\omega_{sp} & k & -\frac{M_{sr}}{\sigma L_s L_r} \omega & \frac{M_{sr}}{\sigma L_s L_r^2} R_r \\ \frac{M_{sr}}{L_r} R_r & 0 & -\frac{R_r}{L_r} & \omega_{rp} \\ 0 & \frac{M_{sr}}{L_r} R_r & -\omega_{rp} & -\frac{R_r}{L_r} \end{bmatrix} \begin{bmatrix} i_{sd} \\ i_{sq} \\ \Phi_{rd} \\ \Phi_{rq} \end{bmatrix} + \begin{bmatrix} \frac{1}{\sigma L_s} & 0 & 0 & 0 \\ 0 & \frac{1}{\sigma L_s} & 0 & 0 \\ 0 & 0 & 1 & 0 \\ 0 & 0 & 0 & 1 \end{bmatrix} \begin{bmatrix} v_{sd} \\ v_{sq} \\ v_{rd} \\ v_{rq} \end{bmatrix} \quad \text{(IV.30)}$$

With

$$k = -\frac{1}{\sigma L_s}\left(R_s + \frac{M_{sr}^2}{L_r^2} R_r\right)$$

The electromagnetic torque is given by :

$$C_{em} = p\frac{M_{sr}}{L_r}\left(\Phi_{rd} i_{sq} - \Phi_{rq} i_{sd}\right) \quad \text{(IV.31)}$$

The fundamental mechanical equation of the generator which link the electromagnetic torque to the speed variation is :

$$J\frac{d\Omega}{dt} = C_{em} - C_r - F\Omega \quad \text{(IV.32)}$$

The machine model use the park coordinates which turn a the rotor speed ω_{rp}

$$\omega_{sp} = \omega + \omega_{rp} \quad \text{(IV.33)}$$

After making a variable change, our system is representing below as non linear state space.

$x_1 = i_{ds}$; $x_2 = i_{qs}$; $x_3 = \Phi_{dr}$. $x_4 = \Phi_{qr}$; $x_5 = \Omega$; $u_1 = v_{ds}$; $u_2 = v_{qs}$; $u_3 = v_{dr}$; $u_4 = v_{qr}$; $u_5 = C_r$

.

Our system (IV.26) becomes

$$\begin{aligned}
\dot{x}_1 &= a_1 x_1 + w_s x_2 + a_2 x_3 + a_3 x_4 x_5 + \frac{v_{ds}}{L_s \sigma} \\
\dot{x}_2 &= a_1 x_2 - w_s x_1 + a_2 x_4 + a_3 x_3 x_5 + \frac{v_{qs}}{L_s \sigma} \\
\dot{x}_3 &= \frac{M_{sr}}{T_r} x_1 + w_s x_4 - p x_4 x_5 - \frac{1}{T_r} x_3 + vdr \\
\dot{x}_4 &= \frac{M_{sr}}{T_r} x_2 - w_s x_3 + p x_3 x_5 - \frac{1}{T_r} x_4 + vqr \\
\dot{x}_5 &= a_4 x_2 x_3 - a_4 x_1 x_4 - p x_4 x_5 - \frac{K_f}{J} x_5 - \frac{1}{J} C_r
\end{aligned} \qquad \text{(IV.34)}$$

Where:

$$R_{sm} = R_s + \frac{M_{sr}^{\ 2}}{L_r^2} R_r \ ; \quad a_1 = \frac{-R_{sm}}{\sigma L_s} \ ; \quad a_2 = \frac{M_{sr}}{\sigma L_s L_r} \frac{1}{T_r} \ ; \quad a_3 = \frac{p M_{sr}}{\sigma L_s L_r} \ ; \quad a_4 = \frac{p M_{sr}}{J L_r} \ .$$

4.13 Linearization of DFIG:

Linearization of the plant is performed to make the use of linear design methods possible in this thesis. The linearization procedure is performed using the steps shown below[65].[66]

1. Determine the operating point equation by solving the non-linear equation in a stationary point.

2. Replace the variables with operating point values plus small signal values, i.e.

$x(t) = \bar{x} + \Delta x(t)$

and approximate the non-linear expressions with first order Taylor approximations.

3. Subtract the operating point equation from the Taylor approximation. The result is a linear equation in small signal values. In order to set up a linear model of the wind turbine system, two equations for the aerodynamics have to be linearized. Furthermore, the output power equation is linearized in order to be included in an output equation of the system. Linearizing the expressions is accomplished in the next three sections. Notice that this appendix is inspired by [67]

$$\begin{cases} \dot{x} = f(x) + g(x)u \\ y = h(x) \end{cases} \quad \begin{cases} \dot{x} = Ax + Bu \\ y = Cx \end{cases} \qquad \text{(IV.34)}$$

Using Lyaponove theorem

$$A=\left.\frac{df}{dx}\right|_{X=X_0}=\begin{bmatrix} \frac{\delta f_1}{\delta x_1} & \frac{\delta f_1}{\delta x_2} & \frac{\delta f_1}{\delta x_3} & \frac{\delta f_1}{\delta x_4} & \frac{\delta f_1}{\delta x_5} \\ \frac{\delta f_2}{\delta x_1} & \frac{\delta f_2}{\delta x_2} & \frac{\delta f_2}{\delta x_3} & \frac{\delta f_2}{\delta x_4} & \frac{\delta f_2}{\delta x_5} \\ \frac{\delta f_3}{\delta x_1} & \frac{\delta f_3}{\delta x_2} & \frac{\delta f_3}{\delta x_3} & \frac{\delta f_3}{\delta x_4} & \frac{\delta f_3}{\delta x_5} \\ \frac{\delta f_4}{\delta x_1} & \frac{\delta f_4}{\delta x_2} & \frac{\delta f_4}{\delta x_3} & \frac{\delta f_4}{\delta x_4} & \frac{\delta f_4}{\delta x_5} \\ \frac{\delta f_5}{\delta u_1} & \frac{\delta f_5}{\delta u_2} & \frac{\delta f_5}{\delta u_3} & \frac{\delta f_5}{\delta u_4} & \frac{\delta f_5}{\delta u_5} \end{bmatrix}=\begin{bmatrix} a_1 & w_s & a_2 & a_3x_5 & a_3x_4 \\ -w_s & a_1 & -a_3x_5 & a_2 & -a_3x_3 \\ \frac{M_{sr}}{T_r} & 0 & -\frac{M_{sr}}{T_r} & w_s-px_5 & \\ 0 & \frac{M_{sr}}{T_r} & -w_s+px_5 & -\frac{M_{sr}}{T_r} & -px_4 \\ -a_4x_4 & -a_4x_3 & -a_4x_2 & -a_4x_1 & px_3 \end{bmatrix}$$

(IV.35)

$$B=\left.\frac{df}{du}\right|_{X=X_0}=\begin{bmatrix} \frac{\delta f_1}{\delta u_1} & \frac{\delta f_1}{\delta u_2} & \frac{\delta f_1}{\delta u_3} & \frac{\delta f_1}{\delta u_4} & \frac{\delta f_1}{\delta u_5} \\ \frac{\delta f_2}{\delta u_1} & \frac{\delta f_2}{\delta u_2} & \frac{\delta f_2}{\delta u_3} & \frac{\delta f_2}{\delta u_4} & \frac{\delta f_2}{\delta u_5} \\ \frac{\delta f_3}{\delta u_1} & \frac{\delta f_3}{\delta x_2} & \frac{\delta f_3}{\delta u_3} & \frac{\delta f_3}{\delta u_4} & \frac{\delta f_3}{\delta u_5} \\ \frac{\delta f_4}{\delta u_1} & \frac{\delta f_4}{\delta u_2} & \frac{\delta f_4}{\delta u_3} & \frac{\delta f_4}{\delta u_4} & \frac{\delta f_4}{\delta u_5} \\ \frac{\delta f_5}{\delta x_1} & \frac{\delta f_5}{\delta x_2} & \frac{\delta f_5}{\delta x_3} & \frac{\delta f_5}{\delta x_4} & \frac{\delta f_5}{\delta x_5} \end{bmatrix}=\begin{bmatrix} \frac{1}{\sigma L_s} & 0 & 0 & 0 & 0 \\ 0 & \frac{1}{\sigma L_s} & 0 & 0 & 0 \\ 0 & 0 & 1 & 0 & 0 \\ 0 & 0 & 0 & 1 & 0 \\ 0 & 0 & 0 & 0 & -\frac{1}{J} \end{bmatrix} \quad \text{(IV.36)}$$

$$C=\left.\frac{dh}{dx}\right|_{X=X_0}=\begin{bmatrix} \frac{\delta h}{\delta x_1} & \frac{\delta h}{\delta x_2} & \frac{\delta h}{\delta x_3} & \frac{\delta h}{\delta x_4} & \frac{\delta h}{\delta x_5} \end{bmatrix} \quad \text{(IV.37)}$$

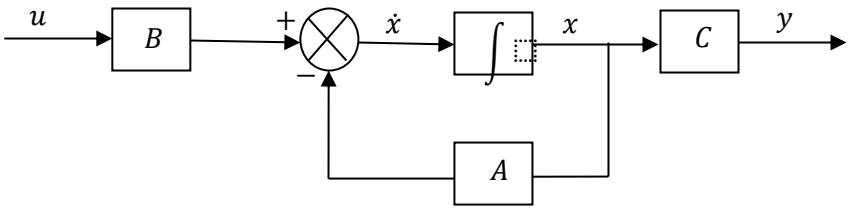

Figure 46. Linear DFIG Space state representation

From linear model we will calculate the feedback gain k

$$\sum \Rightarrow \begin{cases} \dot{x} = Ax + Bu \\ y = Cx \end{cases} \qquad \hat{\sum} \Rightarrow \begin{cases} \dot{\hat{x}} = A\hat{x} + Bu + L(y - \hat{y}) \\ \hat{y} = C\hat{x} \end{cases} \tag{IV.38}$$

$$u = -Kx + r$$

$$e = x - \hat{x}; \dot{e} = \dot{x} - \dot{\hat{x}}$$

$$\dot{e} = Ax + Bu - A\hat{x} - Bu - L(y - \hat{y})$$

$$\Rightarrow \dot{e} = A(x - \hat{x}) - LC(x - \hat{x})$$

$$\Rightarrow \dot{e} = (A - LC)(x - \hat{x})$$

$$\Rightarrow \dot{e} = (A - LC)e \tag{IV.39}$$

$$(A - LC)^T = A^T - C^T L^T$$

We can Use place or acker command on MATLAB

$$L^T = place(A, C, poles)$$

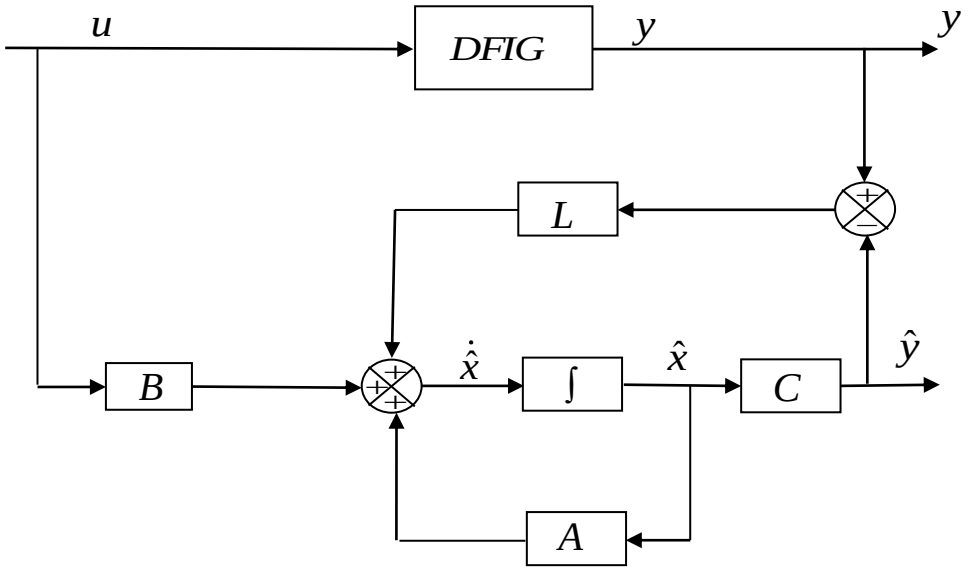

Figure 47. Luenberger observer

4.14 SIMULATION

The last part of the thesis shows the simulation of the whole system behavior with a turbine emulator controlled with the MPPT strategy including actuator faults.

The system described above is simulated using Matlab simulation Program a stochastic wind speed has been generated with a mean value of 12 [m/s] , we apply a short-circuit of 10% on

phase (a) at 1sec.The dynamic responses for both PI and the LQG controllers are illustrated in Figure 71, Figure 73 and Figure 75 for the active and reactive powers ,The Figure 72, Figure 74 and Figure76 represent the stator currents in faulty mode in case PI and LQG controller ,It can be noticed that controllers based on LQG method show a better response than the other one based PI method. It can also be observed that the fluctuations of the active and reactive power are less. The proposed controllers show a better performance and robustness against external load variation. To validate the proposed method, the results show this observer performs well in tracking the dynamics of states with high accuracy and sensitivity.

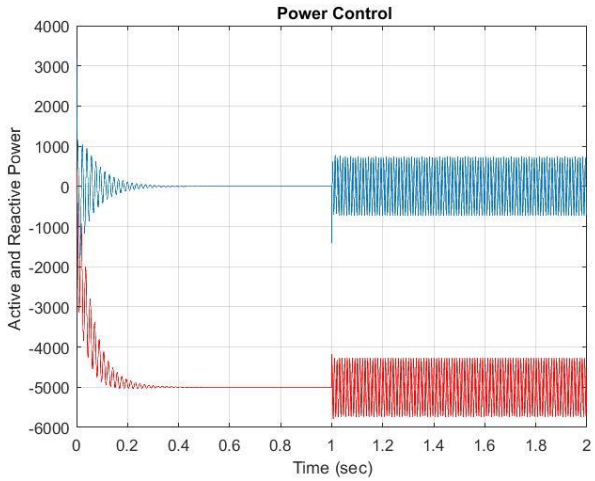

Figure 48. Active and Reactive power PI controller

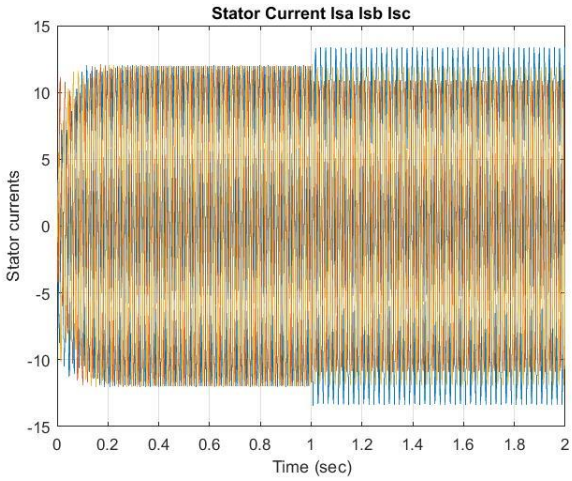

Figure 49. Stator current in case PI controller

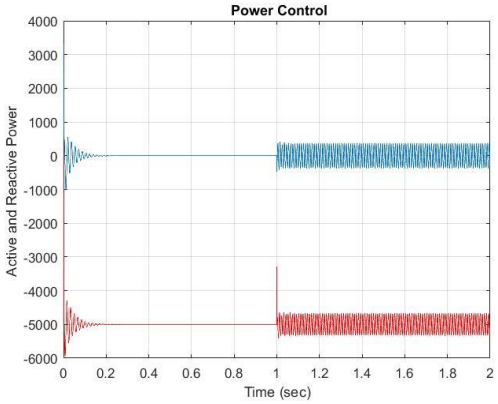

Figure 50. Active and Reactive power using LQG controller

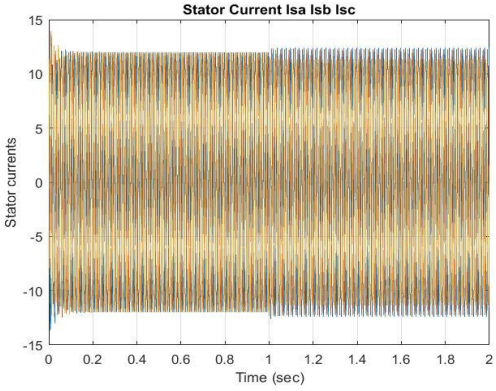

Figure 51. Stator current in case LQG controller

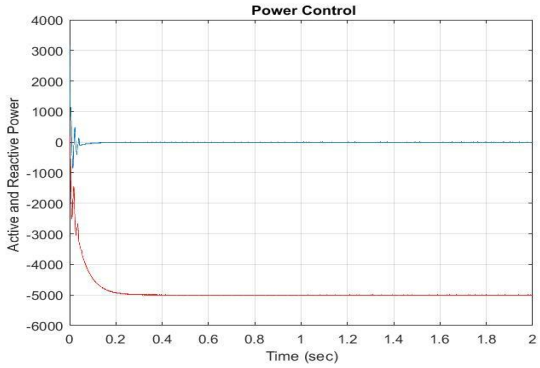

Figure 52. Active and Reactive power SM controller

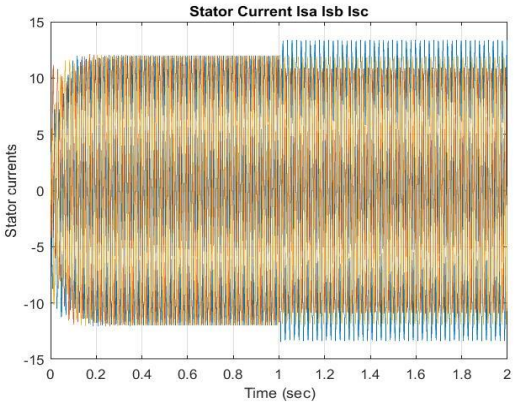

Figure 53. Stator currents SM controller

5. Conclusion

In Chapter 4, we tested the fault-tolerant control system, and it demonstrated its ability to manage the wind turbine effectively even when faced with faults. This is possible because we use a similar structure for the fault diagnosis algorithms. With observers and different control types . These algorithms can keep things running by adjusting the system based on the fault, ensuring it stays reliable even when there are issues.

GENERAL CONCLUSION

GENERAL CONCLUSION

Fault-tolerant control (FTC) is a vital field in control engineering aimed at ensuring the continued functionality and stability of complex systems, even in the presence of faults, failures, or unexpected disruptions. In practical terms, it involves designing control systems that can detect, diagnose, and adapt to faults or anomalies within a system to prevent critical failures. FTC has applications in a wide range of industries, including aerospace, automotive, manufacturing, and power systems, where system reliability and safety are paramount.

In this study, we have introduced a comprehensive system designed for the generation of electrical energy using a doubly-fed induction generator, coupled with a wind turbine. Initially, we have detailed the control mechanisms governing the machine, primarily aimed at overseeing the exchange of active and reactive powers between the machine and the grid. We have also explored several advanced control techniques, comparing their effectiveness.

Our investigation has extended to evaluating the performance of power reference tracking with the doubly-fed induction generator under ideal conditions, as well as when subjected to perturbations, including variations in parameters and external disturbances. We have conducted robustness tests to assess its ability to maintain stable performance in the face of these challenges.

Based on the results obtained in this project, it is concluded that the reliability of wind turbines can be improved by applying fault diagnosis and fault-tolerant control. This is possible since the fault-tolerant capabilities allow wind turbines to continue operation in cases of sensor and actuator faults. Especially for incipient faults, the developed fault-tolerant control system benefits from its model-based approach, which allows faults to be accommodated based on parameter estimates.

This improves the performance of the wind turbine control system in terms of minimizing mechanical loads and increasing efficiency

Recommandations for Future Work

With respect to fault-tolerant control, the choice between active and passive fault-tolerant approaches is problem-specific. It is recommended to utilize an active fault-tolerant controller, when this allows significantly improved performance compared to a passive fault-tolerant controller. This is expected to happen in situations where a fault causes severe changes in the dynamics of the system and where a reliable diagnosis system exists. Otherwise, it is recommended to apply passive fault-tolerant controllers, since they have no risk of making wrong decisions.

- It is considered that the active fault-tolerant controller is suited for controlling the wind turbine in case of high air content in the oil, but that the passive fault-tolerant controller is preferable when the generator speed measurement is unavailable, since this effect dominates the control problem resulting in similar performance of both controllers. Generally, the active fault-tolerant controller approach show slightly better performance, since it is adapted to the condition of the system, by exploiting information from the fault diagnosis algorithms
- Laboratory or field validation: this would be more relevant for testing complex control algorithm to show the feasibility and validate the benefit with respect to simpler alternatives.
- Analysis of the dynamical behavior of a multi-DFIG wind farm: The interests would be to identify the dynamics that determine the overall behavior at the common point of coupling, the effect of unequal wind speed distribution on the mechanical and electrical power variation within the wind farm, the cases in which these dynamics would be relevant (e.g. voltage control, power extraction optimization) and when they would need to be controlled.[68]

BIBLIOGRAPHY

Bibliography

[1] Xingjia Yao, Changchun Guo, Zuoxia Xing, Yan Li, Shu Liu, and Xiaodong Wang, “Pitch regulated LQG controller design for variable speed wind turbine,” in *2009 International Conference on Mechatronics and Automation*, Changchun, China, Aug. 2009, pp. 845–849, doi: 10.1109/ICMA.2009.5246272.

[2] E. B. Muhando, T. Senjyu, E. Omine, and T. Funabashi, “Full state feedback digital control of WECS with state estimation by stochastic modeling design,” in *2008 IEEE Power and Energy Society General Meeting - Conversion and Delivery of Electrical Energy in the 21st Century*, Pittsburgh, PA, USA, Jul. 2008, pp. 1–8, doi: 10.1109/PES.2008.4596132.

[3] A. Bakouri, H. Mahmoudi, and A. Abbou, “Modelling and optimal control of the doubly fed induction generator wind turbine system connected to utility grid,” in *2016 International Renewable and Sustainable Energy Conference (IRSEC)*, Marrakech, Morocco, Nov. 2016, pp. 807–812, doi: 10.1109/IRSEC.2016.7984000.

[4] Rui Fan, Z. Huang, Shaobu Wang, R. Diao, and Da Meng, “Dynamic state estimation and parameter calibration of a DFIG using the ensemble Kalman filter,” in *2015 IEEE Power & Energy Society General Meeting*, Denver, CO, USA, Jul. 2015, pp. 1–5, doi: 10.1109/PESGM.2015.7285990.

[5] M. Debbou and M. Pietrzak-David, “Novel tolerant fault DFIM drive for naval propulsion,” in *IECON 2013 - 39th Annual Conference of the IEEE Industrial Electronics Society*, Vienna, Austria, Nov. 2013, pp. 3006–3011, doi: 10.1109/IECON.2013.6699609.

[6] T. M. Letcher, Ed., *Wind energy engineering: a handbook for onshore and offshore wind turbines*. London ; San Diego: Academic Press, an imprint of Elsevier, 2017.

[7] S. Karim, A. Taibe, and T. Mohamed, “LQG Controller for the Control of Active and Reactive Power of DFIG Operating Under Inter-Turn Short Circuit Fault,” p. 1.

[8] M. Stiebler, *Wind energy systems for electric power generation*. Berlin: Springer, 2008.

[9] “Wind energy: fundamentals, resource analysis and economics,” *Choice Rev. Online*, vol. 44, no. 01, pp. 44-0337-44–0337, Sep. 2006, doi: 10.5860/CHOICE.44-0337.

[10] H. Abu-Rub, M. Malinowski, and K. Al-Haddad, “Power Electronics for Renewable Energy Systems, Transportation,” p. 827.

[11] S. E. Aimani, “Modèlisation de différentes technologies d’éoliennes,” p. 226.

[12] Z. Jin, “Control Studies of DFIG based Wind Power Systems,” p. 110.

[13] J. F. Manwell, “Wind Energy Explained: Theory, Design and Application,” p. 705.

[14] R. Babouri, D. Aouzellag, and K. Ghedamsi, “Introduction of Doubly Fed Induction Machine in an Electric Vehicle,” *Energy Procedia*, vol. 36, pp. 1076–1084, 2013, doi: 10.1016/j.egypro.2013.07.123.

[15] M. FRANCOISE, “SMALL-SIGNAL MODELLING AND ANALYSIS OF DOUBLY-FED INDUCTION GENERATORS IN WIND POWER APPLICATIONS,” PhD Thesis, Control and Power Group Dept of Electrical and Electronic Engineering Imperial College London University, London.

[16] A. Bakouri, A. Abbou, H. Mahmoudi, and K. Elyaalaoui, “Direct torque control of a doubly fed induction generator of wind turbine for maximum power extraction,” in *2014 International Renewable and Sustainable Energy Conference (IRSEC)*, Ouarzazate, Morocco, Oct. 2014, pp. 334–339, doi: 10.1109/IRSEC.2014.7059799.

[17] M. Vijayalaxmi and N. Shanmugavadivoo, “APPLICATION OF SUPERVISORY CONTROL FOR DOUBLY FED INDUCTION GENERATOR BASED WIND ENERGY CONVERSION SYSTEM,” *J. Electr. Eng.*, p. 8.

[18] E. Ritchie and K. Leban, “Doubly Fed Induction Generator Fault Simulation,” p. 63.

[19] J. Tian, “Optimal Power Control in DFIG Turbine Based Wind Farm Considering Wake Effect and Lifetime.” Aalborg University Press, 2017, doi: 10.5278/vbn.phd.eng.00010.

[20] J. Zafar and S. A. Rajput, “Integration of Wind Energy Converters into an Existing Distribution Grid,” p. 124.

[21] S. Abdelmalek, A. Gencer, and S. Rezazi, “Multiple Models Representation for a Doubly-Fed Induction Generator based Wind Energy Conversion Systems,” in *2019 1st Global Power,*

Energy and Communication Conference (GPECOM), Nevsehir, Turkey, Jun. 2019, pp. 348–352, doi: 10.1109/GPECOM.2019.8778585.

[22] E. S. Abdin and W. Xu, "Control Design and Dynamic Performance Analysis of a Wind Turbine-Induction Generator Unit," *IEEE Trans. ENERGY Convers.*, vol. 15, no. 1, p. 6, 2000.

[23] F. Hachicha and L. Krichen, "Performance analysis of a wind energy conversion system based on a doubly-fed induction generator," in *Eighth International Multi-Conference on Systems, Signals & Devices*, Sousse, Mar. 2011, pp. 1–6, doi: 10.1109/SSD.2011.5767481.

[24] A. Yazidi, H. Henao, G. A. Capolino, L. Capocchi, and D. Federici, "Double-fed three-phase induction machine model for simulation of inter-turn short circuit fault," in *2009 IEEE International Electric Machines and Drives Conference*, Miami, FL, USA, May 2009, pp. 571–576, doi: 10.1109/IEMDC.2009.5075263.

[25] . N. H., "DOUBLE FLUX ORIENTATION CONTROL FOR A DOUBLY FED INDUCTION GENERATOR BASED WIND TURBINE," *Int. J. Res. Eng. Technol.*, vol. 02, no. 03, pp. 380–384, Mar. 2013, doi: 10.15623/ijret.2013.0203025.

[26] A. A. R. Al Tahir, R. Lajouad, F. Z. Chaoui, R. Tami, T. Ahmed-Ali, and F. Giri, "A Novel Observer Design for Sensorless Sampled Output Measurement: Application of Variable Speed Doubly Fed Induction Generator," *IFAC-Pap.*, vol. 49, no. 13, pp. 235–240, 2016, doi: 10.1016/j.ifacol.2016.07.957.

[27] F. Poitiers, T. Bouaouiche, and M. Machmoum, "Advanced control of a doubly-fed induction generator for wind energy conversion," *Electr. Power Syst. Res.*, vol. 79, pp. 1085–1096, 2009.

[28] V. Vidyanagar and V. Vidyanagar, "Simulation of Active and Reactive Power Control of DFIG," *Am. J. Eng. Res.*, p. 8, 2014.

[29] M. Abid, A. G. Aissaoui, Y. Ramdani, and A. K. Zeblah, "SLIDING MODE SPEED AND FLUX CONTROL OF FIELD-ORIENTED INDUCTION MACHINE," vol. 7, no. 1, p. 7, 2007.

[30] D. Kairous, R. Wamkeue, and B. Belmadani, "Advanced control of variable speed wind energy conversion system with DFIG," in *2010 9th International Conference on Environment and Electrical Engineering*, Prague, May 2010, pp. 41–44, doi: 10.1109/EEEIC.2010.5490021.

[31] L. Barazane, S. Kharzi, A. Malek, and C. Larbès, "A sliding mode control associated to the field-oriented control of asynchronous motor supplied by photovoltaic solar energy," p. 11.

[32] Y. Djeriri, A. Meroufel, A. Massoum, and Z. Boudjema, "DIRECT POWER CONTROL OF A DOUBLY FED INDUCTION GENERATOR BASED WIND ENERGY CONVERSION SYSTEMS INCLUDING A STORAGE UNIT," *J. Electr. Eng.*, p. 8.

[33] A. Boumassata and D. Kerdoun, "Direct powers control of DFIG through direct converter and sliding mode control for WECS," in *2015 3rd International Conference on Control, Engineering & Information Technology (CEIT)*, Tlemcen, Algeria, May 2015, pp. 1–5, doi: 10.1109/CEIT.2015.7233058.

[34] S. Arnalte, J. C. Burgos, and J. L. Rodríguez-Amenedo, "Direct Torque Control of a Doubly-Fed Induction Generator for Variable Speed Wind Turbines," *Electr. Power Compon. Syst.*, vol. 30, no. 2, pp. 199–216, Feb. 2002, doi: 10.1080/153250002753427851.

[35] K. Cristian, P. Puleston, and M. Mayosky, *Sliding-Mode Control of PEM Fuel Cells (2012).pdf*, Springer. 2012.

[36] D. Mulik, G. S. Phadke, and S. Salunkhe, "Sliding Mode Speed Controller for Vector Controlled Induction Motor," vol. 02, no. 05, p. 5.

[37] B. Hamane, M. L. Doumbia, A. M. Bouhamida, and M. Benghanem, "Direct active and reactive power control of DFIG based WECS using PI and sliding mode controllers," in *IECON 2014 - 40th Annual Conference of the IEEE Industrial Electronics Society*, Dallas, TX, USA, Oct. 2014, pp. 2050–2055, doi: 10.1109/IECON.2014.7048784.

[38] S. Nourdine, H. Camblong, I. Vechiu, and G. Tapia, "Comparison of wind turbine LQG controllers designed to alleviate fatigue loads," in *IEEE ICCA 2010*, Xiamen, China, Jun. 2010, pp. 1502–1507, doi: 10.1109/ICCA.2010.5524385.

[39] P. N. Paraskevopoulos, *Modern control engineering*. New York: Marcel Dekker, 2002.

[40] R. Barrera-Cardenas and M. Molinas, “Optimal LQG Controller for Variable Speed Wind Turbine Based on Genetic Algorithms,” *Energy Procedia*, vol. 20, pp. 207–216, 2012, doi: 10.1016/j.egypro.2012.03.021.
[41] F. Lin, *Robust control design: an optimal control approach*. Chichester, West Sussex, England ; Hoboken, NJ: John Wiley/RSP, 2007.
[42] H. Noura, Ed., *Fault-tolerant control systems: design and practical application*. Dordrecht: Springer, 2009.
[43] Z. Zhao, S. Jiang, R. Ni, S. Fu, Z. Han, and Z. Yu, “Fault-tolerant control of clutch actuator motor in the upshift of 6-speed dry dual clutch transmission,” *Control Eng. Pract.*, vol. 95, p. 104268, Feb. 2020, doi: 10.1016/j.conengprac.2019.104268.
[44] Q. Zhang and M. Feng, “Fast Fault Diagnosis Method for Hall Sensors in Brushless DC Motor Drives,” *IEEE Trans. Power Electron.*, vol. 34, no. 3, pp. 2585–2596, Mar. 2019, doi: 10.1109/TPEL.2018.2844956.
[45] A. Zolghadri, D. Henry, J. Cieslak, D. Efimov, and P. Goupil, *Fault Diagnosis and Fault-Tolerant Control and Guidance for Aerospace Vehicles: From Theory to Application*. London: Springer London, 2014.
[46] F. Shi and R. Patton, “An active fault tolerant control approach to an offshore wind turbine model,” *Renew. Energy*, vol. 75, pp. 788–798, Mar. 2015, doi: 10.1016/j.renene.2014.10.061.
[47] M. Witczak, P. Majdzik, R. Stetter, and B. Lipiec, “A fault-tolerant control strategy for multiple automated guided vehicles,” *J. Manuf. Syst.*, vol. 55, pp. 56–68, Apr. 2020, doi: 10.1016/j.jmsy.2020.02.009.
[48] L. Zhong, “Contribution to fault tolerant flight control under actuator failures,” p. 248.
[49] R. J. Patton, “FAULT-TOLERANT CONTROL SYSTEMS: THE 1997 SITUATION,” p. 22.
[50] C. Nie and R. J. Patton, “Fault estimation and MRC-based active FTC,” *IFAC Proc. Vol.*, vol. 44, no. 1, pp. 14808–14813, Jan. 2011, doi: 10.3182/20110828-6-IT-1002.00586.
[51] A. Pakstas, I. Shagaev, and J. Zalewski, “Redundancy classification principles for the design of the fault-tolerant computer controlled systems,” *IFAC Proc. Vol.*, vol. 33, no. 20, pp. 119–125, Jul. 2000, doi: 10.1016/S1474-6670(17)38036-9.
[52] H. Merabet, Tahar. Bahi, and N. Halem, “Condition Monitoring and Fault Detection in Wind Turbine Based on DFIG by the Fuzzy Logic,” *Energy Procedia*, vol. 74, pp. 518–528, Aug. 2015, doi: 10.1016/j.egypro.2015.07.737.
[53] P. Kachroo and K. Ozbay, “Feedback Control Theory for Dynamic Traffic Assignment,” p. 214.
[54] R. E. Bavili, M. J. Khosrowjerdi, and R. Vatankhah, “Active Fault Tolerant Controller Design using Model Predictive Control,” *CONTROL Eng. Appl. Inform.*, p. 9.
[55] “INTELLIGENT FAULT DETECTION, IDENTIFICATION AND CONTROL OF SATELLITE FORMATION FLYING:,” in *Proceedings of the 8th International Conference on Informatics in Control, Automation and Robotics*, Noordwijkerhout, Netherlands, 2011, pp. 85–90, doi: 10.5220/0003529600850090.
[56] M. Blanke, R. Izadi-Zamanabadi, S. A. Bøgh, and C. P. Lunau, “F A U L T - T O L E R A N T C O N T R O L S Y S T E M S - A H O L I S T I C V I E W,” *Control Eng. Pract.*, vol. 5, no. 5, pp. 693–702, May 1997, doi: 10.1016/S0967-0661(97)00051-8.
[57] J. Zhang, Z. Pang, Y. Zhou, and C. Han, “Active fault tolerant control for networked control systems with actuator fault,” in *2016 35th Chinese Control Conference (CCC)*, Chengdu, China, Jul. 2016, pp. 7521–7525, doi: 10.1109/ChiCC.2016.7554548.
[58] G. J. J. Ducard, *Fault-tolerant flight control and guidance systems: practical methods for small unmanned aerial vehicles*. London: Springer, 2009.
[59] S. Simani, C. Fantuzzi, and R. Patton, *Model-based fault diagnosis in dynamic systems using identification techniques*. London; New York: Springer, 2003.
[60] S. Pourmohammad and A. Fekih, “Fault-Tolerant Control of Wind Turbine Systems - A Review,” in *2011 IEEE Green Technologies Conference (IEEE-Green)*, Baton Rouge, LA, USA, Apr. 2011, pp. 1–6, doi: 10.1109/GREEN.2011.5754880.
[61] X. Yao, S. Liu, G. Shan, Z. Xing, C. Guo, and C. Yi, “LQG Controller for a Variable Speed Pitch Regulated Wind Turbine,” in *2009 International Conference on Intelligent Human-Machine*

Systems and Cybernetics, Hangzhou, Zhejiang, China, 2009, pp. 210–213, doi: 10.1109/IHMSC.2009.176.

[62] K. P. B. Chandra, H. Alwi, and C. Edwards, "Fault Reconstruction for a Quadrotor Using an LPV Sliding Mode Observer 1," *IFAC-Pap.*, vol. 48, no. 21, pp. 374–379, 2015, doi: 10.1016/j.ifacol.2015.09.555.

[63] M. Tadjine, H. Chekireb, and M. Djemai, "On a sliding mode control and observer of induction motor," in *SMC'03 Conference Proceedings. 2003 IEEE International Conference on Systems, Man and Cybernetics. Conference Theme - System Security and Assurance (Cat. No.03CH37483)*, Washington, DC, USA, 2003, vol. 2, pp. 1371–1377, doi: 10.1109/ICSMC.2003.1244603.

[64] M. Messaoudi, L. Sbita, and M. N. Abdelkrim, "A robust nonlinear observer for states and parameters estimation and on-line adaptation of rotor time constant in sensorless induction motor drives," *Int J Phys Sci*, p. 9.

[65] J. G. Andersen, "Restricting access to social protection for immigrants in the Danish welfare state," vol. 15, no. 3, p. 13, 2007.

[66] M. Jouili, K. Jarray, Y. Koubaa, and M. Boussak, "Luenberger state observer for speed sensorless ISFOC induction motor drives," *Electr. Power Syst. Res.*, vol. 89, pp. 139–147, Aug. 2012, doi: 10.1016/j.epsr.2012.02.014.

[67] T. Esbensen and C. Sloth, "Fault Diagnosis and Fault-Tolerant Control of Wind Turbines," p. 177.

[68] A. O, M. Bekravi, and N. Ghadimi, "Intelligent controller based wide-area control in power system," *Int. J. Uncertain. Fuzziness Knowl.-Based*, vol. 25.01, 2017.

APPENDIX

DFIG parameters

- Stator voltage Vs=450 v
- Rated Power Pn=1.5 Kw
- Stator resistance Rs= 1.557 Ω.
- Rotor resistance Rr=2.62 Ω.
- Number of pole pairs P=2.
- Stator inductance Ls =0.195H
- Rotor inductance Lr =0.195H
- Mutual inductance Lm=0.177H
- Friction coefficient f =7.1e-3
- Shaft inertia J=0.001 Kg.m2
- Slip g=0.04

Parameters of Turbine

Radius R=30 m.

- Gear ratio G= 90.
- Air density $\rho = 1.22 Kg / m^3$.